

Review

Targeting Strategies for Multifunctional Nanoparticles in Cancer Imaging and Therapy

Mi Kyung Yu, Jinho Park, Sangyong Jon✉

Cell Dynamics Research Center, School of Life Sciences, Gwangju Institute of Science and Technology, 261 Chemdangwagi-ro, Gwangju 500-712, Republic of Korea.

✉ Corresponding author: Dr. Sangyong Jon. Tel: 82-62-715-2504; E-mail: syjon@gist.ac.kr.

© Ivyspring International Publisher. This is an open-access article distributed under the terms of the Creative Commons License (<http://creativecommons.org/licenses/by-nc-nd/3.0/>). Reproduction is permitted for personal, noncommercial use, provided that the article is in whole, unmodified, and properly cited.

Received: 2011.08.30; Accepted: 2011.09.28; Published: 2012.01.01

Abstract

Nanomaterials offer new opportunities for cancer diagnosis and treatment. Multifunctional nanoparticles harboring various functions including targeting, imaging, therapy, and etc have been intensively studied aiming to overcome limitations associated with conventional cancer diagnosis and therapy. Of various nanoparticles, magnetic iron oxide nanoparticles with superparamagnetic property have shown potential as multifunctional nanoparticles for clinical translation because they have been used as magnetic resonance imaging (MRI) contrast agents in clinic and their features could be easily tailored by including targeting moieties, fluorescence dyes, or therapeutic agents. This review summarizes targeting strategies for construction of multifunctional nanoparticles including magnetic nanoparticles-based theranostic systems, and the various surface engineering strategies of nanoparticles for *in vivo* applications.

Key words: Multifunctional nanoparticles, magnetic nanoparticles, targeting ligand, bioconjugation, surface engineering, long circulation

Introduction

Cancer remains one of the most deadly diseases in the world, and the number of new cases increases each year [1]. Despite rapid advances in diagnostic procedures and treatments, the overall survival rate from cancer has not improved substantially over the past 30 years [2]. There is a need, therefore, to develop novel approaches for the accurate detection of early-stage of cancer and for targeted therapies based on the cancer-specific markers, which could lead to personalized medicine. Recent advances in nanomaterials have explored passive and active targeting strategies for enhancing intratumoral drug concentrations while limiting the unwanted toxicity to healthy tissue [3-5]. The targeted delivery of nanomaterials can overcome difficulties associated with conventional free anticancer drugs, including insolubility under

aqueous conditions, rapid clearance, and a lack of selectivity, resulting in nonspecific toxicity toward normal cells and lower the dose of drugs delivered to the cancer cells [6]. Inorganic nanomaterials with a variety of unique intrinsic physical properties have attracted growing interest for use in biomedical imaging applications [7,8]. Among the imaging nanoprobes, magnetic iron oxide nanoparticles have been widely used as MRI contrast agents for cancer imaging, helping to provide anatomical details and furthermore real-time monitoring of the therapeutic response [9,10]. In this review, we first discuss selective targeting strategies using nanoparticles for achieving effective cancer detection and treatment; secondly, we discuss the various targeting moieties used as 'escort' molecules to specific tumor tissues; third, we discuss

methods of conjugating the functional moieties to nanoparticles; finally, we discuss strategies for optimizing the nanoparticle surfaces for *in vivo* applications. We highlight the potential utility of magnetic nanoparticle-based theranostic systems, which thus far are shown to be suitable for clinical use.

Passive and active targeting

Most nanoparticles are expected to accumulate in tumors due to the pathophysiologic characteristics of tumor blood vessels. Delivery of nutrients to an actively growing tumor with a volume greater than 2 mm³ becomes diffusion-limited, and new blood vessel formation is required to supply nutrients and oxygen [11]. The incomplete tumor vasculature results in leaky vessels with enlarged gap junctions of 100 nm to 2 μm, depending on the tumor type, and macromolecules easily access the tumor interstitium [12-14]. Tumors also have a compound retention time higher than that of normal tissues because tumors lack a well-defined lymphatic system [15,16]. These features provide an enhanced permeability and retention (EPR) effect, which constitutes an important mechanism for the passive targeting and selective accumulation of nanoparticles in the tumor interstitium. Doxil[®], a poly(ethylene glycol)-coated (PEGylated) liposomal system for doxorubicin (Dox) delivery, and Abraxane[®], albumin-bound paclitaxel nanoparticles for the treatment of metastatic breast cancer, are representative examples of US Food and Drug Administration (FDA)-approved nanocarrier-based drugs for cancer therapy. These agents circulate in the body with a half-life about 100 times longer than that of free anticancer drugs while simultaneously reducing systemic toxicity [17-21].

However, passive targeting approaches suffer from several limitations. Targeting cancer cells using the EPR effect is not feasible in all tumors because the degree of tumor vascularization and porosity of tumor vessels can vary with the tumor type and status [12,22]. In addition, cancer cells can display a reduced number of specific interactions that lead to internalization of nanoparticles. In addition to preventing interactions between nanoparticles and opsonins, PEGylated surfaces can also reduce interactions between nanoparticles and cell surfaces [23-26]. The lack of control can lead to drug expulsion and induce cancer cells to develop resistance toward a variety of drugs (multiple drug resistance, MDR), which inevitably reduces any therapeutic effects [27]. One approach to overcoming these limitations is to attach targeting moieties to the nanoparticle surfaces. Nanoparticles that present targeting moieties can bind to target cells through ligand-receptor interactions that

induce receptor-mediated endocytosis and drug release inside the cell. Efficient binding and internalization requires that receptors are expressed exclusively on target cancer cells (10⁴-10⁵ copies per cell) relative to normal cells, and expression should be homogeneous across all targeted cells [28]. This delivery strategy achieves a high targeting specificity and delivery efficiency, while avoiding nonspecific binding and the MDR efflux mechanism [29]. At present, several targeted delivery systems are under clinical trials, such as transferrin receptor targeted cytotoxic platinum-based oxaliplatin in a liposome (MBP-426), transferrin receptor targeted cyclodextrin-containing nanoparticles with siRNA payload (CALAA-01), or prostate-specific membrane antigen (PSMA) targeted polymeric nanoparticles containing docetaxel (BIND-014). Table 1 lists the nanoparticle-based drugs that are approved or under clinical development. Although ligand-mediated targeting technologies have not yet made a considerable clinical impact on human health, it will soon be feasible to develop targeted nanoparticle candidates for clinical translation [30].

Multifunctional nanoparticles for targeted imaging and therapy

The multifunctional properties of nanoparticles convey unique advantages for the cancer-specific delivery of imaging and therapeutic agents [42]. Several ligands with therapeutic, diagnostic, or barrier-avoiding properties can be incorporated across the large nanoparticle surface area in a single nanoparticle system. Multivalent targeting significantly increases the binding affinity of a particle toward a target cell [43]. Magnetic iron oxide nanoparticles have been shown to be suitable for use as theranostic agents by employing their intrinsic diagnostic capabilities in the context of MRI applications. Surface modifications may be easily introduced through conjugation with targeting moieties (e.g., antibodies, peptides, small molecules, or aptamers), fluorescence dyes, genes, or drugs to provide multimodal functionalities [44-47]. In the following section, multifunctional nanoparticle systems that feature a variety of targeting moieties for *in vitro* and/or *in vivo* cancer imaging and therapy, including magnetic nanoparticles, will be discussed.

2. Types of targeting moieties

Targeting moieties are classified as proteins (mainly antibodies and their fragments), peptides, nucleic acids (aptamers), small molecules, or others (vitamins or carbohydrates). Although monoclonal

antibodies (mAbs) have been widely used as escort molecules for the targeted delivery of nanoparticles, several limitations including large size and difficulty in conjugation to nanoparticles have hampered their uses. Thus, other smaller-sized ligands including

peptides have attracted greater attention these days. This section will discuss the types of targeting moieties that may be used for decorating multifunctional nanoparticles, as well as their potential benefits and drawbacks.

Table 1. Nanoparticle-based drugs that have been approved or are being tested in the clinic.

Commercial name	Platform	Targeting ligand	Active pharmaceutical ingredient	Indication	Status	ref
Nanoparticle systems without targeting ligands						
DaunoXome	liposomes		daunorubicin	Kaposi's sarcoma	approved	28
Myocet	liposomes		doxorubicin	combinational therapy of recurrent breast, ovarian cancer	approved	29
Doxil/Caelyx	PEG-liposomes		doxorubicin	refractory Kaposi's sarcoma, recurrent breast, ovarian cancer	approved	30
Onco TCS	liposomes		vincristine	relapsed aggressive non-Hodgkin's lymphoma	approved	31
Abraxane	albumin-bound paclitaxel nanoparticles		paclitaxel	metastatic breast cancer	approved	32
Genexol-PM*	PLA-PEG micelle		paclitaxel	metastatic breast cancer	approved	33
Nanoparticle systems with targeting ligands						
CALAA-01	cyclodextrin-containing polymeric nanoparticle	transferrin	siRNA	solid tumor	Phase I	34
MBP-426	liposome	transferrin	oxaliplatin	gastric, esophageal, gastricesophageal adenocarcinoma	Phase Ib/II	35
MCC-465	liposome	F(ab') ₂ fragment of human Ab GAH	doxorubicin	metastatic stomach cancer	Phase I (not continued)	36
BIND-014	PLGA-PEG nanoparticle	PSMA-specific peptide	doxetaxel	solid tumor	Phase I	37
SGT53-01	liposome	transferrin receptor-specific-scAb	p53 gene	solid tumor	Phase I	38

Antibody-based targeting

Targeted ligand development over the past several decades has focused on antibodies as a class. The presence of two epitope binding sites in a single molecule offers an exceedingly high selectivity and binding affinity for the target of interest. Rituximab (Rituxan®) for non-Hodgkin's lymphoma treatment [48], Trastuzumab (Herceptin®) for breast cancer treatment [49], Bevacizumab (Avastin®) designed to inhibit angiogenesis [50], and Cetuximab (Erbix®) for advanced colorectal cancer treatment [51] have been developed and approved by FDA for use as therapeutic antibodies. However, these are large, expensive to manufacture, and there is some degree of variation from batch to batch. Antibodies can potentially induce an immunogenic response. To mitigate such a response, recent developments in the field of antibody engineering have yielded humanized, chimeric, or fragmented antibodies.

Hadjipanayis *et al.* employed an anti-epidermal

growth factor receptor (EGFR) deletion mutant antibody to fabricate iron oxide nanoparticles for targeted imaging and therapeutic treatment of glioblastoma [52]. The EGFR variant III (EGFRvIII) deletion mutant is specifically expressed in malignant glioma cells but not in normal brain tissue. Selective binding to this mutant EGFR protein was achieved by creating a polyclonal rabbit antibody toward the chemically synthesized 14-amino-acid fusion junction sequence (EGFRvIIIAb). Covalent conjugation of the purified rabbit polyclonal EGFRvIIIAb to the amphiphilic triblock copolymer-coated iron oxide nanoparticles [53] yielded a stable glioblastoma-targeting theranostic agent (EGFRvIIIAb-IONPs) (Figure 1A). The EGFRvIIIAb-IONPs were effectively delivered to the intratumoral and peritumoral regions in the brain using convection enhanced delivery (CED), which is a continuous method of injection under a pressure gradient formed by the fluid containing the therapeutic agent [54]. Generally, CED prevents nanoparticles from becoming trapped in the liver, spleen, or circu-

lating macrophages after intravenous administration, and it helps in bypassing the blood-brain barrier (BBB). CED is, therefore, increasingly used to distribute therapeutic agents for the treatment of malignant gliomas [55-57]. Athymic nude mice implanted with a human U87ΔEGFRvIII glioma model underwent CED of EGFRvIII-IONPs to test the accuracy of MRI monitoring and the efficacy of the antitumor effects. The T2-weighted MRI signal at the tumor site decreased after CED of EGFRvIII-IONPs, and the total area in which a signal drop was observed was larger 7 days after CED, showing that the nanoparticles had dispersed. A significant increase in survival was observed in animals that underwent CED with EGFRvIIIAb or EGFRvIIIAb-IONPs as a result of the inhibition of EGFR phosphorylation, whereas CED with the untreated control or IONPs did not result in an increase in the survival rate (Figures 1B-1F). These results indicated that the MRI-guided CED of EGFRvIIIAb-IONPs resulted in specific targeting of the devastating brain tumors.

Wei and Gao *et al.* used a single chain anti-prostate stem cell antigen (PSCA) antibody (scAb_{PSCA}) as a specific 'address tag' for prostate cancer targeted imaging and therapy [58]. Prostate stem cell antigen is a prostate-specific glycosyl phosphatidylinositol-anchored glycoprotein that is marginally expressed in normal prostate and overexpressed in prostate cancer tissues [59]. As shown in Figure 2A, the scAb_{PSCA} was prepared by cleaving intact Ab_{PSCA}

with mercaptoethylamine (MEA), followed by linking to maleimide-PEG-carboxyl (MAL-PEG-COOH) and covalent conjugation to multifunctional polymeric vesicles that had been formed by the entrapping of superparamagnetic iron oxide (SPIO) nanoparticles and docetaxel (Dtxl) by amine-terminated poly(lactic-co-glycolic) acid. The scAb_{PSCA}-Dtxl/SPIO-NPs were 147 nm in size, as determined by dynamic light scattering (DLS), and the amounts of SPIOs and Dtxl in the polymer matrix were 23 wt% and 6.02 wt%, respectively. The high drug encapsulation efficiency was due to partitioning of Dtxl into the oleic acid and oleylamine shell of the SPIOs, which acted as a drug reservoir, thereby exhibiting a triphasic drug release pattern rather than the common two-phase kinetic release pattern, including burst effects of an initial release stage, as observed in vesicles without SPIOs. An *in vitro* cytotoxicity study demonstrated the antiproliferative effects of the multifunctional vesicles toward prostate cancer cells. As indicated in Figures 2B and 2C, PC3 cells incubated with scAb_{PSCA}-Dtxl/SPIO-NPs produced distinct darkened regions in the T2-weighted MRI compared to the polymeric vesicles without scAb_{PSCA} or Endorem® (a commercial contrast, Guerbet, France). This result demonstrated that the scAb_{PSCA}-Dtxl/SPIO-NPs could be used as MRI contrast agents for prostate-targeted imaging and real-time monitoring of therapeutic effects.

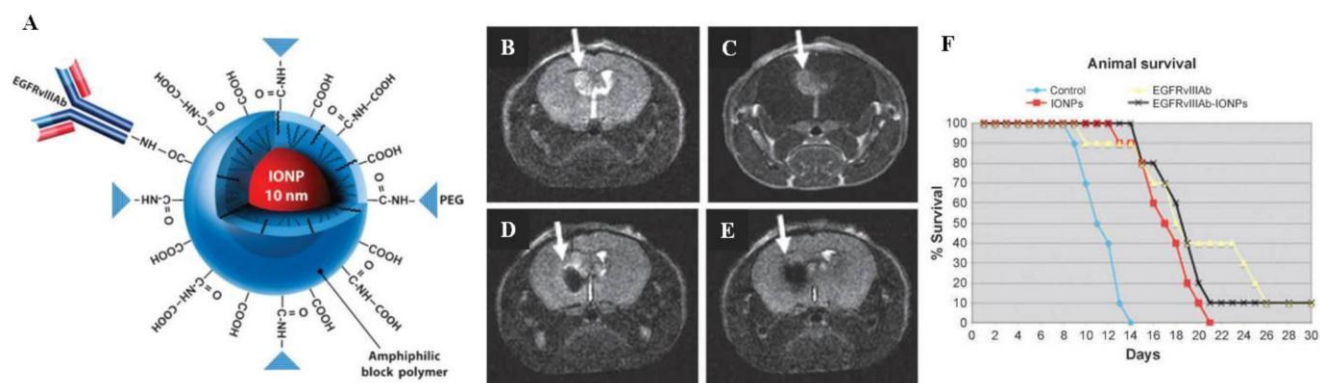


Figure 1. (A) Schematic diagram showing EGFRvIII-IONPs. (B-F) Survival studies of nude mice implanted with the U87ΔEGFRvIII glioma model. (B) T2-weighted MRI showing a tumor region with a bright signal 7 days after tumor implantation (arrow). (C) A tumor is shown (arrow) after injection of a gadolinium contrast agent (Gd-DTPA). (D) The MRI signal decreased (arrow) after CED of EGFRvIIIAb-IONPs. (E) EGFRvIIIAb-IONP dispersion and T2 signal decrease (arrow) 4 days after CED. (F) Survival curve of the nude mice bearing U87ΔEGFRvIII cells after a treatment regimen of MRI-guided CED: the untreated control, IONPs, EGFRvIIIAb, or EGFRvIIIAb-IONPs. Reproduced with permission from ref. [52].

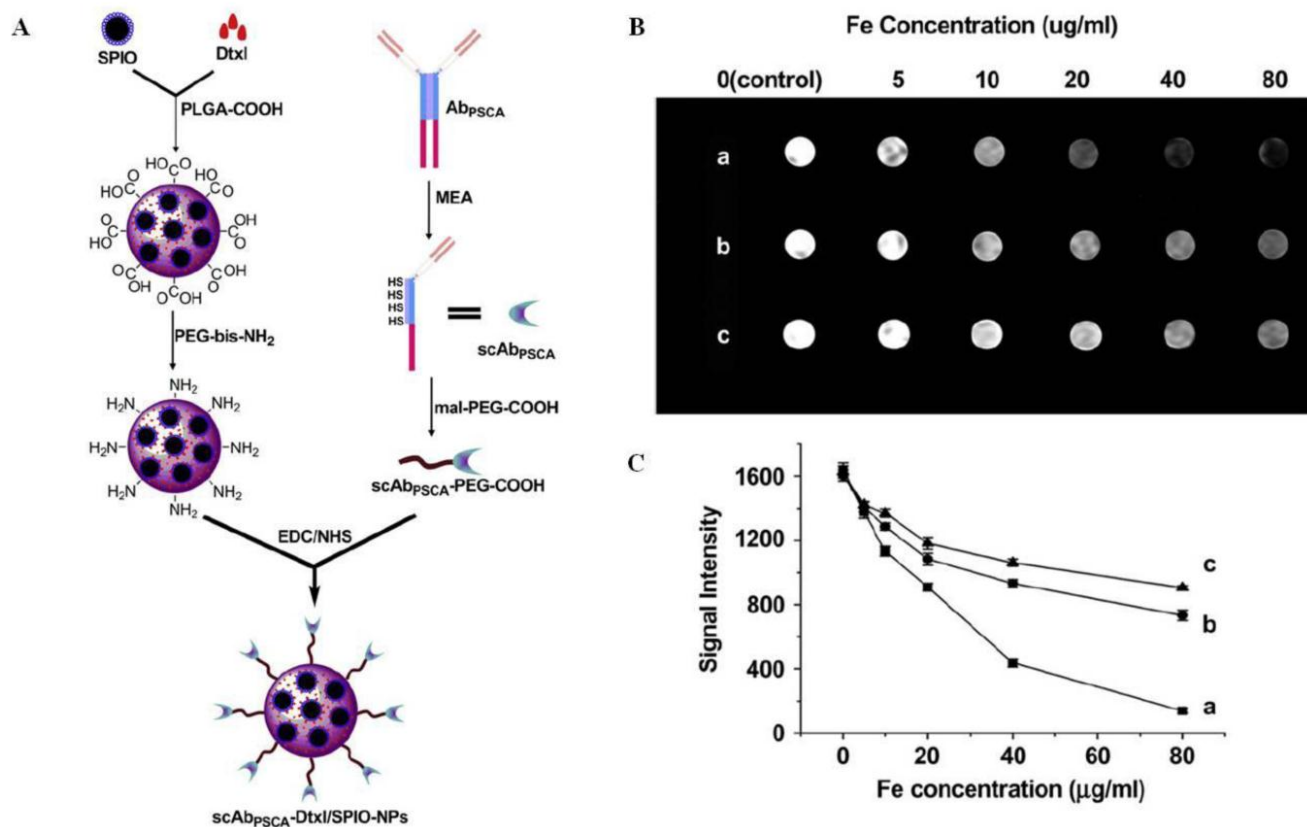


Figure 2. (A) Schematic diagram showing the formulation of $scAb_{PSCA}$ -Dtxl/SPIO-NPs. T2-weighted imaging (B) and the MR signal intensity (C) of PC3 cells (1×10^6) after 2 h incubation with (a) $scAb_{PSCA}$ -Dtxl/SPIO-NPs, (b) PEG-PLGA-Dtxl/SPIO-NPs, or (c) Endorem[®] with 1.5 T MRI scanning. Reproduced with permission from ref. [58].

In a similar manner, Chen and Shuai *et al.* used $scAb$ as a targeting molecule. They designed a CD3 single chain antibody ($scAb_{CD3}$) functionalized nonviral polymeric vector for gene delivery to T cells [60]. This polymeric vector was first complexed with superparamagnetic iron oxide nanoparticles (SPIOs), then was used to condense a therapeutic gene plasmid as a dual-purpose probe (T lymphocyte targeted gene delivery and MRI contrast agent). In mature T cells, engagement of T cell antigen receptors, such as the CD3 receptor, can lead to the initiation of anergy, and such receptors can potentially mediate targeted gene delivery to T cells. Thus, the $scAb_{CD3}$ -conjugated, poly(ethylene glycol)-grafted polyethyleneimine (PEG-g-PEI)-coated SPIOs ($scAb_{CD3}$ -PEG-g-PEI-SPIO) were synthesized by bioconjugation and ligand exchange methods [61]. The targeting polyplexes ($scAb_{CD3}$ -PEG-g-PEI-SPIO/DNA) were then prepared by incorporating a diacylglycerol kinase (DGK α) gene that could impair T cell receptor (TCR) signaling and, consequently, resulted in the anergy of T cells [62,63]. The $scAb_{CD3}$ -immobilized polyplexes were efficiently

taken up by the target T cells (HB8521) via CD3 receptor-mediated endocytosis, as indicated by the T2-weighted MRI. Interestingly, although gene transfection of T cells is generally difficult, quantitative flow cytometric analysis indicated that the gene transfection efficiency of the targeted polyplexes was high (81.95%) compared to the efficiency of polyplexes without $scAb_{CD3}$ functionalization (7.39%). Additionally, after DGK α genes were transferred into HB8521 cells, lower levels of cell proliferation and IL-2 expression were observed in response to immune stimulation in cells transfected with the targeted polyplexes than in cells that hadn't been pre-transfected during stimulation, demonstrating that MRI-visible targeted nanoparticles can dampen TCR-induced diacylglycerol signaling.

Immunoliposomes (antibody-directed liposomes) are common pharmaceutical carriers for targeted drug delivery because of their unique ability to encapsulate both hydrophilic and hydrophobic therapeutic agents and due to their simple preparation. Wu *et al.* developed *in vivo* lung cancer targeted immunoliposomes using an anti-c-Met antibody [64].

The receptor for hepatocyte growth factor (HGF), c-Met, is abundantly expressed in 25% of non-small cell lung cancer patients, and activation of this protein is reported to trigger cancer cell proliferation, migration, and invasion [65, 66]. Wu *et al.* prepared individual targeted therapeutic vehicles and imaging probes. First, an anti-c-Met single chain variable fragment (scFv) antibody was identified by phage display (Ms20, Kd value; 9.14 nM), and cysteine residues were fused for site-direct conjugation with maleimide-modified PEG-terminated liposomal Dox. The resulting Ms20-conjugated liposomal Dox (Ms20-LD) was used as a therapeutic vehicle. Inorganic quantum dots (QD) were also utilized to prepare targeted diagnostic tools (Ms20-QD). Because c-Met expression appeared in angiogenic endothelium as well as in tumor cells [67], the dual targeting properties, including inhibition of tumor growth and prevention of angiogenesis, were observed in an Ms20-LD-injected H460-bearing SCID mouse xenograft model. In addition, Ms20-LD improved chemotherapeutic drug delivery by inhibiting c-Met-transient or c-Met-constitutive activation of cancer cells. An *in vivo* tumor homing study of Ms20-QD supported that Ms20 provided selective delivery to solid tumors and was potentially useful as a lung tumor targeted theranostic agent.

Peptide-based targeting

Peptides are attractive targeting molecules due to their small size, low immunogenicity, and ease of manufacture at small costs [68]. Peptide-based targeting ligands may be identified via several methods. Most commonly, they are obtained from the binding regions of a protein of interest. Phage display techniques can also be used to identify peptide-targeting ligands. In a phage display screen, bacteriophages present a variety of targeting peptide sequences in a phage display library (~10¹¹ different sequences), and target peptides are selected using a binding assay [69]. Cilengitide, a cyclic peptide with integrin binding affinity, is currently in phase II clinical trials for the treatment of non-small cell lung cancer and pancreatic cancer [70]. In 2006, an Adnectin for human VEGF receptor 2 (Angiocept), a 40 amino acid thermostable and protease-stable oligopeptide, entered phase I clinical trials for the treatment of advanced solid tumors and non-Hodgkin's lymphoma. Although peptides can have drawbacks, such as a low target affinity and susceptibility to proteolytic cleavage, these issues may be ameliorated by displaying the peptides multivalently or by synthesizing them using D-amino acids. Recently, peptides have been used to fabricate multifunctional nanoparticles for targeted cancer im-

aging and therapy.

Medarova *et al.* synthesized a breast tumor-targeted nanodrug designed to specifically shuttle siRNA to human breast cancer while simultaneously allowing for the noninvasive monitoring of the siRNA delivery process [71]. The nanodrug consisted of SPIONs for MRI monitoring, Cy5.5 fluorescence dye for near-infrared (IR) optical imaging, and siRNA to target the tumor-specific antiapoptotic gene *BIRC5*. Magnetic iron oxide nanoparticles are extensively used as multimodal imaging probes in combination with optical fluorescence dyes to obtain the benefits of optical imaging, such as rapid screening and high sensitivity. Because tumor-associated underglycosylated mucin-1 (uMUC-1) antigen is overexpressed in >90% of breast cancers and in >50% of all cancers in humans [72], researchers have decorated nanodrugs with uMUC-1-targeting EPPT synthetic peptides for selective tumor targeting. As shown in Figure 3A, amine-functionalized superparamagnetic iron oxide nanoparticles with a cross-linked dextran coating (MN) have been prepared, and a Cy5.5 dye was conjugated to the surface of nanoparticles to produce MN-Cy5.5. Subsequently, thiol-modified, FITC-labeled EPPT peptides and siRNA were coupled to MN-Cy5.5 via a heterofunctional cross-linker, *N*-succinimidyl 3-(2-pyridyldithio) propionate (SPDP). The resulting therapeutic and diagnostic nanodrug (MN-EPPT-siBIRC5) exhibited superparamagnetic and fluorescence properties. After intravenous injection of the nanodrugs into mice with BT-20 breast tumors, the tumors were clearly imaged, as verified simultaneously by T2 MRI and near-IR optical imaging (Figure 3B). Systemic administration of the nanodrug once a week over 2 weeks induced considerable levels of necrosis and apoptosis in the tumors as a result of the siBIRC5-mediated inhibition of the antiapoptotic survivin protooncogene, translating into a significant decrease in tumor growth rate (Figure 3C). This tumor-targeted, imaging-capable nanodrug highlights the potential of MRI-guided tumor treatment, which can be used to quantify changes in the tumor volume over the treatment schedule as well as to guide selection of an optimal treatment time course.

Treatment of malignant brain tumors is one of the most formidable challenges in oncology due to the difficulties associated with drug delivery across the BBB to the tumor. Zhang *et al.* developed an *in vivo* brain tumor targeting magnetic/optical nanoprobe capable of selectively accumulating in brain tumors across the BBB via chlorotoxin (CTX) [73]. CTX is a 36-amino acid peptide that functions well as a tumor-targeting ligand due to its permeation across an

intact BBB as well as its strong affinity for tumors of neuroectodermal origin [74]. The nanoprobe comprised an iron oxide nanoparticle coated with a PEGylated chitosan-branched copolymer (NPCP) that included exposed amine groups, to which *N*-succinimidyl-*S*-acetylthioacetate (SATA)-functionalized CTX and the near-IR dye Cy5.5 were conjugated via iodoacetate and amide linkages, respectively (Figure 4A). *In vivo* MRI contrast enhancement and optical imaging were then evaluated in a transgenic mouse model, ND2:SmoA1 that closely resembles human medulloblastoma [75], which arises spontaneously in the cerebellum [76] and maintains an intact BBB [77]. After administration of the targeted NPCP-CTX via tail vein injection, a significant increase in the MRI-derived R2 values (s^{-1}) was observed at the periphery of the cerebellum (tu-

mor-containing tissue) in ND2:SmoA1 mice, whereas images of the frontal lobe region (healthy tissue) of these mice or nontargeting NPCP injected mice did not show apparent R2 shifts between pre-injection and post-injection (Figure 4B). Additionally, wild-type mice (bearing no tumors) injected with these nanoprobe showed no considerable accumulation in the brain (Figure 4C), implying the specific accumulation of nanoprobe in the tumor after crossing the BBB with minimal accumulation in normal tissues. Near-IR optical imaging also confirmed the preferential accumulation of NPCP-Cy5.5-CTX only in brain tumor regions at both 2 h and 120 h post-injection (Figure 4D and 4E). This nanoprobe platform may be tailored and further developed toward brain tumor targeted therapeutic nanoparticle systems.

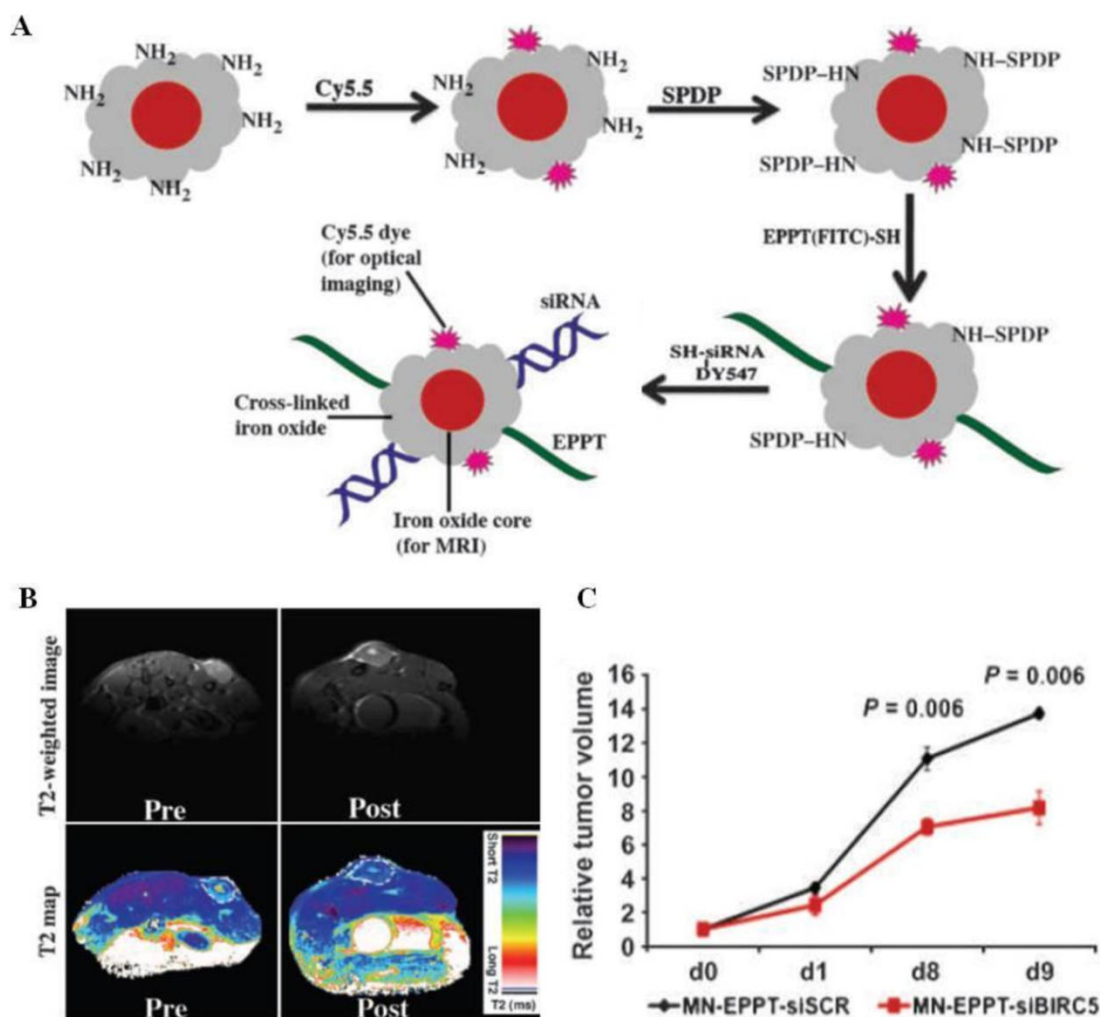


Figure 3. (A) Schematic diagram showing the synthesis of MN-EPPT-siBIRC5. (B) Representative pre-contrast images and 24 h post-contrast T2-weighted images (top), and color-coded T2 maps (bottom) of the tumor-bearing mice intravenously injected with MN-EPPT-siBIRC5 (10 mg/kg Fe). (C) Relative tumor volume measurements of MN-EPPT-siBIRC5- and MN-EPPT-siSCR-injected animals over the course of treatment. Reproduced with permission from ref. [71].

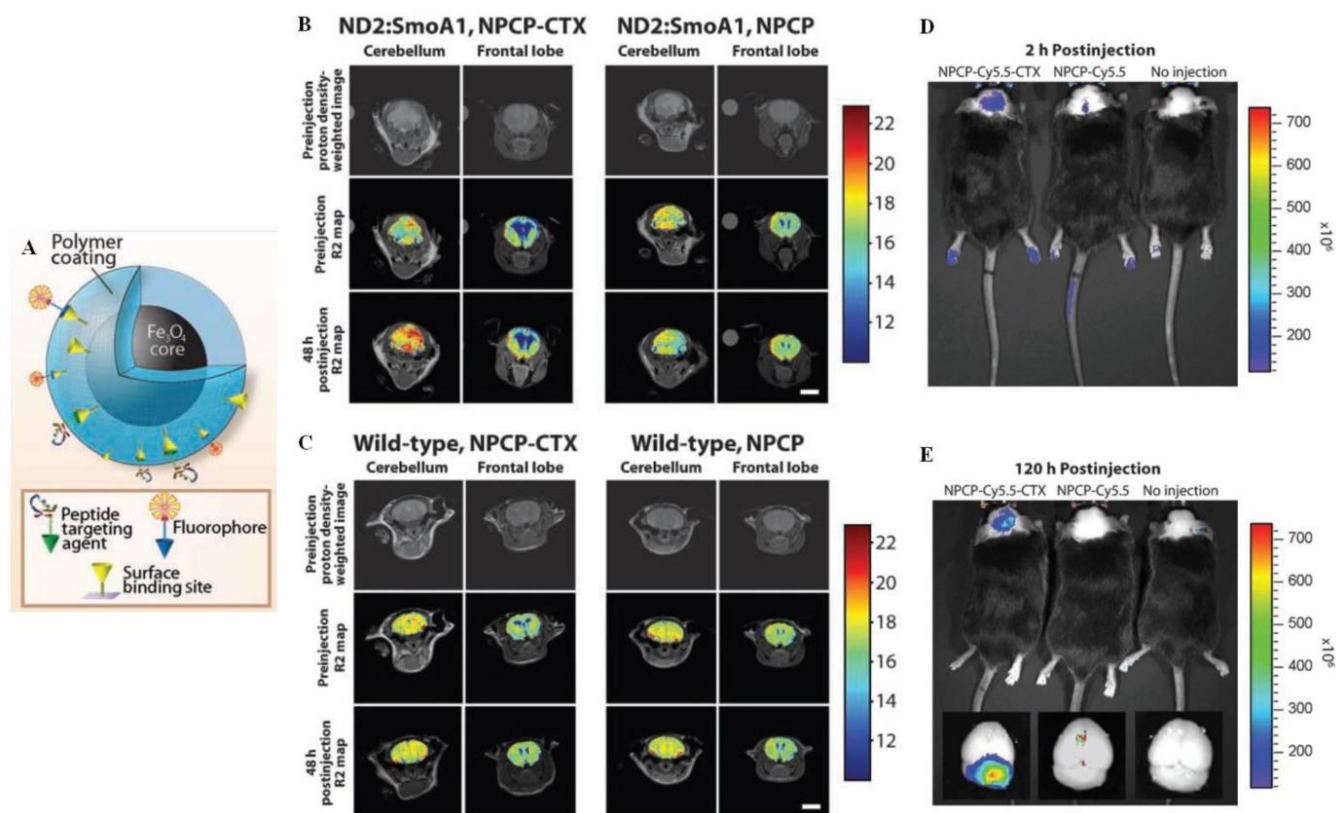


Figure 4. (A) Schematic diagram of the NPCP-Cy5.5-CTX nanoprobe. *In vivo* MR images of ND2:SmoA1 (B) and wild-type mice (C) acquired before and 48 h after administration of either NPCP-CTX or the NPCP nanoprobe. Colorized R2 maps of the brain region were superimposed onto the proton density-weighted images. (D-E) *In vivo* near-IR fluorescence images of autochthonous medulloblastoma tumors in ND2:SmoA1 mice injected with NPCP-Cy5.5-CTX or NPCP-Cy5.5, alongside those receiving no injection: 2 h post-injection (D) and 120 h post-injection (E). *Ex vivo* fluorescence images of mice brains from the same mice following necropsy (inset). The spectral gradient bar corresponds to the fluorescence intensity ($p/s/cm^2/sr$) in the images. Reproduced with permission from ref. [73].

An acidic extracellular tumor microenvironment (pH 5.8–7.1) provides another strategy for increasing tumor selectivity. A hypoxic metabolic state creates acidic conditions around a tumor, which can provide a triggering signal for the cancer-targeted drug delivery of nanoparticles [78–80]. Using this strategy, Zhang *et al.* designed a glioma targeting pH-sensitive siRNA nanovector using CTX [81]. The nanovector was composed of an iron oxide magnetic nanoparticle core coated with three different types of functional molecule: the primary amine group-blocked polyethyleneimine (PEI) as a pH-sensitive coating layer, siRNA as a therapeutic payload, and CTX as a tumor targeting ligand. As an amine blocker of PEI, citraconic anhydride (2-methylmaleic anhydride) reacted with the primary amine group of PEI to provide a terminal carboxylate, which could be hydrolyzed only under acidic conditions. This reversible charge conversion from positive to negative under acidic conditions in a pH-sensitive manner may reduce the cyto-

toxicity of PEI and minimize nonspecific cellular uptake at physiological pH conditions [78,82]. To synthesize the nanovector, amine-functionalized iron oxide nanoparticles (NPs) were prepared by coating with amine-terminated PEG. The primary amine groups on the NPs were reacted with Traut's reagent to provide thiol-modified NPs. The amine groups in PEI that remained after the citraconylation reaction were then activated with SPDP for conjugation onto the NPs. The resultant pH-sensitive PEI-coated NPs exhibited negligible cytotoxicity at pH 7.4 as a result of the surface-exposed carboxylates on NPs, however, the surface charge on the NPs increased under acidic conditions due to both deblocking of the primary amine groups and protonation of amine groups remaining in the PEI, thereby triggering cytotoxicity. The group tested the targeted delivery and therapeutic properties of NPs by additional conjugation with thiol-modified CTX and siRNA via succinimidyl ester-PEG-maleimide (NHS-PEG-MAL) linkages. *In*

in vitro MRI scans of C6 cells incubated in the presence of the NP-PEI-siRNA-CTX exhibited intracellular uptake that was higher than that observed for NP-PEI-siRNA, suggesting that the presence of CTX on the NP surfaces facilitated cellular internalization of the nanovectors. Gene silencing effects indicated CTX-mediated selectivity. The extent of GFP gene expression by cells incubated with NP-PEI-siRNA-CTX at pH 6.2 was significantly reduced, whereas GFP gene expression was almost unchanged in cells treated with the same nanovector at pH 7.4. These results suggested that the nanovector system has a good safety profile and may potentially be used as a brain tumor targeted theranostic agent.

Integrin $\alpha\beta 3$ is an ideal vascular target receptor because it is highly expressed on angiogenic endothelium, and expression of this receptor on tumor vessels correlates with disease progression [83]. The targeting of molecular imaging agents or therapeutic delivery agents to integrin $\alpha\beta 3$ provides an attractive strategy for the treatment of cancer. Cheresh *et al.* used an arginine-glycine-aspartic acid (RGD) peptide sequence, an effective targeting molecule for integrin $\alpha\beta 3$, to fabricate liposomal Dox for treating metastatic disease [84]. RGD-immobilized liposomes were synthesized from distearoylphosphatidylcholine (DSPC), chole-

sterol, dioleoylphosphatidylethanolamine (DOPE), distearoylphosphatidylethanolamine (DSPE)-mPEG2000, and DSPE-cyclic RGDfK via dehydration/rehydration and sonication. Dox was added to the liposomes at 55°C to provide RGD-Dox-NPs (Figure 5A). Mice containing s.c. Matrigel plugs loaded with basic fibroblast growth factor (bFGF) were injected intravenously with the RGD-Dox-NPs (targeted) or RAD-Dox-NPs (nontargeted). After 7 days, animals treated with RGD-Dox-NPs displayed vascular pruning compared with the normal vascular structure of PBS-treated animals, whereas RAD-Dox-NPs showed only a marginal reduction in neovascularization relative to the control animals (Figure 5B), demonstrating strong antiangiogenic effects of the integrin $\alpha\beta 3$ -targeted nanoparticles. Furthermore, RGD-Dox-NPs produced a modest reduction of the primary tumor growth (23%) and a significant reduction of metastasis (82%) in an orthotopic pancreatic tumor model that included metastatic lesions in the hepatic hilar lymph node (Figure 5C). On the other hand, RAD-Dox-NPs or free Dox did not provide apoptotic effects. These results suggest that integrin-targeted nanoparticles influenced the invasive behavior of the primary tumor and its ability to metastasize.

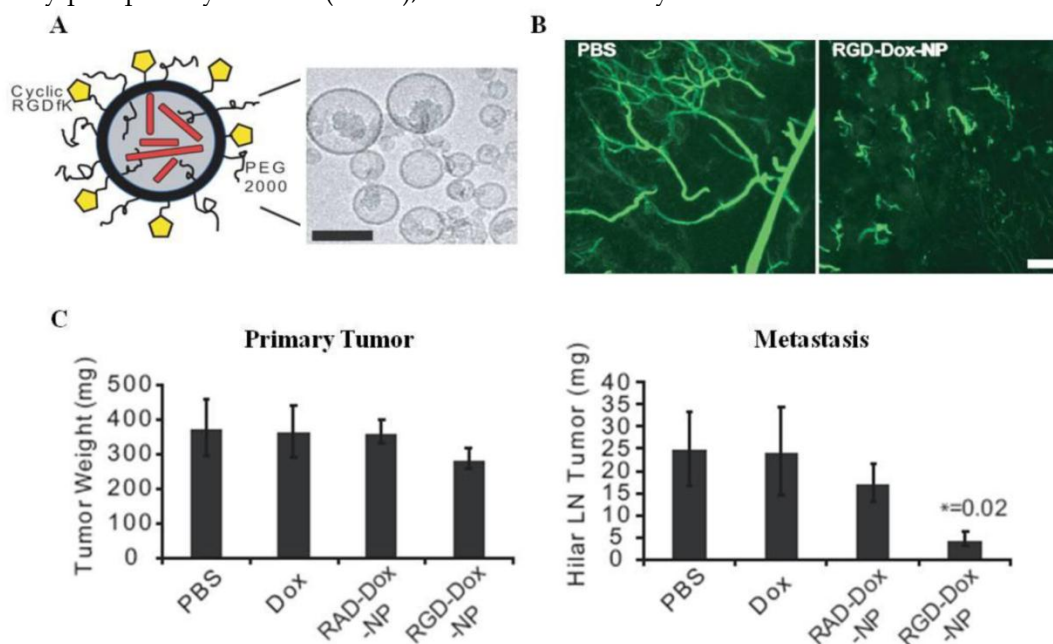


Figure 5. (A) Schematic representation and TEM image of RGD-Dox-NP (scale bar indicates 100 nm). (B) Vascular disruption in the mouse Matrigel model with intravenous injection of PBS or $\alpha\beta 3$ -targeted RGD-Dox-NPs on days 1, 3, and 5. After treatment, mice were intravenously injected with fluorescein-labeled *G. simplicifolia* lectin, and the plugs were removed and imaged by scanning confocal microscopy. (C) Suppression of metastasis in an orthotopic model of pancreatic cancer. After surgical implantation of the cells, mice were treated on days 5, 7, and 9 with RGD-Dox-NPs, RAD-Dox-NPs, free Dox, or PBS (each with 1 mg/kg total Dox per dose). On day 11, the primary tumor and the hepatic hilar lymph node were resected and weighed. Reproduced with permission from ref. [84].

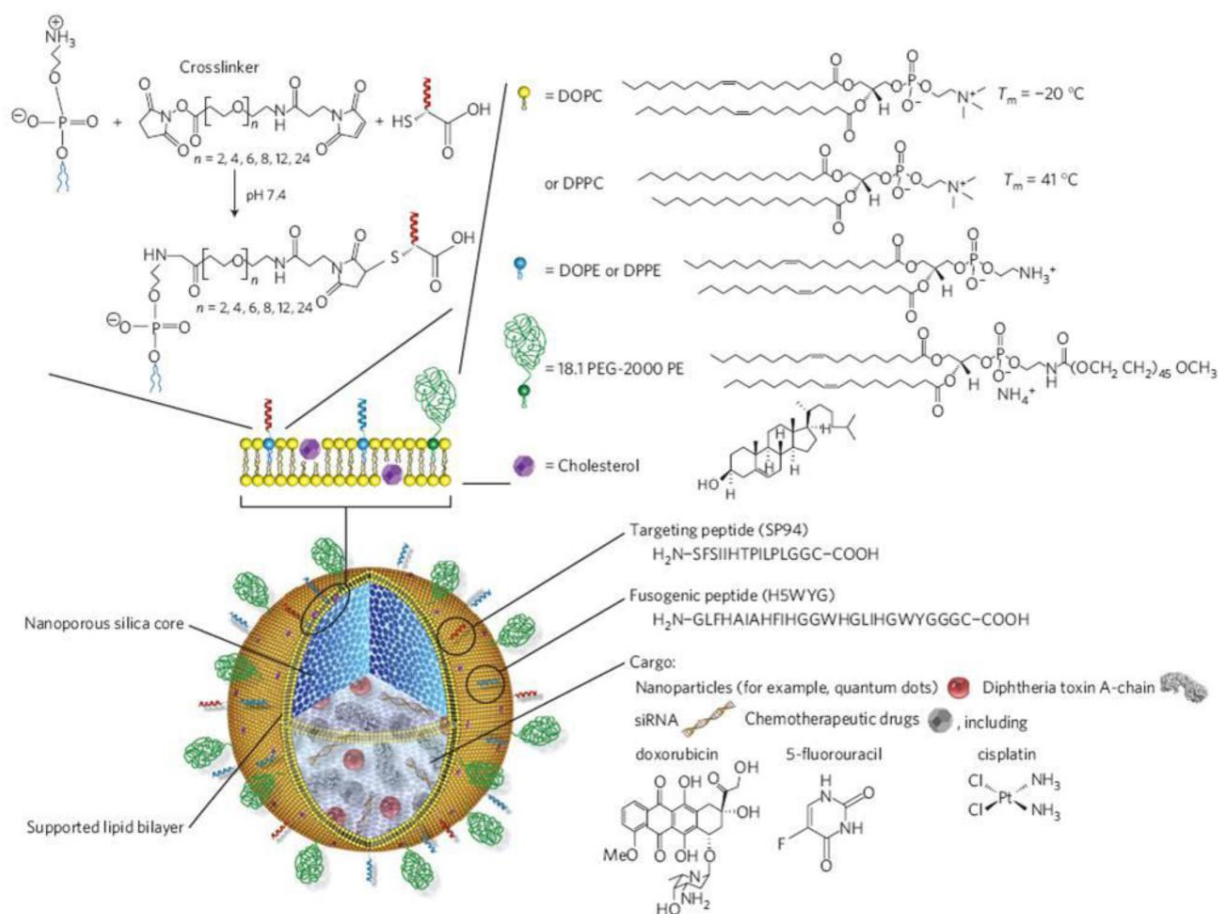


Figure 6. Schematic illustration of the silica nanoporous particle-supported lipid bilayer, depicting the disparate types of therapeutic and diagnostic agents that can be loaded within the nanoporous silica core, as well as the ligands that can be displayed on the surface of the nanoparticle. Reproduced with permission from ref. [86].

Lee *et al.* decorated liposomal Dox with a lung tumor targeted peptide [85]. Lung cancer is the leading cause of death due to cancer, and its high mortality rate appears to derive from a low therapeutic index for chemotherapy and late detection due to a lack of sensitive diagnostic biomarkers [2]. The identification of novel biomarkers for early lung cancer detection remains a challenge. In this study, a novel peptide (CSNIDARAC) with a high binding affinity for lung tumors was identified by *in vitro* screening of a phage display peptide library, and CSNIDARAC peptide-conjugated liposomal Dox (Lipo-Dox) was synthesized. The *in vivo* tumor targeting capabilities and the therapeutic efficacy were evaluated in the H460 tumor xenograft mice. To minimize the interactions between the targeted peptide and the surface of the liposome, the amount of PEG on the surface of the liposome was reduced from 5–20 mol% (general use) to 1.3 mol% of total lipids. Tumor growth inhibition of the peptide-targeted Lipo-Dox was superior to that of the untargeted Lipo-Dox or free Dox administered at

an equivalent dose, and this result was consistent with the levels of apoptosis measured by TUNEL staining. Near-IR Cy7.5 dye-labeled peptide-conjugated Lipo-Dox also showed a distinct fluorescence signal at the tumor, whereas untargeted Lipo-Dox did not show such a strong signal intensity, suggesting the potential utility of this lung tumor-targeting peptide as a diagnostic agent.

Nanoporous silica offers a higher surface area and binding capacity for therapeutic and diagnostic agents compared to similarly sized liposomes, and, therefore, provides an attractive drug delivery system. Multicomponent cargos are easily loaded onto nanoporous silica cores, and the resultant nanocarriers can potentially be used for targeted multicomponent delivery. Ashley *et al.* developed porous silica nanoparticle-supported lipid bilayers (protocells, 100–150 nm in diameter) that synergistically combined the features of mesoporous silica particles and liposomes to address the multiple challenges of targeted delivery (Figure 6) [86]. Protocells were modi-

fied with an SP94-targeted peptide that binds to human hepatocellular carcinoma and a histidine-rich fusogenic peptide that promotes endosomal escape of the protocells and cytosolic dispersion of the encapsulated cargos. The nanoporous support resulted in greater stability and enhanced lateral bilayer fluidity compared with both liposomes and non-porous particles, thereby promoting multivalent interactions between the protocell and the target cancer cell using a minimal number of targeting peptides via peptide recruitment to the cell surface. The high surface area and porosity of their nanoporous cores conveyed a one-thousand-fold higher capacity of the protocells for Dox than the similarly sized liposomes. The unique properties of protocells solve the problem of simultaneously achieving high targeting specificity, high cytotoxicity toward the target cell, and low collateral damage to non-cancerous cells. Cell viability tests indicated that Dox-loaded protocell treatment maintained greater than 90% normal hepatocyte viability while killing nearly 97% MDR1+ hepatocellular carcinoma (Hep3B). In contrast, Dox-loaded liposomes or protocells without fluidity on their surface were less efficient at killing Hep3B and caused considerable cytotoxicity to non-cancerous cells. The Dox-loaded protocells demonstrated good therapeutic ability compared to both free Dox and Dox-loaded liposomes.

Ruoslahti *et al.* described self-amplifying tumor homing nanoparticles [87]. The system was based on a CREKA peptide that not only recognizes clotted plasma proteins around tumor vessel walls or tumor stroma but also induces localized tumor clotting [88-90]. Fluorescein-labeled peptides, including the sulfhydryl group of the single cysteine residue, were coupled to amino dextran-coated iron oxide nanoparticles (CREKA-SPIO), and nanoparticles with at least 8,000 peptide molecules per particle were used for *in vivo* experiments. To reduce reticuloendothelial system (RES) uptake, a major obstacle to the homing of the nanoparticles, chelated Ni²⁺-liposome or liposomes as potential decoy particles were introduced prior to CREKA-SPIO injection. CREKA-SPIO treatment after pretreatment with the decoy particles displayed primary localization in the tumor vessels, and fewer particles were seen in the liver. The tumor-targeted nanoparticles were distributed along a meshwork in the clots, presumably formed by fibrin, suggesting that the nanoparticles infiltrated the

depths of the clots. The tumor magnetization was quantitatively analyzed using a superconducting quantum interference device (SQUID), revealing that heparin injection prior to injection of CREKA-SPIO reduced the tumor accumulation of nanoparticles by >50% by eliminating intravascular clotting, although the treatment series did not considerably reduce the number of vessels. Thus, binding of CREKA-SPIO to tumor vessels did not require clotting activity, but intravascular clotting attracted more nanoparticles to the tumor, suggesting that tumor targeting was amplified.

A disease-targeting multifunctional integrated nanosystem can be constructed by combining two different functional nanoparticles that communicate with one another to amplify tumor targeting *in vivo*. Bhatia *et al.* designed communicating nanosystems using 'signaling' modules (gold nanorods, NRs, or tumor-targeted tissue factor, tTF) as selective tumor-activating agents and 'receiving' nanoparticles (magnetofluorescent iron oxide nanoworms, NWs, or Dox-loaded liposomes, LPs) as targeted imaging or therapeutic agents (Figure 7A) [91]. NWs, which were previously developed by Bhatia *et al.*, are elongated nanostructures formed by the assembly of iron oxide cores that exhibit strong magnetic properties and efficient tumor targeting [92]. As shown in Figure 7B, two 'signaling' modules specifically activated the coagulation cascade in tumors to broadcast the tumor's location to receivers in circulation. The NRs passively targeted tumors and converted external electromagnetic energy into heat to locally disrupt tumor vessels. tTF, which included the RGD peptide motif, induced coagulation upon binding to the angiogenic $\alpha v \beta 3$ receptors. The receiving nanoparticles targeted regions of coagulation. NWs and LPs were derivatized with a peptide substrate for the coagulation transglutaminase FXIII or a fibrin-binding peptide. After injecting the signaling modules into MDA-MB-435 bearing mice, at 45°C, the 'receiving' NWs or LPs indicated prominent extravascular accumulation around the tumor and amplified the therapeutic outcome (Figures 7C and 7D, respectively), demonstrating a heat-dependent increase in the passive accumulation and specific biochemical recognition of the coagulation process. Communication through the coagulation cascade improved the accumulation of the receiving modules in tumors by a factor of 40 relative to the receiving modules without communication.

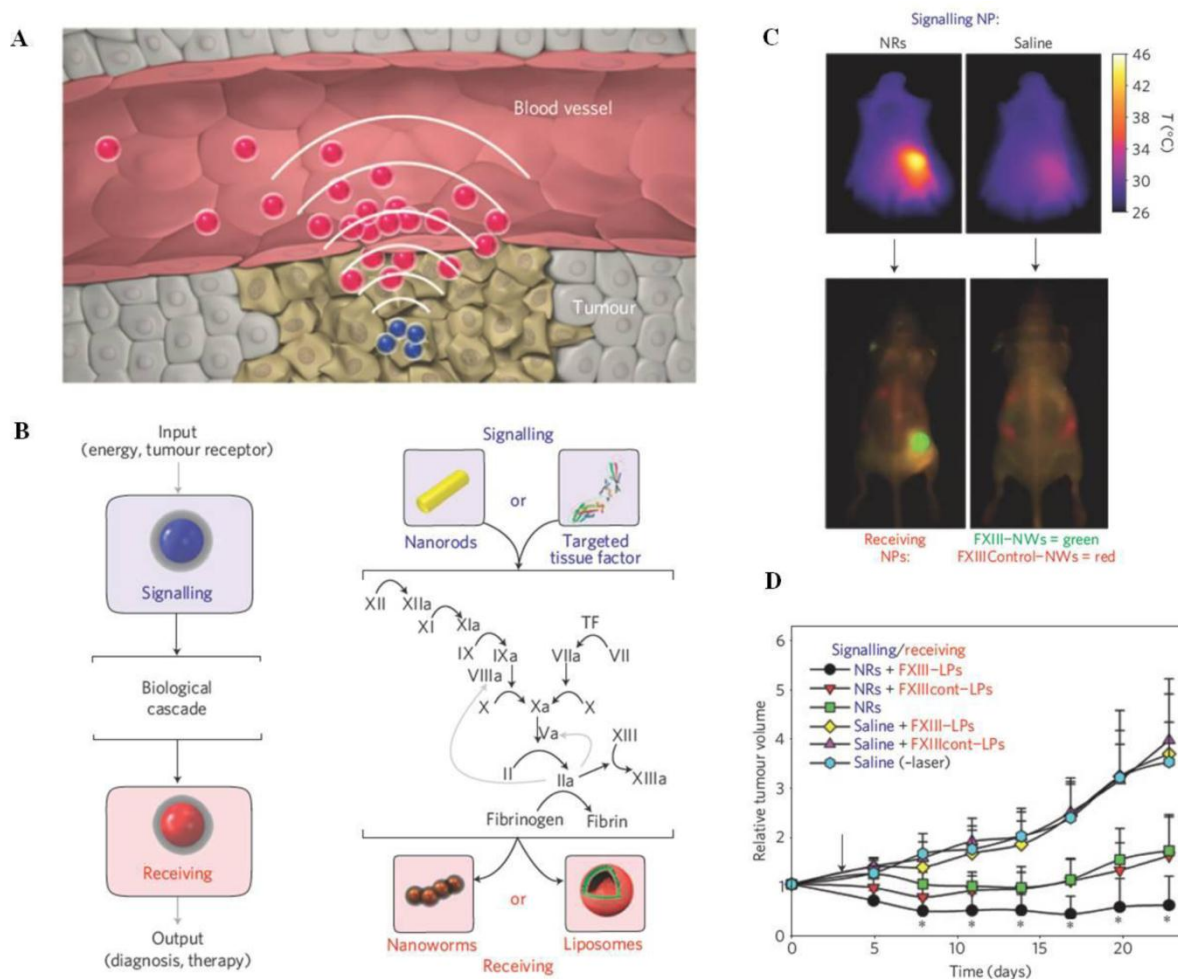


Figure 7. (A) Schematic representation of nanoparticle communication to achieve amplified tumor targeting. Tumor-targeted signaling nanoparticles (blue) broadcast the tumor location to the receiving nanoparticles (red) present in circulation. (B) Shown are the harnessing of the biological cascade to transmit and amplify nanoparticle communication and the molecular signaling pathway between the signaling and receiving components. (C) Thermographic images of the photothermal NRs with heating. Seventy-two hours after NR or saline injection, mice were co-injected with FXIII-NWs and untargeted control-NWs, and their right flanks were broadly irradiated (top). Twenty-four hours post-irradiation, whole-animal fluorescence imaging revealed the distribution of the receiving nanoparticles (bottom). (D) Amplified tumor therapy with communicating nanoparticles. Tumor volumes following a single treatment with the communicating nanoparticle systems and controls. Reproduced with permission from ref. [91].

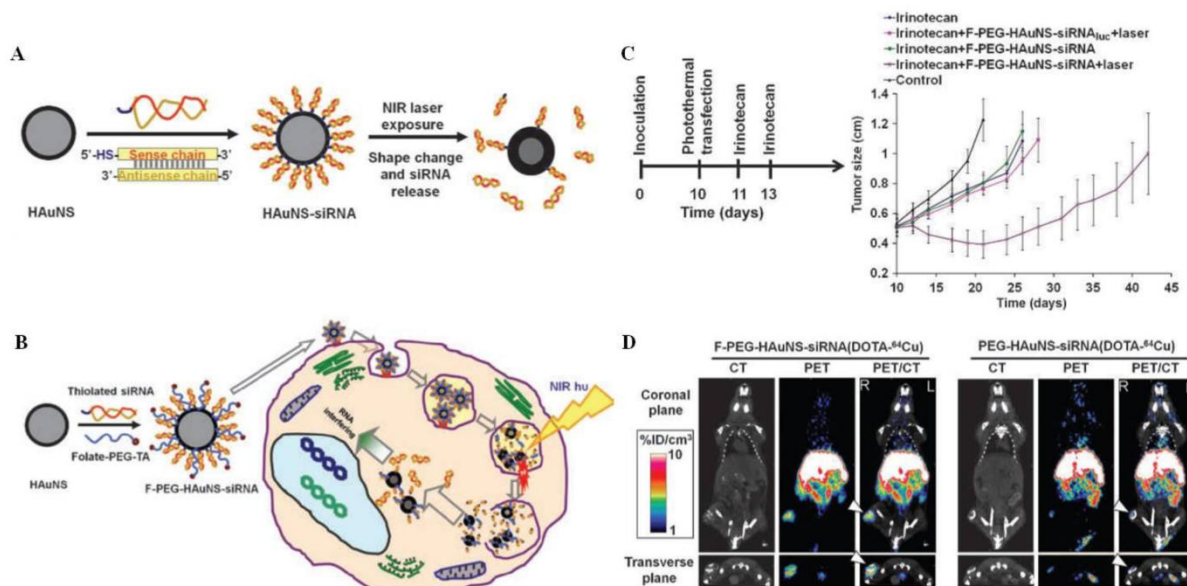


Figure 8. (A) Schematic diagram showing bioconjugation of HAuNS-siRNA and photothermal-induced siRNA release. (B) Schematic diagram showing the synthesis of F-PEG-HAuNS-siRNA and the proposed intracellular events following near-IR irradiation. (C) Effect of p53 siRNA photothermal transfection combined with irinotecan delivered to nude mice bearing HeLa cancer xenografts. (D) Micro-PET/CT imaging of nude mice bearing HeLa cervical cancer xenografts in right rear leg 6 h after intravenous injection of F-PEG-HAuNS-siRNA(DOTA-⁶⁴Cu) or PEG-HAuNS-siRNA(DOTA-⁶⁴Cu). Arrowheads indicate the tumors. Reproduced with permission from ref. [98].

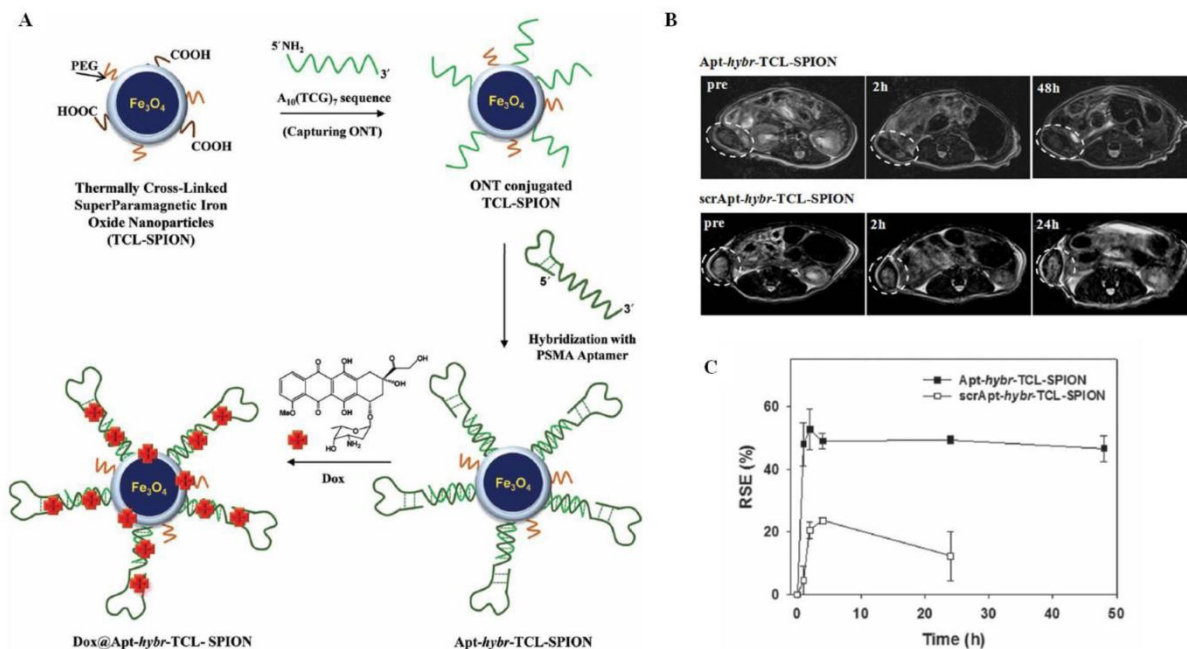


Figure 9. (A) Schematic diagram showing the preparation of Apt-hybr-TCL-SPIONs and Dox@Apt-hybr-TCL-SPIONs. (B) T2-weighted fast spin echo images at the level of the LNCaP tumor on the right side of the mouse taken 0, 2, 24, and 48 h after injection of Apt-hybr-TCL-SPIONs or scrApt-hybr-TCL-SPIONs. The dashed circle indicates the xenograft tumor region. (C) The RSE (%) in the tumor areas of the Apt-hybr-TCL-SPION- and scrApt-hybr-TCL-SPION-treated mice were recorded from the T2-weighted images as a function of time. Reproduced with permission from ref. [123].

Small molecule-based targeting

Small molecules with infinitely diverse structures and properties are inexpensive to produce and have great potential as a class of targeting moieties. One of the most widely studied small molecules as a targeting moiety for the delivery of agents is folic acid (folate). Folate is a water-soluble vitamin B6 and is essential in humans for rapid cell division and growth, especially during embryonic development [69]. In cancers, folate receptors are overexpressed on tumor cells, so folate, which has a high binding affinity for the folate receptor ($K_d = 10^{-9}$ M) enables the targeted delivery of imaging and therapeutic agents to tumors. ^{111}In -DTPA-folate, $^{99\text{m}}\text{Tc}$ -folate conjugate (EC20), folate-linked fluorescent hepten (EC17), and diacetylvinylblastine hydrazide-folate conjugate (EC145) are currently being tested in clinical trials as cancer imaging agents and therapeutics. Folate has been combined with drug delivery vehicles or inorganic nanoparticles to produce targeted delivery of theranostic agents. Carbohydrates form another class of small molecule targeting ligands that selectively recognize cell surface receptors, such as lectin [93]. The asialoglycoprotein receptor (ASGP-R) is present only on hepatocytes at a high density of 500,000 receptors per cell [94,95], and it readily binds carbohydrates, such as galactose, mannose, arabinose, which can thereby serve as effective liver-targeted drug delivery systems *in vivo* [96,97].

Li *et al.* designed folate receptor-targeted hollow gold nanospheres carrying siRNA recognizing NF- κ B, a transcription factor related to the expression of genes involved in tumor development [98,99]. In this case, the photothermal effects of gold nanospheres were utilized to regulate drug release and as a therapeutic tool. Core/shell-structured hollow gold nanospheres (HAuNS, 40 nm) were initially synthesized, consisting of a thin gold wall with a hollow interior, and the structures displayed strong surface plasmon resonance (SPR) tunability in the near-IR region [100-103]. Thiol-modified siRNA duplexes directed toward the NF- κ B p65 subunit were then introduced to the surface of HAuNS. Folates were coupled to the nanoparticles through a thioctic acid-terminated PEG linker to produce F-PEG-HAuNS-siRNA (Figure 8A and 8B). Irradiation with a pulsed near-IR laser (800 nm) altered the absorption spectra of the HAuNS-siRNA solutions significantly, indicating a loss in the structural integrity and triggering the dissociation of siRNA from HAuNS, when demonstrated by TEM and fluorescence microscopy images. This mode of action is termed 'photothermal transfection'. Intravenous injection of the nanospheres into HeLa

xenografts resulted in the distinct downregulation of the NF- κ B p65 subunit only for the folate-conjugated nanosphere treatment combined with near-IR laser irradiation, suggesting that selective targeting and endolysosomal escape of the nanoparticles was activated by near-IR irradiation at the tumor site. *In vivo* tests, in which therapy was combined with administration of irinotecan, a chemotherapeutic agent that increases sensitivity to NF- κ B inhibition, yielded a substantially enhanced apoptotic response (Figure 8C). *In vivo* micro-positron emission tomography (PET)/computed tomography (CT) imaging also confirmed the folate-mediated tumor-targeted theranostic properties of the nanostructures (Figure 8D). Although significant uptake of the nanoparticles was observed in the liver, spleen, kidney, and lung, no significant downregulation of p65 in these organs was observed as a result of the tumor-selective near-IR irradiation.

Riboflavin is an essential vitamin for cellular metabolism, and the riboflavin carrier protein (RCP) is highly upregulated in metabolically active cells [104,105]. Thus, flavin mononucleotide (FMN), an endogenous RCP ligand, was used as a small molecule targeting ligand for metabolically active cancer or endothelial cells. Kiessling and co-workers synthesized FMN-coated ultrasmall superparamagnetic iron oxide nanoparticles (FLUSPIO) as MRI/optical dual probes for cancer detection [106]. USPIO was coated with FMN through the phosphate groups of FMN, and guanosine monophosphate was added to stabilize the colloid. The hydrodynamic radius of FLUSPIO was 97 ± 3 nm, and an intense fluorescence emission band was observed at 530 nm due to FMN. *In vitro* cellular uptake of FLUSPIO was investigated by MRI (3T), TEM, and fluorescence microscopy of PC3 cells and HUVEC cells. Both PC3 cells and HUVEC cells showed a significantly higher R2 relaxation rate after 1 h incubation with FLUSPIO than with nontargeted USPIO. Such an uptake was considerably reduced by competitive blocking of RCP with free FMN. A strong green fluorescence in the cells was observed after FLUSPIO incubation. The perinuclear fluorescence signal suggested endosomal localization of the nanoparticles, consistent with TEM results, suggesting that FMN could serve as a versatile building block for generating tumor-targeted imaging and therapeutic modalities.

Jeong *et al.* demonstrated the use of galactose-conjugated SPIONs as a hepatocyte-targeted dual contrast agent (nuclear imaging/ MRI) in a mouse model [107]. Generally, SPIONs are nonspecifically phagocytosed or endocytosed by RES in the liver, spleen, lymph, and bone marrow after i.v. injection.

Therefore, hepatocyte-selective imaging was needed for the evaluation of hepatocytic function under certain clinical conditions, such as partial liver transplant or hepatitis, as well as for monitoring the disease progress. This research group synthesized lactobionic acid- (LBA) with a high affinity for ASGP-R, and immobilized the LBA onto SPIONs via amide linkages between the dopamine-modified SPIONs bearing a primary amine group and the lactobionic acid using 1-ethyl-3-(3-(dimethylamino)-propyl) carbodiimide/*N*-hydroxysuccinimide (EDC/NHS) chemistry. To radiolabel nanoparticles with ^{99m}Tc , diethylene triamine pentaacetic acid (DTPA) was then conjugated to the remaining amine groups of dopamine-SPIONs. After tail vein injection, *in vivo* micro-single photon emission computed tomography (SPECT)/CT images and T2-weighted MR images indicated that the ^{99m}Tc -LBA-SPION mainly accumulated in the liver within a few minutes. A competition study involving blocking of the ASGP-R with free galactose showed a large decrease in the liver uptake, suggesting ASGP-R-mediated uptake of ^{99m}Tc -LBA-SPIONs. TEM analysis confirmed that the LBA-SPIONs were located in the mitochondrial matrix as well as in the cytoplasm, indicating ASGP-R-mediated internalization of the nanoparticles into hepatocytes.

Aptamer-based targeting

Aptamers are small nucleic acid ligands (15–40 bases) that bind to targets with high specificity due to the ability of the molecules to fold into unique conformations with three-dimensional structures [108]. Aptamers are identified via a selection processes similar to phage display, involving the systematic evolution of ligands by exponential enrichment (SELEX) [109]. From libraries of 10^{15} random oligonucleotides, aptamers displaying high affinity and specificity for a target can be selected. This targeting moiety has potential advantage over antibodies, such as the small in size (15 kDa), low immunogenicity, and easy scale-up preparation without batch-to-batch variations. To date, more than 200 aptamers have been isolated [110,111]. Pegaptanib, a VEGF₁₆₅ targeted aptamer, was approved by the FDA in 2004 for the treatment of neovascular macular degeneration. AS1411, a nucleolin targeted aptamer, is in phase II of clinical development [112–114]. However, aptamers possess several deleterious properties, such as rapid blood clearance, largely due to nuclease degradation. To overcome this difficulty, pyrimidine modifications at the 2'-fluorine position or chemical modifications with PEG have been used to enhance the bioavailability and pharmacokinetic properties [115]. The best-characterized aptamers for targeted delivery are

2'-fluoro-pyridine-RNA aptamers generated against the extracellular domain of prostate-specific membrane antigen (PSMA) [116]. These aptamers have been used to deliver Dox [117], self-assembled polymeric nanoparticles [118–120], and QDs [121]. Recently, the PSMA aptamer-siRNA chimera system, extended at the 3' end to contain a complementary nucleotide sequence directed toward the antisense strand of the siRNA, was generated [122].

Jon *et al.* designed a CG-rich duplex containing a PSMA aptamer conjugated iron oxide nanoparticles as a prostate cancer-specific nanotheranostic agent [123]. As shown in Figure 9A, simultaneous prostate tumor detection and therapy were achieved *in vivo* by conjugating the (CGA)₇-elongated PSMA aptamers to complementary oligonucleotides (ONTs) (5'-(TCG)₇-3') immobilized thermally cross-linked iron oxide nanoparticles (TCL-SPIONs). The resulting CG-rich duplex aptamer-hybridized TCL-SPIONs enabled loading of multiple Dox molecules onto the nanoparticles (Dox@Apt-*hybr*-TCL-SPIONs). The size of the targeted nanoparticles was 65 ± 12 nm, as determined by DLS, and the Dox molecules were present on the surface at a concentration of 2.9 wt%. The drug release profile of Dox@Apt-*hybr*-TCL-SPIONs in plasma indicated the quick release of electrostatically associated drug molecules in the early stages and the subsequently gradual release of drug through degradation of the CG-rich duplex-containing PSMA aptamer by serum nucleases, demonstrating that the Dox molecules loaded in the nucleotides were quite stable. *In vivo* T2-weighted MRI showed the selective accumulation of Apt-*hybr*-TCL-SPIONs at the tumor site in LNCaP (PSMA+)-bearing xenograft mice with a 48% relative signal enhancement (RSE). The signal drop persisted up to 48 h, indicating PSMA aptamer-mediated selective targeting (Figure 9B and 9C). In contrast, scrambled aptamer-hybridized nanoparticles (scrApt-*hybr*-TCL-SPIONs) as a negative control indicated a lower RSE (21%), and the signal drop gradually recovered from the tumor over 24 h, suggesting tumor targeting through an EPR effect. *In vivo* therapeutic efficacy also demonstrated the superiority of the Apt-*hybr*-TCL-SPIONs and suggested the possibility of enhancing the accuracy of treatment using MRI-guided real-time monitoring of the nanoparticles.

Kim *et al.* reported cancer-targeted multimodal imaging probes capable of concurrent radionuclide imaging, MRI, and fluorescence imaging *in vivo* [124]. Magnetic cobalt ferrite cores were encased by a silica shell containing fluorescent rhodamine, and were modified with various organosilicon compounds, such as (MeO)₃Si-PEG or 3-aminopropyl triethox-

ysilane. Further conjugation of the AS1411 aptamer as a nucleolin-targeting ligand [125] and *p*-SCN-Bn-NOTA for ^{67}Ga -citrate incorporation provided MFR-AS1411. Twenty-four hours after injection of the nanoparticles into C6-bearing nude mice, the specific tumor targeting of MFR-AS1411 was observed in radionuclide images via ^{67}Ga radioactivity. In contrast, the MFR-AS1411 mutant (MFR-AS1411mt)-administered mice showed rapid clearance through the bloodstream. T2-weighted MR images of MFR-AS1411-injected mice also showed black spots at the tumor site. These results were further confirmed by *ex vivo* fluorescence imaging, and high fluorescence signals were obtained from the intestine, liver, and tumors, demonstrating the tumor-specific accumulation of MFR-AS1411. This multimodal imaging system offers the benefits of complementary modalities by eliminating the shortcomings of individual imaging modalities, and it provides for a broad range of diagnostic and therapeutic imaging possibilities in human applications [126].

A newly identified anti-EGFR aptamer and its specific 'escort' and internalization properties were demonstrated by Ellington *et al.* via conjugation with gold nanoparticles (GNPs) [127]. Aptamers specific to EGFR were identified by generating an RNA pool that spanned 62 random sequence positions. Selective binding species were obtained after round 12, and one aptamer predominated (aptamer J18) with a K_d of 7 nM. The aptamer J18 was conjugated to GNPs (20 nm) by coating the GNPs with capture ONTs, followed by hybridization of an extended aptamer complementary to the capture ONTs. A flow cytometry-based internalization assay and fluorescence microscopy results indicated that only specific binding was observed in the A431 cells incubated with the aptamer J18-GNPs at 37°C, demonstrating that aptamers directed toward cell surface EGFR could lead to the specific internalization of GNP via receptor-mediated endocytosis. This finding suggests that receptor-specific nucleic acids can overcome non-specific absorption and internalization of GNPs, which convey chronic disadvantages during therapy.

Others

A major challenge to the use of siRNA in mammals is the intracellular delivery to specific tissues and organs that express the target gene. The first demonstrations of siRNA-mediated gene silencing in a human were achieved by Davis *et al.* using a targeted nanoparticle delivery system (the clinical version is denoted CALAA-01) [128]. In this system, a human transferrin protein was used as a targeting ligand for binding to the transferrin receptor, which is upregu-

lated in malignant cells [129]. The nanoparticles consisted of a cyclodextrin-containing cationic polymer (CDP), adamantane (AD)-terminated PEG (AD-PEG), and transferrin-conjugated AD-PEG (AD-PEG-TF), which formed inclusion complexes with surface cyclodextrins to achieve steric stabilization and targeting, respectively. The nanoparticles delivered an siRNA designed to reduce expression of the ribonucleotide reductase (RRM2), an established anti-cancer target (Figure 10A) [130]. To examine whether the targeted delivery system (70 nm diameter nanoparticles) provided effective delivery of the functional siRNA to human tumors, Davis *et al.* treated biopsy specimens from three patients, all of whom had metastatic melanoma, with three dose regimens (18, 24, and 30 mg/m² siRNA, indicated as A, B, and C, respectively). Among the stained tumor sections, the C1_{post} and C2_{post} samples showed the highest intensity, whereas A_{post} did not show the presence of the stain (Figure 10B), indicating dose-dependent accumulation of the targeted nanoparticles in human tumors. Tumor RRM2 mRNA and protein levels were measured by quantitative real-time reverse-transcriptase polymerase chain reaction (qRT-PCR) and western blotting, respectively (Figure 10C). Consistent with tumor staining results, the C2_{pre} and C2_{post} samples provided direct evidence for RRM2 mRNA or protein reduction after siRNA treatment with the nanoparticles. 5'-RNA-ligand-mediated rapid amplification of the complementary DNA ends (5'-RLM-RACE) using PCR techniques confirmed that the observed therapeutic results could be attributed to an RNAi mechanism.

Hyaluronic acid (HA), a copolymer of *N*-acetyl D-glucosamine and D-glucuronic acid, is a widely used targeting macromolecule that can bind to cluster determinant 44 (CD44), which is overexpressed in various tumors [131-133]. Zhou *et al.* used this targeting ligand to develop a thermo-responsive hybrid nanogel for simultaneous temperature sensing, cancer cell targeting, fluorescence imaging, and combined chemo-photothermal treatment [134]. The spherical hybrid nanogel was prepared by templated Ag nanoparticle synthesis using a thermo-responsive nonlinear PEG-based hydrogel coating as a shell, HA immobilization on the surface via strong hydrogen bonding between HA and PEG oligomers, and finally, addition of AuCl₄⁻ to the hybrid nanogel to form a Ag-Au bimetallic core. The Ag-Au@PEG-HA hybrid nanogels showed a high drug loading capacity (46.5 wt%) that was stabilized by hydrogen bonds between the ether oxygen atoms of the nonlinear PEG gel shell and the amide groups of Temozolomide (TMZ), a

model drug. Confocal imaging revealed a significantly higher fluorescence intensity in Ag-Au@PEG-HA hybrid nanogel-incubated B16F10 cells (CD44+) than in the nanogel without HA, indicating selective tumor targeting. The drug release profile demonstrated that near-IR irradiation generated localized heat and enhanced drug delivery by promoting a gradual transition from a hydrophilic to a hydrophobic PEG network. This transition not only broke the PEG-TMZ bonds, but also reduced the mesh size of the nanogels, thereby promoting diffusion of the drug molecules from the nanocages. The effects of

combined chemo-photothermal treatment were investigated by measuring the cell viability in B16F10 cells incubated with empty or TMZ-loaded hybrid nanogels and submitted to near-IR irradiation. The combination of TMS and photothermal treatment was much more cytotoxic than other chemotherapy or photothermal treatments alone. In particular, combined therapy showed a substantially higher therapeutic efficacy than the additive therapeutic index achieved from chemo- and photothermal therapies, suggesting that the nanogels displayed synergistic effects.

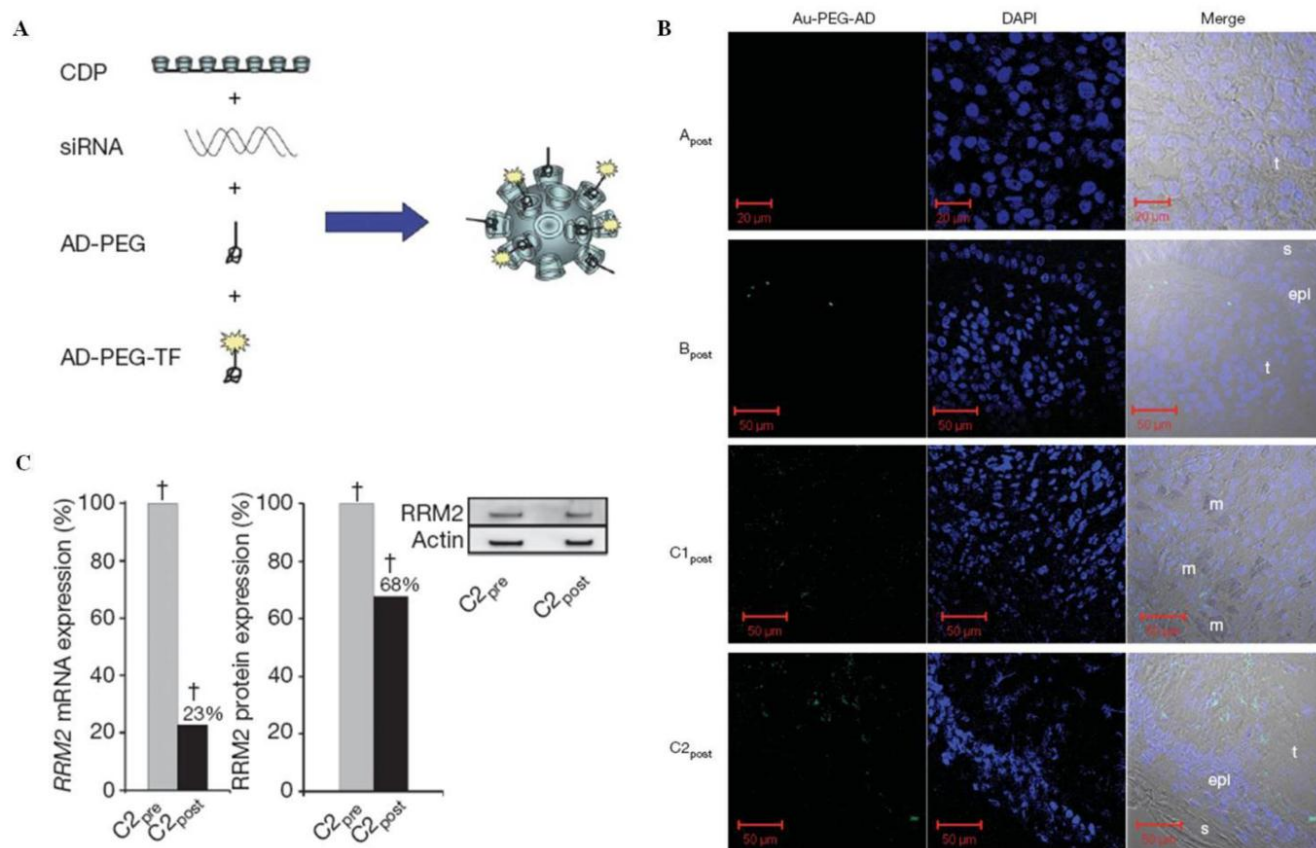


Figure 10. (A) Schematic representation of the transferrin targeted nanoparticle system. (B) Confocal images of post-treatment biopsy sections from patients A, B, and C. Left, Au-PEG-AD stain; middle, DAPI stain; right, merged images. The abbreviations are as follows: epi, epidermis; m; melanophage; s, skin side; t, tumor side. (C) qRT-PCR and western blot analysis of RRM2 protein expression in patient samples C2_{pre} and C2_{post}. The asterisk denotes the archived samples; the dagger denotes the samples obtained during the trial. Reproduced with permission from ref. [128].

3. Methods of conjugating the functional moieties for nanoparticle fabrication

A broad spectrum of chemical approaches has been used to conjugate targeting moieties, therapeutic molecules, or contrast agents to nanoparticle surfaces. These methods can be categorized as conventional bioconjugation strategies (direct conjugation, linker

chemistry, physical interactions), click chemistry, or hybridization methods (Table 2). The primary goal of targeted ligand conjugation is to bind a targeting moiety without losing its functionality after attachment to the nanoparticle. For example, binding of an antibody to a nanoparticle without consideration for the recognition site can shield the functional regions and reduce the targeting properties. Conjugated

therapeutic agents, such as drugs and siRNA, must be designed to release from a nanoparticle system after cellular uptake to show therapeutic effects. In the following sections, the unique advantages and drawbacks of each strategy will be discussed, and several examples of the strategy, including decoration of iron oxide nanoparticle surfaces with the above-listed targeting moieties will be highlighted.

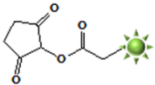
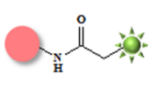
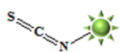
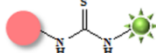
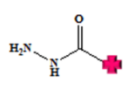
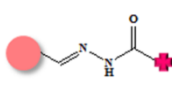
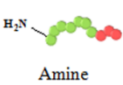
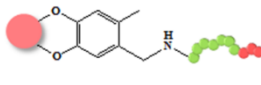
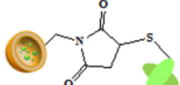
Conventional bioconjugation strategies

Direct conjugation

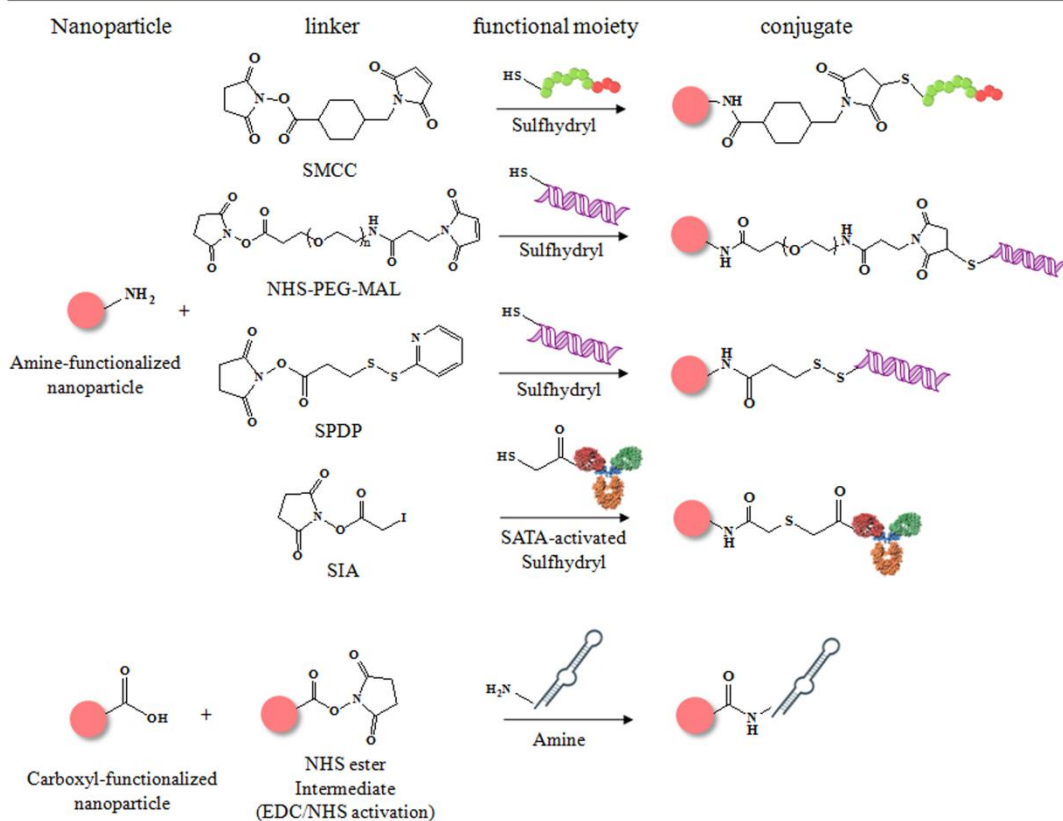
Direct reaction strategies involve nanoparticle surface functionalization with amine, aldehyde, or

active hydrogen groups. The functional groups on the nanoparticle surfaces depend on the coating layer applied during the nanoparticle preparation steps. These strategies are particularly suitable for conjugating fluorescence dyes, chelators for nuclear imaging, or drugs. In general, antibody-based or peptide-based targeting moieties that are unmodified prior to conjugation are not natively reactive with these nanoparticles. However, liposomes that include maleimides on their surfaces or GNPs can be used for direct conjugation with thiol group-containing biomolecules, such as antibodies, peptides, or ONTs.

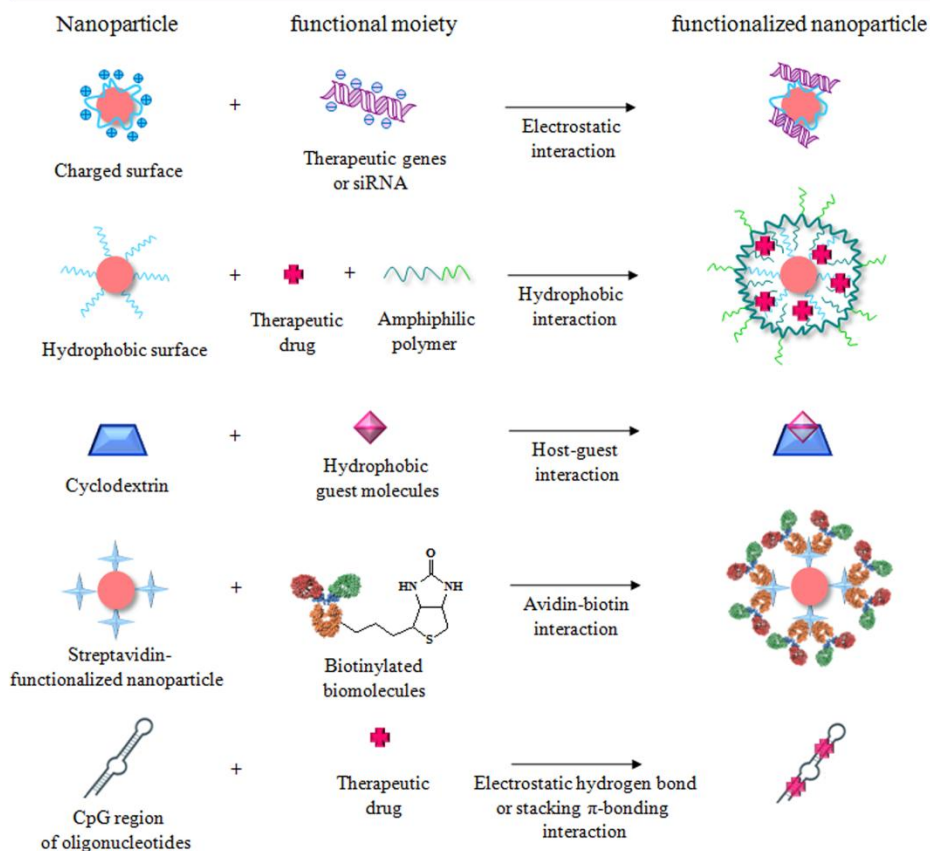
Table 2. Methods of conjugating functional moieties during nanoparticle fabrication.

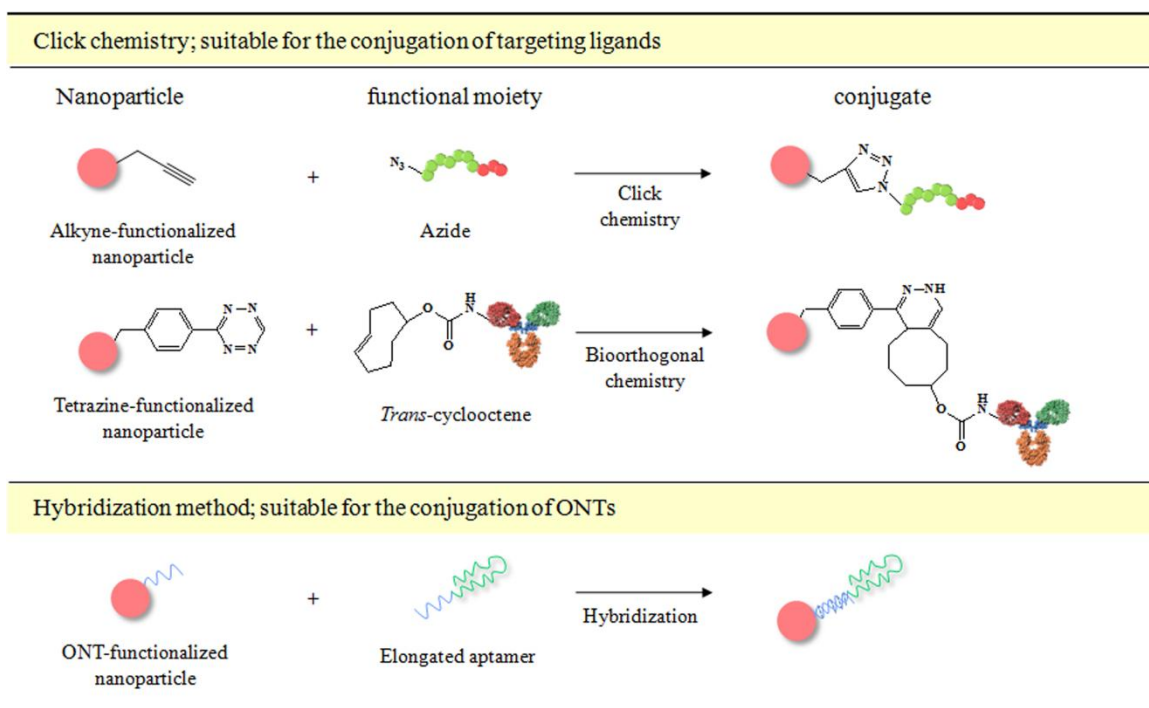
Conventional bioconjugation strategies		
Direct conjugation; suitable for the conjugation of fluorescence dyes, chelators, and drugs.		
Nanoparticle	functional moiety	conjugate
 Amine-functionalized nanoparticle	 Succinimidyl ester	
 Amine-functionalized nanoparticle	 Isothiocyanate	
 Aldehyde-functionalized nanoparticle	 Hydrazone	 Schiff-base condensation
 Active hydrogen-functionalized nanoparticle	 Amine	 Mannich reaction
 Maleimide-functionalized liposome	 Sulfhydryl	
 Gold nanoparticle	 Sulfhydryl	

Linker chemistry; suitable for the attachment of targeting ligands .



Physical interaction; suitable for the assembly of therapeutic agents onto the nanoparticles.





Nanoparticles functionalized with amine groups easily react with commercially available fluorescence dyes, such as fluorescein isothiocyanate (FITC) and the Cy5.5 NHS ester. Gu *et al.* described fluorescence dye-modified chitosan-coated magnetic nanoparticles as efficient cancer cell imaging probes [135]. Optical labeling of the nanoparticles was achieved by reacting the primary amine groups of chitosan with the isothiocyanate groups of FITC, and the magnetic nanoparticles were then coated with FITC-labeled chitosan. Recently, near-IR fluorescent dyes, such as cyanine, have been the most commonly used contrast agents for biomedical applications. To develop dual imaging probes for cancer *in vivo*, Jon *et al.* synthesized amine-modified iron oxide nanoparticles by reaction between the carboxyl group-containing polymer coating layer on a nanoparticle and 2,2'-(ethylenedioxy)bis-(ethylamine) [136]. The Cy5.5 NHS ester was then coupled to the amine-modified nanoparticles. The animal tumor was clearly visualized by MRI and optical microscopy. As reported for use of the Cy5.5-labeled nanoprobe, the combination of MRI and near-IR fluorescence imaging can potentially allow disease site mapping using MRI prior to surgical resection, and real-time imaging guidance can be achieved using fluorescent imaging techniques by delineating the tumor margins during surgery [137,138]. Trimodal imaging probes have been designed by adding a third imaging modality to the dual MRI and optical imaging probes. As described above,

cancer-targeted multimodal imaging probes capable of radionuclide imaging, MRI, and fluorescence imaging *in vivo* have been developed by Kim *et al.* [124]. First, the fluorescence properties were achieved by introducing a rhodamine-containing silica shell coating onto the magnetic cobalt ferrite core. The nanoparticles were then further modified with 3-aminopropyl triethoxysilane to produce an amine functionality on the surfaces. The isothiocyanate group of the radioactive ^{67}Ga chelator, *p*-SCN-Bn-NOTA, was then reacted with the amine-functionalized nanoparticles. ^{67}Ga incorporation provided the final trimodal imaging probes.

Aldehyde-functionalized nanoparticles can react directly with functional moieties containing a hydrazide group via the hydrazone ligation chemistry. Dawson *et al.* synthesized tumor-targeted multifunctional viral nanoparticles using a stepwise assembly strategy based on an efficient hydrazone ligation reaction [139]. The cowpea mosaic virus (CPMV) has recently been explored as a nanoparticle delivery system for a number of diseases targeting applications, and its use has been demonstrated in the context of biomedical imaging and targeted drug delivery [140-142]. In a study, CPMV was modified with sulfo-succinimidyl 4-formylbenzoic acid to yield benzaldehyde-labeled CPMV. VEGFR-1 antagonist peptides that included a hydrazide moiety at the C-terminus, prepared by solid phase peptide synthesis, and hydrazide-modified PEG molecules were

then added to the benzaldehyde-labeled CPMV. This ligation strategy enabled the sequential introduction of different peptides in a ratio that was controlled by the reaction conditions, and the modular nature of the chemistry could be tailored for specific applications. The hydrazide-functionalized nanoparticles could be conjugated to anticancer drugs containing a carbonyl group. Misra *et al.* developed a magnetic drug-targeting carrier encapsulated by a thermosensitive smart polymer [143]. This group utilized the acid-labile hydrazone bond in the drug carrier system to achieve pH-sensitive drug release. As shown in Figure 11, the surfaces of the magnetic nanoparticles were functionalized with 3-mercaptopropionic acid hydrazide via Fe-S covalent bonding. The carbonyl group of Dox was chemically adsorbed to the magnetic nanoparticle surfaces through a hydrazone bond. The Dox-loaded magnetic nanoparticles were then encapsulated with a thermosensitive biodegradable polymer to enable the on-off drug triggering mechanism. The release of drug followed the collapse of the thermosensitive polymer and the cleavage of the acid-labile hydrazone linkage. The proposed carrier is useful as a magnetic drug targeting system with a drug release profile that could be controlled by changes in the external temperature and pH.

Recently, Chen and Sun *et al.* used the Mannich reaction to couple biomolecules to nanoparticles [144]. In this work, iron oxide nanoparticles functionalized with active hydrogen groups were reacted with amine group-containing cyclic RGD peptides to develop ultrasmall c(RGDyK)-coated Fe₃O₄ nanoparticles (with an 8.4 ± 1.0 nm hydrodynamic diameter) as *in vivo* tumor-targeted imaging agents. Nonspecific uptake of the iron oxide nanoparticles by RES in the blood stream complicates the development of small biocompatible nanoparticles with targeting capabilities. Initially, they synthesized Fe₃O₄ nanoparticles via the thermal decomposition of Fe(CO)₅ in benzyl ether in the presence of 4-methylcatechol, as a surfactant, followed by air oxidation. The 4-methylcatechol formed a tight thin coating layer over the nanoparticle surface via formation of a strong chelating bond between the iron and the catechol unit. The aromatic ring of the 4-methylcatechol on the nanoparticles was directly coupled with the amine group of a lysine residue in the cyclic RGD peptide, c(RGDyK) (Figure 12). High-resolution transmission electron microscopy (HRTEM) images of the nanoparticles indicated an

iron oxide core size of 4.5 nm and a coating layer containing the c(RGDyK) peptide 2 nm in thickness, close to the size in water.

The simple process of preparing functional group-immobilized liposomes has facilitated the coupling of biomolecules to liposomal surfaces without the need for complex surface coating steps. In particular, liposomes functionalized with thiol-reactive maleimide groups may be easily prepared using commercially available maleimide-modified phospholipids in the liposome preparation step. Immunoliposomes are commonly synthesized by direct bioconjugation between maleimide-modified liposomes and thiol group-containing antibody fragments. As described above, lung cancer targeting liposomes fabricated using an anti-c-Met antibody were prepared via the conjugation of a cysteine residue-fused anti-c-Met scFv antibody to the maleimide-modified PEG-terminated liposomal Dox [64]. In another case, Mulder *et al.* reported the preparation of integrin $\alpha\beta 3$ -targeted paramagnetic lipid-coated silica nanoparticles with a QD core as a novel contrast agent platform [145]. QDs were encapsulated by silica spheres via the reverse micelle method, and the silica surface was coated with hydrophobic octadecanol. Addition of a mixture of phospholipids (PEG-DSPE, maleimide-modified PEG-DSPE, and Gd-DTPA-bis(stearylamide)) yielded water-soluble QD/silica nanoparticles enclosed by a lipid monolayer. The thiol moieties of the hydroxylamine pretreated cyclic RGD peptides (c(RGDf(-S-acetylthioacetyl)K)) were conjugated to the surfaces of the maleimide groups on the nanoparticles to obtain integrin-targeted multimodal imaging probes.

GNPs can couple to thiol-modified functional moieties without the need for additional functional groups. Because Au is highly reactive toward thiol groups, forming a strong Au-S bond, a variety of thiol-functionalized biomolecules may be conjugated to GNP surfaces in a straightforward manner. Oligonucleotide-based molecules, such as siRNA, are usually chemically synthesized to contain sulfhydryl groups that can then be conjugated to GNPs. When Li *et al.* synthesized the folate-receptor targeted hollow gold nanospheres carrying siRNA, they conjugated thiol-modified siRNA duplexes directly to the surfaces of H AuNS [98].

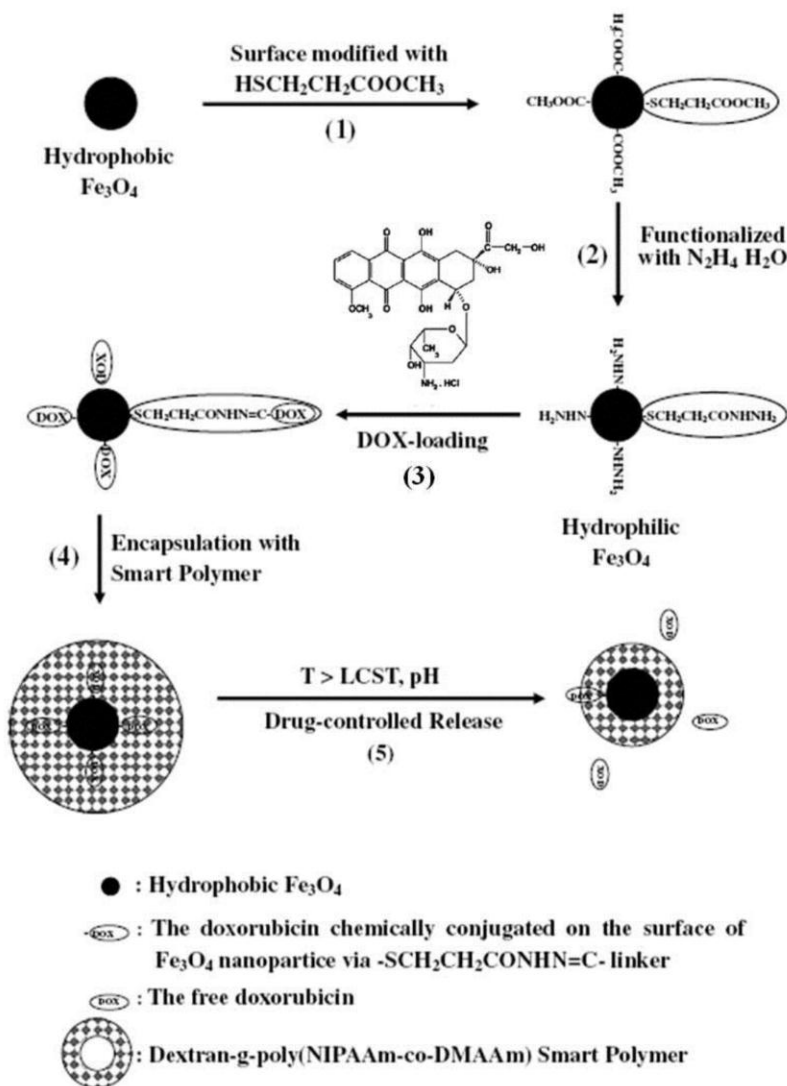


Figure 11. Schematic diagram of the sequence of steps in the synthesis of a magnetic drug targeted carrier encapsulated in a thermosensitive smart polymer, and the drug release process. Reproduced with permission from ref. [143].

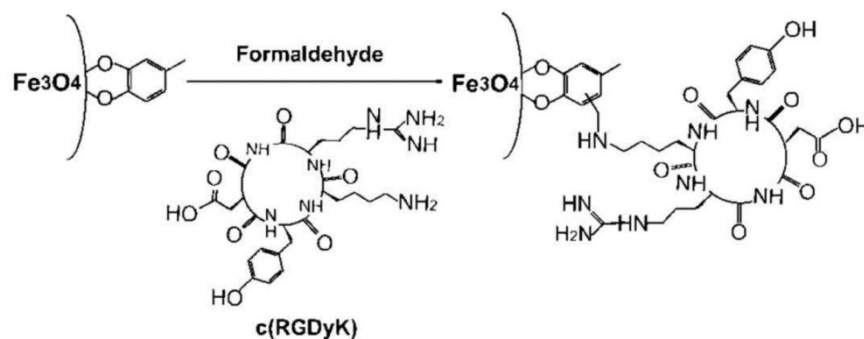


Figure 12. Schematic illustration of the coupling of the c(RGDyK) peptide to Fe_3O_4 nanoparticles. Reproduced with permission from ref. [144].

Linker chemistry

Linker molecules can control the binding orientations of ligands, thus, bioconjugation via linker chemistry is preferred over direct conjugation strategies for the attachment of targeting moieties to nanoparticles. Antibodies, peptides, and small molecules may be conjugated to nanoparticles using a variety of linkers. The most common linker chemistry relies on the reaction between amine-modified nanoparticles and sulfhydryl-containing biomolecules. Cysteine residues may be present or introduced into proteins and peptides, or the peptide may be chemically modified to gain this functionality. For example, the primary amine groups of lysine residues can be thiolated using Traut's reagent (2-iminothiolane) or SATA (*N*-succinimidyl *s*-acetylthioacetate). This bioconjugation strategy has employed a variety of linker molecules, including SIA (*N*-succinimidyl iodoacetate), SMCC (succinimidyl-4-(*N*-maleimidomethyl) cyclohexane-1-carboxylate), SPDP (*N*-succinimidyl-3-(2-pyridyldithio)-propionate), or heterobifunctional PEG molecules (NHS-PEG-MAL). Heterobifunctional linker molecules include amine-reactive succinimidyl esters in one region of the molecule and thiol-reactive iodoacetate, maleimide, or pyridyldithio groups on the other end. The reaction methods can form covalent complexes between nanoparticles and ligands, thereby requiring stepwise nanoparticle modification prior to ligand attachment or purification between each step [138]. Carboxyl group-presenting nanoparticles may be covalently bonded to amine group-bearing functional moieties through EDC/NHS linkers, which form an amide linkage. This approach is effective for the attachment of molecules that have a single amine group, although it is difficult to control the binding orientations of ligands with multiple amines, often leading to loss of functionality of the targeting ligands.

Ross *et al.* developed brain cancer-targeted multifunctional polymeric nanoparticles consisting of tumor vascular targeting F3 peptides, photosensitizers for photodynamic therapy (PDT), and iron oxide for MRI [146]. The targeted delivery of photodynamic agents to tumor sites via nanoparticles is one approach to overcoming the disadvantages of prolonged cutaneous photosensitization during PDT. To conjugate targeting peptides onto the nanoparticles specifically, first, amine-functionalized, photofrin and iron oxide-encapsulated polyacrylamide nanoparticles were prepared, and the water-soluble sulfo-SMCC was added to couple with surface amines on nanoparticles. The reaction mixture was further treated with succinimidyl succinate ester of PEG2000. And

the thiol groups of F3 peptides, pretreated with Traut's reagent, were lastly conjugated to the maleimide-functionalized nanoparticles. The targeted nanoparticles performed well during PDT and significantly improved survival rate in a glioma-bearing orthotopic rat model. SMCC may be replaced by heterobifunctional PEG molecules (NHS-PEG-MAL) to functionalize amine-modified nanoparticles. Zhang *et al.* used NHS-(PEG)₂-MAL and NHS-(PEG)₁₂-MAL to introduce maleimide functionalities onto the magnetic nanoparticles [81]. A thiol-modified siRNA and CTX were attached to the amine-functionalized pH-sensitive PEI-coated iron oxide nanoparticles via NHS-(PEG)₂-MAL and NHS-(PEG)₁₂-MAL, respectively (Figure 13A). The dodecaethyleneglycol linker for CTX facilitated targeted ligand delivery by providing a more flexible linker, thereby enhancing the peptide's ability to bind to a target receptor. pH-sensitive surface coating layers improved the presentation and availability of cationic CTX on the nanovector surfaces by introducing electrostatic charge repulsion between CTX and surface moieties (Figure 13B).

Pyridyl disulfide linkers include cleavable disulfide bonds, which facilitates a quantitative evaluation of the reaction efficiency. Jon *et al.* calculated the concentration of surface-bound peptide molecules on the nanoparticles by quantifying the released pyridine-2-thione [147]. In an effort to develop integrin-targeted iron oxide nanoparticles as theranostic agents, amine-modified iron oxide nanoparticles were synthesized, and SPDP was added to convert the primary amine groups on the nanoparticles to sulfhydryl-reactive pyridyldisulfide groups. Conjugation between the thiol group-containing cyclic RGD peptides and the SPDP-activated nanoparticles produced pyridine-2-thione, which was immediately collected by spin filtering (at 100 K). The immobilized cRGD molecules were quantified based on the ultraviolet (UV) absorbance at 343 nm of the collected pyridine-2-thione filtrate, indicating that the average number of conjugated cRGD peptides on each nanoparticle was 0.39 wt%. This linker is useful for enhancing the intracellular gene silencing properties of siRNA. Bhatia *et al.* studied the gene-silencing efficacy of siRNA-conjugated QDs using cleavable (sulfo-LC-SPDP) or noncleavable (sulfo-SMCC) cross-linkers [148]. They immobilized thiol-modified siRNA specific for EGFP to amine-functionalized QDs via sulfo-LC-SPDP or sulfo-SMCC linkers and quantified the EGFP fluorescence intensity. The siRNA attached QDs via the sulfo-LC-SPDP linker provided greater silencing efficiency than those attached via the sulfo-SMCC linker. The cleavable disulfide

cross-linker released siRNA from the nanoparticles into the intracellular reducing environment, which affected the interactions between the siRNA and the RNA induced silencing complex (RISC), which is necessary for gene knockdown.

Stable linkages between nanoparticles and functional moieties may be provided by iodoacetate linkers. Using this linker, Zhang *et al.* synthesized a CTX-mediated brain tumor targeting magnetic/optical nanoprobe [73]. As shown in Figure 14, amine-functionalized nanoparticles were prepared by synthesizing a PEG-grafted chitosan polymer. Methoxy-PEG was oxidized to yield PEG-aldehyde, which was then reacted with the primary amines of depolymerized chitosan by formation of a Schiff base. Subsequently, iron oxide nanoparticles were coated with a PEGylated chitosan-branched copolymer (NPCP). SATA-pretreated CTX was then conjugated to the nanoparticles via an SIA cross-linker. The nanoparticles were linked to fluorescence imaging dyes by conjugating the amine groups remaining on the iron oxide nanoparticles to a Cy5.5 NHS ester, producing

NPCP-Cy5.5-CTX as a brain tumor targeting magnetic/optical nanoprobe.

Amine coupling using EDC/NHS chemistry is a practical approach to conjugating small molecules, peptides, and ONTs. EDC reacts with the carboxyl groups of nanoparticles to form an active ester, but this reactive complex is subject to rapid hydrolysis under aqueous conditions. Formation of a sulfo-NHS ester intermediate prevents hydrolysis and extends the half-life of the activated carboxylates, permitting their reaction with the primary amine groups of functional moieties. As described above, Jeong *et al.* synthesized hepatocyte-targeted LBA-immobilized SPIONs via an amide linkage between the dopamine-modified SPION bearings a primary amine group and lactobionic acid using the EDC/NHS coupling chemistry [107]. Jon and Farokhzad *et al.* also developed prostate-targeted QD aptamer conjugates as theranostic agents by reacting carboxyl QDs with a 5'-amine-modified A10 PSMA aptamer via EDC/NHS chemistry [121].

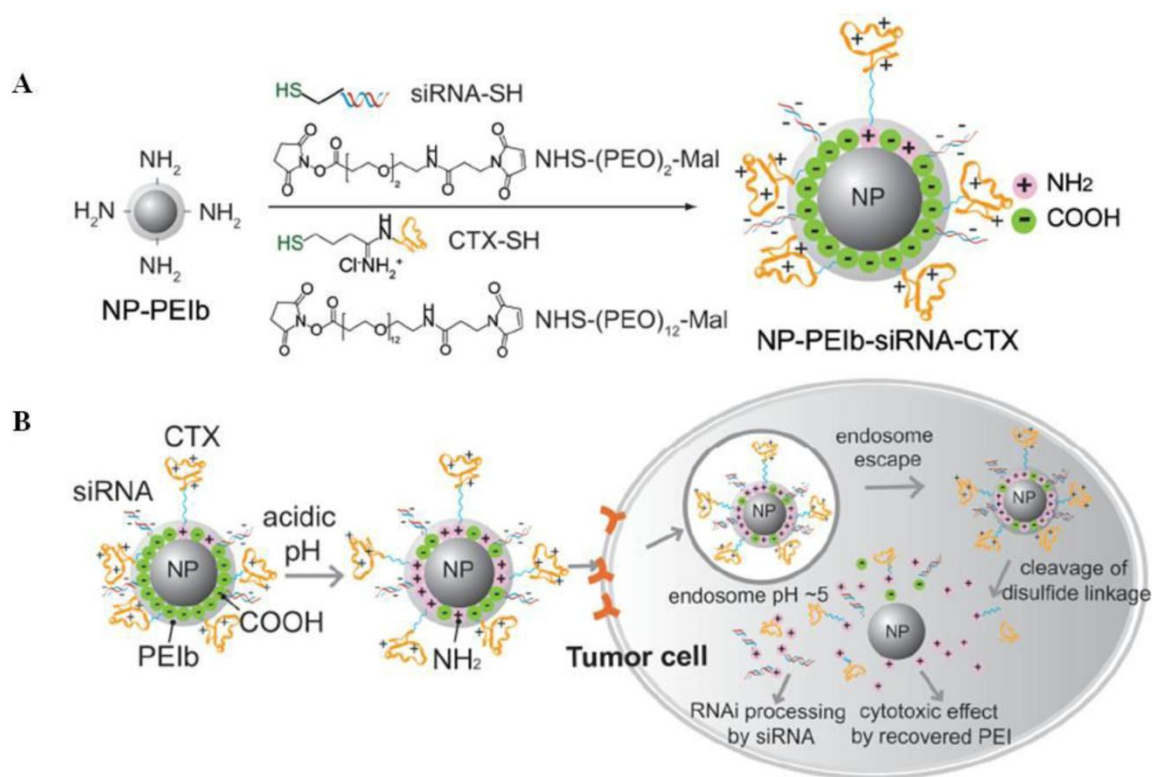


Figure 13. Schematic diagram showing the preparation of (A) the multifunctional NP-PEI-siRNA-CTX nanovector and (B) intracellular uptake, extracellular trafficking, and processing of the nanovector in tumor cells. Reproduced with permission from ref. [81].

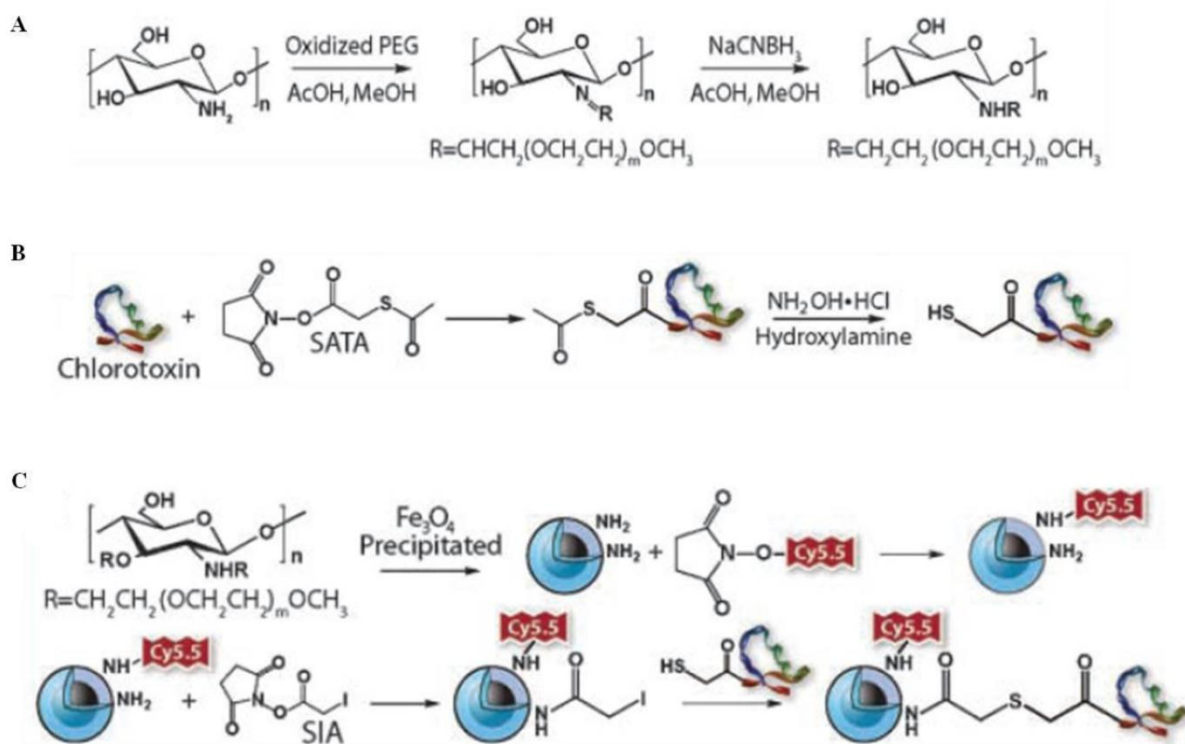


Figure 14. Synthesis of NPCP-Cy5.5-CTX nanoprobe. (A) PEG-grafted chitosan, (B) sulfhydryl functionalization of CTX, and (C) CTX and Cy5.5 conjugation to NPCP. Reproduced with permission from ref. [73].

Physical interactions

Physical interactions encompass electrostatic, hydrophobic, and affinity interactions. Physical conjugation strategies are particularly useful for the assembly of therapeutic agents onto nanoparticles. Electrostatic interactions are useful for loading siRNA onto nanoparticles coated with cationic PEI. Hydrophobic anticancer drugs can adsorb via hydrophobic interactions onto nanoparticles coated with a hydrophobic coating layer, and the drugs may then be released inside cells after degradation of the coating layer. Although these interactions have several unique advantages, including rapid binding and the lack of modification steps, it is difficult to control the molecular orientations of physically bound ligands. This binding mode, therefore, is not appropriate for immobilizing targeting moieties. In contrast, affinity interactions are effective for bioconjugating targeting ligands to nanoparticles. A representative example of affinity interactions is the streptavidin-biotin interaction. This linkage is very stable and shows the strongest known binding affinity among non-covalent linkage reactions ($K_d = 4.0 \times 10^{-14}$ M) [149].

T cell-specific DGK α genes were incorporated onto nanoparticles by Chen and Shuai *et al.* by first

synthesizing PEG-g-PEI-SPIONs as an MRI-visible polymeric vector [60]. The PEG-g-PEI was coated onto the SPIONs using the ligand exchange method. T cell-specific targeted gene delivery was achieved by preparing T cell-targeted scAb_{CD3}-PEG-COOH conjugates. A thioether bond linked MAL-PEG-COOH to the sulfhydryl-containing scAb_{CD3}, and PEG-g-PEI-SPIONs were then added to the solution in the presence of EDC/NHS to produce scAb_{CD3}-PEG-g-PEI SPIONs. The targeting polyplexes (scAb_{CD3}-PEG-g-PEI SPIONs/DNA) were then obtained by loading the DGK α gene onto the scAb_{CD3}-PEG-g-PEI SPIONs via electrostatic interaction. Park *et al.* designed a new class of siRNA structure, multimerized siRNA-linear PEI (LPEI) complexes, to achieve efficient gene silencing [150]. Thiol-modified, single-stranded sense or antisense siRNA were reacted with cleavable or noncleavable cross-linkers, were dimerized, and were annealed to obtain multi-siRNA. The multi-siRNA species formed stable compact nanosized complexes (81.8 ± 47.2 nm) with oppositely charged LPEI via electrostatic interactions. Efficient gene silencing was promoted by the high charge density. Multi-siRNA, with intracellularly cleavable linkages, displayed the capacity for

target sequence-specific gene silencing.

Labhasetwar *et al.* developed a hydrophobic drug carrier system using a water-dispersible oleic acid-Pluronic-coated iron oxide nanoparticle formulation [151]. In their study, Pluronic F-127 was anchored onto the oleic acid-coated iron oxide nanoparticles to improve the dispersibility in aqueous solutions, and hydrophobic Dox molecules were partitioned into the oleic acid shell surrounding the iron oxide nanoparticles via hydrophobic interactions. The amount of Dox that could be loaded was 8.2 wt%. This formulation simplified the drug-loading process relative to chemical conjugation methods. In a similar approach, Wei and Gao utilized this formulation to incorporate a hydrophobic anticancer drug, Dtxl, to the prostate tumor targeted, scAb_{PSCA}-linked multifunctional polymeric vesicles [58]. They synthesized poly(lactic-co-glycolic) acid and entrapped both SPIO and Dtxl into this polymer. At this time, Dtxl was loaded into the oleic acid/oleylamine shell of the SPIO, and the drug loading was 6.0 wt%. The partition of the drug in the shell via hydrophobic interactions, provided for a slow and controlled drug release profile from the multifunctional vesicles. Host-guest interactions provide another example of hydrophobic interactions. Cyclodextrin (CD) is the most common host molecule and displays a particular aptitude for enhancing the solubility of guest molecules, such as a hydrophobic organic solute, by encapsulating it within its central cavity (in the shape of a hollow truncated cone). Davis *et al.* first demonstrated siRNA-mediated gene silencing in a human using a targeted CD-based delivery system [128]. They synthesized a β -CD-containing cation polymer (CDP) by polymerizing a difunctionalized β -CD monomer with a difunctionalized comonomer using dimethylsuberimidate 2HCl and dithiobis(succinimidyl propionate), and this polymeric backbone provided a scaffold for attaching agents [152]. They also prepared adamantane (AD)-PEG by conjugating succinimidyl propionate-PEG5000 with the amine-containing AD. AD is a hydrophobic cage molecule that can fit inside the cavity of β -CD. In this case, the CD-AD interactions were used to assemble non-biofouling PEG molecules or malignant tumor targeting transferrin (Tf) ligands on the surface of the polymeric drug delivery system. To the coupled complex of AD and vinyl sulfone-PEG5000-NHS was coupled transferrin, via a lysine residue, to produce Tf-PEG-AD. Finally, Tf-PEG-AD or PEG-AD was incorporated into the CDP, and siRNA was condensed onto the cationic polymeric systems to provide a targeted nanoparticle siRNA delivery system. Interestingly, transferrin formed strong complexes with nanoparticles while

maintaining its functionality. In addition to the hydrophobic interactions contributing to the complex stability, van der Waals interactions and hydrogen bonding assisted in the host-guest association.

The HER2/neu protein is highly expressed in approximately 25% of human breast cancers, and expression levels of the protein correlate with a poor prognosis for breast cancer or other human cancers [153]. Artemov *et al.* examined the expression levels of HER2/neu using commercially available streptavidin-conjugated superparamagnetic iron oxide nanoparticles [154]. Breast cancer cells expressing different levels of the HER2/neu receptors were pretreated with biotinylated Herceptin, followed by nanoparticles targeted to the receptors. *In vitro* T2-weighted MRI contrast was correlated with the levels of HER2/neu expression on the breast cell membrane, as confirmed by flow cytometry analysis. The noninvasive imaging method was highly sensitive, with a lower limit of detection in the range of 5×10^4 receptors per cell. This sensitivity is comparable to the typical expression levels of HER2/neu receptor in patient samples, in which levels can range from 10^5 to 4.5×10^6 per cell.

In addition to the physical interactions described above, other noncovalent secondary interactions can stabilize bioconjugation. Adriamycin, such as Dox, may intercalate into the DNA double stranded helix via guanine-cytosine d(CpG) site-specific interactions. The drug-DNA complex is stabilized by electrostatic hydrogen bonds and stacking π -bonding interactions between the electron-deficient quinone-based chromophore and the electron-rich purine or pyrimidine bases [155]. Based on this specific interaction, Jon *et al.* designed a CG-rich duplex containing PSMA aptamer-conjugated GNPs and magnetic nanoparticles as a prostate tumor targeting theranostic agent [156, 123]. They demonstrated that a PSMA aptamer containing an appended (CGA)₇ repeating ONT significantly enhanced the Dox-loading capacity compared to the original PSMA aptamer by providing binding sites for at least 6–7 Dox molecules in the extended region, whereas the original PSMA aptamer included only a single Dox molecule binding site. Conjugation of the elongated PSMA aptamer to nanoparticles proceeded by coating the nanoparticles with aptamer-binding ONTs comprising an A₁₀ spacer and a 5'-(TCG)₇-3' complementary sequence. Once the PSMA aptamers had been conjugated onto the nanoparticles, several Dox molecules intercalated among the surface-bound CG-rich duplex containing a PSMA aptamer. The resulting nanoparticles displayed prostate-targeted diagnostic and therapeutic abilities when analyzed by CT imaging/MRI or a tu-

mor-bearing animal model.

Click chemistry

The Huisgen 1,3-dipolar cycloaddition, also known as the 'click reaction' was developed by Sharpless *et al.* almost a decade ago [157]. The Cu(I)-catalyzed reaction between alkyne and azide groups results in the formation of a stable triazole linkage, which is water-soluble and biocompatible. These reactions are highly specific and occur under mild reaction conditions in aqueous solutions with high yield. The reaction specificity precludes undesirable reaction with other functional groups, ensuring specific conjugation at the desired location on the biomolecules. These features provide highly oriented linkages, thus the click reaction is specifically suited for the conjugation of targeting moieties to the nanoparticles. However, the Cu(I) catalyst, needed to drive the reaction, can cause toxicity, such as hepatitis, neurological disorders, kidney disease, or Alzheimer's disease *in vivo* [158]. Recently, Weissleder *et al.* developed a covalent bioorthogonal reaction between a 1,2,4,5-tetrazine (Tz) and a *trans*-cyclooctene (TCO) as the alternative coupling mechanism [159]. The [4 + 2] cycloaddition is fast, chemoselective, does not require a catalyst, and proceeds in serum. This reaction strategy is therefore attracting increased interest for molecular imaging applications at the cellular level.

Bhatia *et al.* firstly demonstrated the use of 'click' nanoparticles for *in vivo* applications [160]. They synthesized a succinimidyl 4-azidobutyrate and alkyne-containing Lyp-1 peptide (CGNKRTRGC) that binds to p32 mitochondrial protein-overexpressing tumor cells [161]. The succinimidyl 4-azidobutyrate was then linked to a thiol-PEG₅₀₀₀-amine, and the product was added to N-[γ -maleimidobutyryloxy]succinimide ester (GMBS)-activated magneto-fluorescent nanoparticles (MFNP), consisting of amine-functionalized cross-linked iron oxide nanoparticles linked to a cyanine dye (Vivo Tag 680), to generate azido-PEG-nanoparticles. The alkyne-bearing Lyp-1 peptides were clicked to the nanoparticles in the presence of CuSO₄ and sodium ascorbate. Excess copper catalyst and peptides were removed using size exclusion chromatography. Nude mice bearing human MDA-MB-435 were injected intravenously with Lyp-1-iron oxide nanoparticles to test *in vivo* tumor targeting properties. Twenty-four hours post-injection, the mice were sacrificed and the organs were collected for immunohistochemical or whole organ fluorescence analysis. The Lyp-1 'click' nanoparticles appeared to have extravasated from the tumor vasculature, penetrated into the interstitial

spaces of the tumor, and bound to p32-expressing cells. In contrast, non-targeted azido-PEG-nanoparticles were localized within the immediate periphery of blood vessels by passive accumulation. These results demonstrated the successful use of the 'click' attachment strategy in the development of specific tumor targeting theranostic nanoparticles.

Perez *et al.* utilized the click reaction to conjugate folate onto multifunctional iron oxide nanoparticles [162]. They synthesized poly(acrylic acid) (PAA)-coated iron oxide nanoparticles and encapsulated lipophilic fluorescence dyes (dialkylcarbocyanine fluorophores) within the hydrophobic coating layers on the nanoparticles to provide dual imaging capabilities. The nanoparticles were functionalized with alkyne groups via a reaction with propargyl amine and EDC/NHS, followed by further reaction with azide-containing folate via the click chemistry. A hydrophobic anticancer drug, Taxol, was then encapsulated to yield multifunctional theranostic nanoparticles. A thick polymeric coating layer, 40 nm thick according to DLS measurements, played a key role in incorporating hydrophobic guest molecules. The MTT and cellular uptake assessments indicated the folate-decorated nanoparticles' specificity toward target tumor cells (A549). MRI studies demonstrated the ability of those theranostic agents to behave as sensitive MRI contrast agents.

An alternative to the click reaction was reported by Weissleder *et al.*, who described the use of a bioorthogonal chemistry-based targeting nanoparticle platform [163]. This chemistry permitted reconfiguration of the conjugation strategies for targeting nanoparticle sensors, thereby improving the binding efficiency and detection sensitivity. This technique was referred to as 'bioorthogonal nanoparticle detection' (BOND) (Figure 15A). Their study compared two BOND assays to determine the specific cancer cell targeting ability (Figure 15B). In one setting, MFNPs were directly coupled to three types of monoclonal antibody (mAb) prior to cell exposure (BOND-1). Another setting examined a two-step strategy (BOND-2), in which TCO-functionalized monoclonal antibodies mediated primary binding to cells and were coupled to Tz-immobilized MFNPs via the covalent bioorthogonal reaction. In this comparison, amino-MFNP were modified with Tz-NHS to create Tz-MFNP, and lysine groups of the mAbs (anti-HER2 Abs, anti-EpCAM Abs, and anti-EGFR Abs) reacted with the TCO-NHS to produce TCO-mAbs. Nanoparticle binding increased with increased TCO loading until saturation at 20 TCO per antibody. Interestingly, the BOND-2 labeling strategy consistently yielded

higher nanoparticle binding to cells compared to direct labeling such as maleimide/thiol chemistry or BOND-1 (Figure 15C). These results suggested that TCO-decorated mAbs may serve as scaffolds for subsequent nanoparticle attachment and can amplify the achievable signal by increasing the number of available TCO reaction sites. In addition, when compared with streptavidin-biotin coupling mechanism as two-step labeling strategy, the overall signal was considerably lower than BOND-2, confirming the unique and superior bioorthogonal chemistry. The higher probability of binding was attributed to the valency and small size of Tz, which interacted with TCO on the antibody surfaces without introducing steric hindrance. Recently, it has been shown that BOND amplification can be used as a technique for detecting intracellular proteins in rapid sensitive diagnostic applications [164]. The detection of cytoplasmic and nuclear protein markers (cytokeratin, CK, and K_i -67, respectively) as model diagnostic targets was tested by examining several methods for fixing and permeabilizing cells, and a combination of freeze-thaw cycles and saponin treatment provided the best results, with a small increase in background

binding (Figure 16A). As described, the BOND-2 scheme amplified nanoparticle binding to intracellular targets with an order of magnitude higher signal compared to the BOND-1 scheme. This procedure permitted quantification of the target protein expression levels. The cell line panels with varying levels of CK and K_i -67 expression were incubated with the targeted nanoparticles, and the fluorescence intensity was measured. Fluorescent antibody staining and Western blot results indicated that the nanoparticle signals were closely correlated with expression levels, suggesting a chemoselective Tz/TCO cycloaddition reaction. They performed NMR profiling of the intracellular proteins using the diagnostic magnetic resonance (DMR), which was developed as a rapid point-of-care diagnostic technique for analyzing small cell populations [165]. Eight cells were labeled with MFNPs using the BOND scheme, and 1000 cells were analyzed in a 1 μ L sample volume of a hand-held NMR device (Figure 16B). The DMR profiling results correlated with the expression levels of the target proteins, as measured by fluorescent antibody staining in larger samples (10^6 cells).

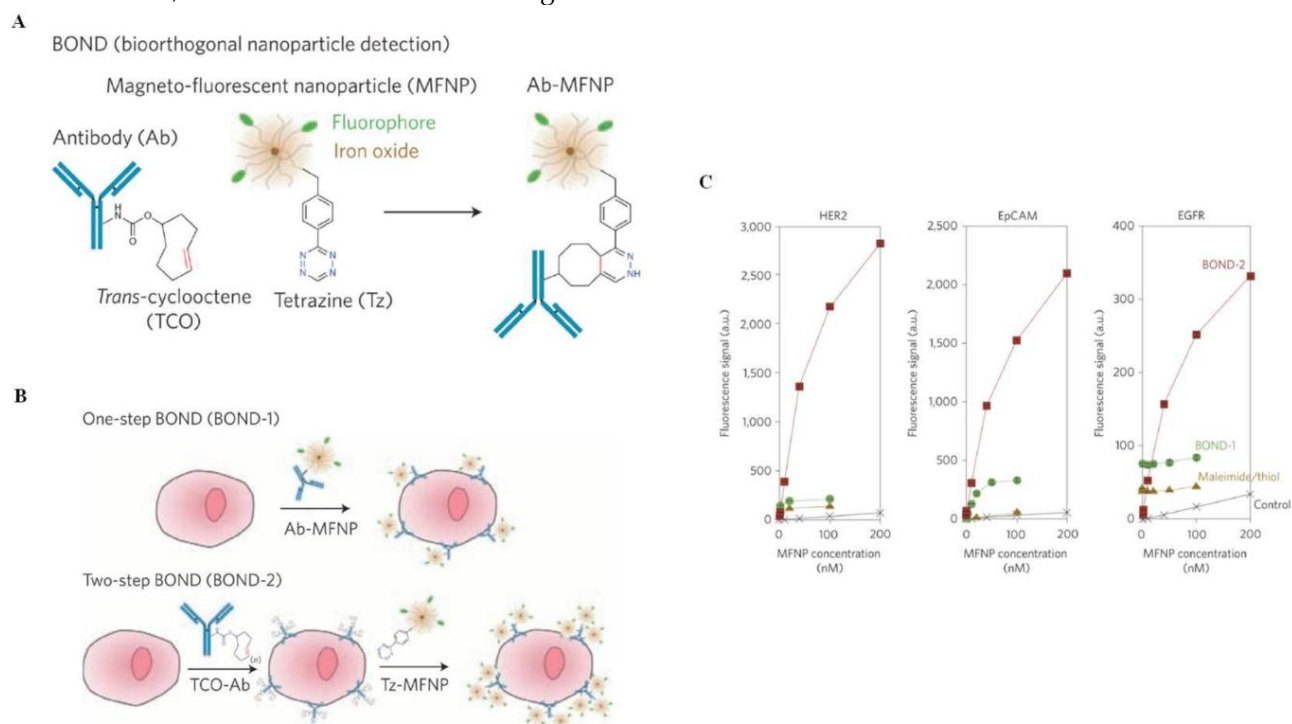


Figure 15. (A) Schematic diagram showing the conjugation chemistry between an antibody and a nanoparticle. (B) Application of BOND for one-step (direct) and two-step targeting of nanoparticles to cells. Note that the antibody and tetrazine are shown to be present in multiple copies per nanoparticle. (C) Comparison of different nanoparticle targeting strategies. SKBR-3, HCT116, and A549 cells were labeled with different concentrations of MFNPs using the two-step BOND-2 or direct MFNP immuno-conjugates, and the fluorescence signal was measured using flow cytometry. MFNP immuno-conjugates were prepared either via maleimide/thiol or TCO/Tz (BOND-1) chemistries. The control samples were incubated with Tz-MFNP only. Reproduced with permission from ref. [163].

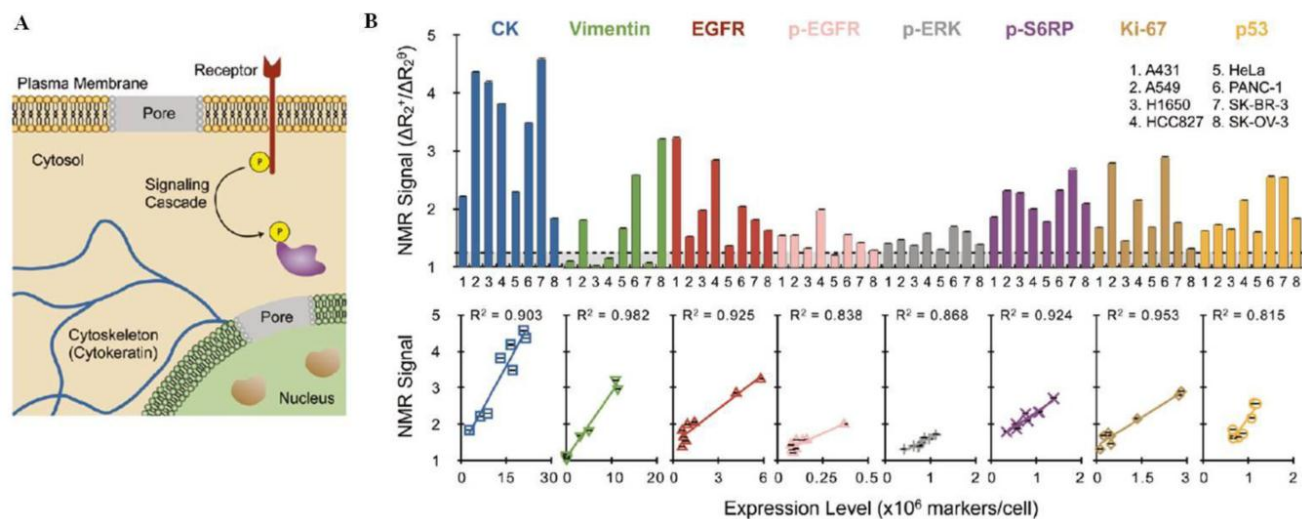


Figure 16. (A) Semipermeabilization of intact cells allows for nanoparticle targeting to a variety of intracellular biomarkers. Indicators of cell growth, activation, and survival. (B) Profiling scant tumor cell populations for key biomarkers of cancer using DMR. Detection of eight biomarkers in eight different cell lines using MFNPs based on NMR signal (top). Magnetic measurements showed an excellent correlation with the marker expression levels determined independently using antibody staining (bottom). Reproduced with permission from ref. [164].

Hybridization method

Richards-Kortum *et al.* reported a novel approach to conjugating nanoparticles and aptamers [166]. The aptamer was extended to provide a hybridization site for complementary ONT-coated nanoparticles. GNPs (20 nm) were coated with thiol-modified capture ONTs containing a hexa(ethylene glycol) spacer and a complementary sequence for the aptamer extension, and the extended anti-PSMA aptamer was hybridized to capture ONT-coated GNPs by heating the solution at 70°C for 5 min, followed by incubation at room temperature for 30 min. The resulting aptamer-GNPs showed targeted detection of LNCaP (PSMA+) cells via reflectance imaging. This conjugation strategy has several advantages. First, the negatively charged phosphate groups of the ONTs prevented aggregation of the nanoparticles through electrostatic repulsion, leading to nanoparticle stability, even in high-salt environments. Second, aptamers were easily conjugated to the surfaces of nanoparticles via complementary sequence hybridization with the capture ONTs, which preserved the aptamer integrity and stability during bioconjugation. A PEG spacer between the thiol group and the complementary capture sequence of capture ONT improved the hybridization efficiency by minimizing steric hindrance between the gold surface and the hybridization site. Third, a small number of aptamers was needed for binding to the nanoparticles through the short cheap

capture ONTs, unlike thiolated aptamers, in which significant concentrations of aptamers are necessary to coat and stabilize the nanoparticles. Finally, multiplexing capabilities can be obtained by incorporating other types of molecules (targeting, delivery, imaging, or therapeutic agents) into the nanoparticles.

Ellington *et al.* used this bioconjugation method to conjugate an anti-EGFR aptamer onto GNPs to demonstrate the targeting specificity of a newly identified aptamer [127]. As described above, they coated GNPs with thiol-modified capture ONTs that hybridized to an extended anti-EGFR aptamer to generate anti-EGFR aptamer-conjugated GNPs. Jon *et al.* utilized the hybridization method to conjugate an anti-PSMA-aptamer to iron oxide nanoparticle surfaces [123]. In their study, CG-rich duplexes were constructed at the ends of the aptamers to achieve multiple Dox-binding on the nanoparticles. They immobilized amine-functionalized capture ONTs (5'-NH₂-A10-(TCG)₇-3') on the surfaces of the carboxyl-modified iron oxide nanoparticles. Magnet purification yielded the capture ONT-coated iron oxide nanoparticles. A (CGA)₇-extended anti-PSMA-aptamer was synthesized by *in vitro* transcription, and the aptamers were added to the ONT-coated nanoparticles to produce Apt-hybr-TCL-SPIONs. Thermal gravimetric analysis (TGA) indicated that PSMA aptamers (28,451 Da) hybridized to approximately 33% of the ONTs (9,708 Da) conjugated to the nanoparticles.

4. Surface engineering strategies for *in vivo* application

In general, nanoparticles tend to aggregate through hydrophobic interactions or attractive van der Waals forces in an effort to minimize the surface energy. In the blood stream, such aggregates can trigger opsonization, the process by which a particle becomes covered with opsonin proteins, thereby making it more visible to the mononuclear phagocytic system (MPS), such as RES. The phagocytic mechanisms render nanoparticles ineffective as theranostic devices by removing them from the bloodstream [167]. Therefore, evading uptake by RES and increasing the blood circulation half-life are major challenges for developing theranostic nanoparticles in clinical applications [168]. Several methods of camouflaging nanoparticles have been developed to yield 'stealth' nanoparticles, which are invisible to MPS. These approaches interfere with the binding of opsonin proteins to the nanoparticle surfaces in support of a long circulation half-life, thereby increasing the chance that the nanoparticles can effectively target tumor sites. In order to impart stealth properties to the nanoparticles, one of the most promising molecules is the FDA-approved PEG. Natural or synthetic polymers, small organic molecules, and core-shell structures have also been utilized for nanoparticle surface coatings. However, a high surface coverage can decrease binding to and uptake by target cancer cells. This section describes the use of several coating molecules as shielding materials. The optimal surface densities of the coating materials and the targeted ligands will be discussed.

Shielding strategy

PEG is a biocompatible linear synthetic polymer that can be prepared in a range of sizes and with a variety of terminal functional groups. PEG is commonly used to achieve stealth properties, due to its hydrophilicity, flexibility, and neutral charge in biological fluids, all of which properties help disperse nanoparticles and increase their blood circulation times [169,170]. Various methods have been used to attach PEG to magnetic nanoparticles, including *in situ* coating under aqueous conditions [171], silane-grafted PEG coating [172], fabrication of amine-functionalized 6-armed PEG derivatives [173], polymerization at nanoparticle surfaces [174], or modification through sol-gel approaches [175]. Covalent attachment of one end of a heterobifunctional PEG to the magnetic nanoparticles and functionalization of the other end with targeting ligands, imaging probes, or therapeutic agents have been described

[176-178]. Jon *et al.* developed a multifunctional poly(TMSMA-*r*-PEGMA-*r*-NAS) capable of covalent anchoring onto iron oxide surfaces (silane functionality), resisting protein absorption (PEG functionality), and binding to functional moieties (carboxyl functionality) [136]. Interestingly, silane functionalities were employed to cross-link polymer coating layers, formed by heat-mediated condensation of hydrolyzed silane groups (-Si(OH)₃), to yield highly stable nanoparticles. This polymer facilitated fabrication of iron oxide nanoparticles and demonstrated their *in vivo* dual imaging (MR/optical) modalities in tumor xenograft animal models.

Copolymers containing PEG residues have been developed as a means of combining the properties of PEG with the desired properties of other moieties. Chen and Shuai synthesized PEG-*g*-PEI copolymers that condense DNA to facilitate gene delivery (PEI functionality) and display a stealth profile necessary for *in vivo* applications (PEG functionality). The copolymers were used to construct PEG-*g*-PEI-SPIONs as MRI-visible gene carriers [60]. Zhang *et al.* prepared a PEGylated chitosan-branched copolymer to coat iron oxide core and develop brain tumor targeting magnetic/optical nanoprobe. Chitosan is a hydrophilic and biocompatible natural polymer that is popular as a theranostic nanocarrier material [179]. In a study by Zhang *et al.*, a PEG-grafted chitosan copolymer was prepared using a Schiff base reaction between PEG-aldehyde and amine-containing depolymerized chitosan, and nanoparticles were synthesized by coprecipitation of ferrous and ferric chloride with ammonium hydroxide in the presence of the copolymer. The chitosan amine groups present on the surfaces of the nanoparticles were coupled to the brain tumor targeting ligand, CTX. The presence of surface chitosan sterically stabilized the nanoparticles by preventing aggregation under physiological conditions. Additionally, the positively charged chitosan cations could interact with the negatively charged brain endothelium via electrostatic interactions to trigger adsorptive-mediated transport across the BBB. Jon *et al.* developed another multifunctional amphiphilic copolymer, poly(DMA-*r*-mPEGMA-*r*-MA), that formed an efficient coating on the surfaces of oleic acid-stabilized SPIONs [180]. Hydrophobic dodecyl methacrylate (DMA) residues on the polymer bound to the oleic acid tail group formed a shell around the SPIONs via hydrophobic and van der Waals interactions. Hydrophilic PEG residues improve the water-dispersibility of nanoparticles and prevent biofouling during *in vivo* molecular imaging. Finally, methacrylic acid (MA) residues can be used to introduce additional functionalities. Sonication of the

immiscible phases containing oleic acid-stabilized SPIONs in hexane or the amphiphilic polymer in water created an oil-in-water emulsion. Evaporation of the hexane left a homogenous aqueous solution containing amphiphilic polymer-coated SPIONs. The *in vivo* diagnostic capabilities were demonstrated in a Lewis Lung Carcinoma cell allograft animal model. In a similar approach, Hadjipanayis *et al.* formed oleic acid-stabilized SPIONs using an amphiphilic triblock copolymer consisting of a polybutylacrylate segment (hydrophobic), a polyethylacrylate segment (hydrophobic), a polymethacrylic acid segment (hydrophilic), and a hydrophobic hydrocarbon side chain [52]. Strong hydrophobic interactions between the oleic acid and the hydrophobic residues of the polymer favored spontaneous encapsulation of the SPIONs. The surface-exposed carboxyl groups of the methacrylic acid segments covalently bound to EGFRvIIIAb to target glioblastoma, and PEG stabilized the dispersion under aqueous conditions.

Polysaccharide dextrans are widely used as surface shielding materials for *in vivo* applications. The biocompatibility and high affinity of dextrans toward iron oxide surfaces, mediated by polar interactions, including hydrogen bonds, provide excellent properties to SPIONs coated with dextrans, and several of the clinically approved SPION preparations are dextran-coated [181-183]. Conventional dextran polymer coatings do, however, suffer some degree of detachment from the nanoparticle surfaces due to the lability of the hydrogen bonds. Weissleder *et al.* developed stable cross-linked iron oxide nanoparticles (CLIO) by cross-linking the dextran polymer using epichlorohydrin or ammonia. Ammonia treatment of CLIOs introduced primary amine groups to the particle surfaces, which facilitated attachment of other functional moieties. The resulting nanoparticles were extensively evaluated in a variety of MRI and theranostic applications [71, 87, 184]. The CLIOs exhibited a long blood circulation time without inducing an acute toxic response [185]; however, the persistence and stability, as well as the presence of trace amounts of the epichlorohydrin reactant, were problematic in the clinical setting, and further development of these agents has slowed [186].

Atomic transfer radical polymerization (ATRP) is another common method for coating iron oxide nanoparticles [187]. Li *et al.* used the ATRP method to synthesize polystyrene-coated iron oxide nanoparticles using divinylbenzene as a cross-linker [188]. Several other polymers, including polyvinyl alcohol (PVA) [189], polyvinyl pyrrolidone (PVP) [190], and polyacrylic acid [191], were described as coating materials for iron oxide nanoparticles. These polymers

provided a steric barrier to prevent nanoparticle agglomeration and enhance the blood circulation time. In addition, a variety of monomeric species, including bisphosphonates [192], dimercaptosuccinic acid (DMSA) [193], and alkoxysilanes [194], has been evaluated as anchors to facilitate attachment of polymers to the nanoparticle surfaces. Cheon *et al.* developed water-soluble iron oxide (WSIO) nanocrystals using DMSA as coating materials [195]. The DMSA formed a stable coating on the magnetic Fe₃O₄ nanocrystals through carboxylic chelating bonds, then further stabilized the shells through intermolecular disulfide cross-linkages. The remaining free DMSA thiol groups were linked to a breast cancer-targeting molecule, Herceptin. The WSIO-Herceptin probes specifically targeted breast cancer cells to provide a targeted MRI contrast agent, as revealed by T2-weighted MRI. Cheon *et al.* also developed a hybrid nanoparticle probe for PET/MR imaging consisting of albumin-stabilized iron oxide nanoparticles [196]. Serum albumins were linked to oleic acid-coated manganese-doped magnetic engineered iron oxide (MnMEIO) nanoparticles via ligand exchange, and the surfaces of the nanoparticles were further stabilized by EDC/NHS-mediated cross-linking between the amine and carboxyl groups of the serum albumin. The resultant MnMEIO nanoparticles showed high colloidal stability over a wide range of pH and at high salt concentrations. The tyrosine residues in the serum albumin could be directly conjugated to ¹²⁴I to introduce radioactive properties. This nanoparticle platform was also used to develop all-in-one target cell-specific magnetic nanoparticles for simultaneous molecular imaging and siRNA delivery [197]. To target αvβ3 integrin-positive cancer cells and to inhibit specific protein expression, SH-PEG-RGD and SH-siRNA-Cy5, respectively, were conjugated to MnMEIO via an SPDP cross-linker. *In vitro* evaluation of MRI and gene suppression demonstrated that these multimodal nanoparticle systems selectively silenced genes, confirming their theranostic behavior.

Liposomes and micellar dispersions provide another shielding strategy. Spherical assemblies of amphiphilic molecules can be used to coat magnetic nanoparticles by incorporating the nanoparticles within hydrophilic or hydrophobic cores to enhance blood circulation time. The amphiphilic substructures can encapsulate additional therapeutic agents or functional molecules within the core to easily achieve multifunctional nanoparticles. Lesieur *et al.* developed magnetic-fluid-loaded liposomes (MFLs) by encapsulating maghemite (γ-Fe₂O₃) nanocrystals in the unilamellar vesicles of (DSPE)-mPEG2000 and egg

phosphatidylcholine [198]. MFLs with a hydrodynamic size of 195 ± 33 nm were prepared by film hydration followed by extrusion. The particles were stable without the need for ferrofluid flocculation under physiological conditions. *In vivo* tests in mice using MR angiography demonstrated that the presence of MFLs enhanced the image contrast significantly, and the particles persisted in the blood 24 h after injection, possibly due to the stealth properties conveyed by PEGylation of the MFLs. Huh and Haam developed multifunctional magneto-polymeric nanohybrids (MNPNs) using polymeric micelles, and they evaluated the *in vivo* uses of the particles for simultaneous diagnosis and therapy [199]. Water solubility was achieved by embedding the hydrophobic magnetic nanocrystals and Dox within amphiphilic poly(ethylene glycol)-block-poly(D,L-lactic-co-glycolic acid) (PEG-PLGA) using nanoemulsion methods, and Herceptin was conjugated to the terminal PEG-PLGA carboxyl groups for selective targeting. Manganese ferrite (MnFe_2O_4) and Dox were present in the MNPNs at 41.7 wt% and 3.3 wt%, respectively. *In vivo* MRI and therapeutic tests in a mouse model bearing NIH3T6.7 cells demonstrated that the Herceptin-conjugated multifunctional polymeric micelles were site-specifically delivered to the tumor tissues that overexpressed HER2/neu receptors. The particles retarded the rapid growth of the tumors. Gao *et al.* used polymeric micelles to prepare $\alpha\beta 3$ integrin targeting theranostic nanoparticles [200]. The amphiphilic block copolymers of maleimide-terminated poly(ethylene glycol)-block-poly(D,L-lactide) (MAL-PEG-PLA) and methoxy-terminated poly(ethylene glycol)-block-poly(D,L-lactide) (MPEG-PLA) were used to form micelles. Oleic acid- and oleylamine-stabilized SPIONs and Dox were encapsulated into polymeric micelles via a solvent evaporation method, and thiol-containing cRGD was attached to the surfaces of the micelles. *In vitro* MRI and cytotoxicity studies confirmed the ultrasensitivity, enhanced MRI contrast properties, and $\alpha\beta 3$ integrin-specific therapeutic response to the multifunctional nanoplatform. The presence of ionizable ammonium groups on Dox ($\text{PK}_a=7$) suggested that the drug release rate should be pH-dependent.

In addition to organic coatings, core-shell structures, such as biocompatible silica- or gold-covered magnetic nanoparticles, have provided an attractive approach to developing stealth nanoparticles. Silica shells serve as protective stable nanoparticle coatings under aqueous conditions. The ability to encapsulate functional molecules within the nanoparticle matrix is a unique feature of these nanostructures. Hyeon and

Moon developed Fe_3O_4 nanocrystal-embedded, core-shell mesoporous silica nanoparticles, and they demonstrated their multifunctional application to simultaneous MR/optical imaging and drug delivery [201]. This study suggested a precise method for controlling the size of the silica nanoparticles smaller than 100 nm. The surfactant cetyltrimethylammonium bromide (CTAB) provided an organic template for the formation of a mesoporous silica shell and stabilized the hydrophobic Fe_3O_4 nanocrystals in an aqueous solution. The sol-gel process occurred through the template by using tetraethylorthosilicate (TEOS) and rhodamine B isothiocyanate (RITC)-labeled aminopropyltriethoxysilane (APS), and generated amine groups containing silica shell, to which PEG was covalently conjugated via succinimidyl end group to render further biocompatibility. Dox molecules loaded onto the as-synthesized $\text{Fe}_3\text{O}_4@m\text{SiO}_2(\text{R})$ -PEG NPs to convey therapeutic properties. The core-shell structure exhibited magnetic and fluorescent properties, as well as a therapeutic index, suggesting the utility of the nanostructure in biomedical theranostic applications. On the other hand, gold provides several advantages as a coating material due to its inertness and its unique ability to absorb near-IR radiation. Hyeon and Cho *et al.* described magnetic gold nanoshells (Mag-GNS) consisting of gold nanoshells encapsulating magnetic Fe_3O_4 nanoparticles as a novel nanomedical platform for simultaneous diagnostic imaging and thermal therapy [202]. Monodisperse 7 nm Fe_3O_4 nanoparticles stabilized with 2-bromo-2-methylpropionic acid (BMPA) were covalently attached to amino-modified silica spheres through a direct nucleophilic substitution reaction between the bromo groups and the amino groups. Gold seed nanoparticles were then attached to the residual amino groups of the silica spheres. Finally, a complete 15 nm thick gold shell embedded with Fe_3O_4 nanoparticles formed around the silica spheres to generate Mag-GNS. To target breast cancer, an anti-HER2/neu antibody was conjugated onto the surfaces of the Mag-GNS. SKBR3 breast cancer cells treated with Mag-GNS could be detected using a clinical MRI system, followed by selective destruction by near-IR radiation.

A new class of non-biofouling zwitterionic materials was recently developed [203]. The low fouling properties with respect to blood serum or plasma were attributed to strong interactions between the zwitterions and the neighboring water molecules, thereby offering good colloidal stability. The zwitterionic state was macroscopically neutral with a net zero charge that provided a non-fouling surface [204-206]. *In vivo* tests of the zwitterion-coated QDs

demonstrated that the surfaces were protein-resistant, which made it possible for the QDs to remain small relative to the PEG-decorated particles [207,208]. Jiang *et al.* developed poly(carboxybetaine acrylamide) (polyCBAA)-functionalized surfaces that were used to stabilize gold nanoparticles using the ATRP method [209]. This surface platform was highly resistant to nonspecific protein adsorption, and it presented abundant carboxyl groups for biomolecule immobilization. However, ATRP reactions require surface-grafted initiators and oxygen-free conditions, which limit their practical application. This problem was addressed by another strategy, the 'graft-to-surface' method [210], in which a zwitterionic poly(carboxybetaine methacrylate) (pCBMA) polymer was grafted onto the surface via two 3,4-dihydroxyphenyl-L-alanine (DOPA) adhesive moieties, and iron oxide nanoparticles were fabricated from the as-synthesized pCBMA-DOPA₂. Amine-containing cRGD peptides were immobilized onto the nanoparticles via the EDC/NHS chemistry. pCBMA-DOPA₂-decorated magnetic nanoparticles exhibited a lower macrophage uptake than the dex-

tran-coated magnetic nanoparticles. Uptake by human umbilical vein endothelial cells (HUVEC) was considerably higher due to cRGD-mediated targeting, as demonstrated by MRI studies.

Optimal density of the non-biofouling moieties and targeting ligands

Non-biofouling moieties, present as shielding materials, not only provide a steric barrier to prevent nonspecific protein absorption, they can tailor the surface properties of the nanoparticles to avoid recognition by the RES. The successful *in vivo* performance of a nanoparticle system relies critically on the non-biofouling properties, the molecular weight, the surface structural conformation, and the surface coverage ratio [211,212]. The surface density and conformation are important features for improving the stealth and targeting efficiency. To this end, PEG-linked liposomal nanoparticle surfaces have been engineered. As shown in Figure 17, individual PEG chains on a liposomal surface exhibited a Flory dimension, R_f , which represents the volume occupied by each flexible PEG molecule [213].

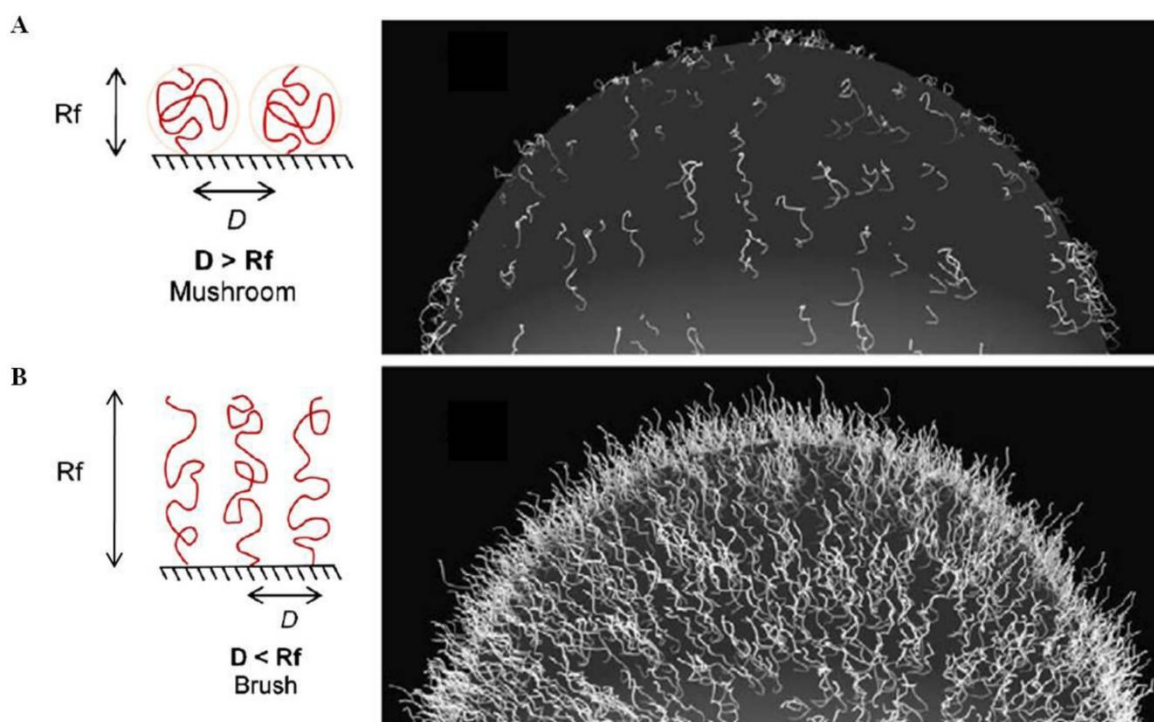


Figure 17. Representations of different PEG conformations, formed through their incorporation onto surfaces at different densities. (A) Low surface coverage levels of PEG lead to the "mushroom" configuration ($D > R_f$). (B) High surface coverage levels restrict the mobility of the PEG chains and lead to the "brush" configuration ($D < R_f$). Reproduced with permission from ref. [213] and [216].

A high surface coverage and a high concentration of the PEG-lipids within a liposomal formulation decrease the distance, D , between each PEG molecule on the nanoparticle surface. If $D > R_f$, the PEG chains self-assemble into a random-coil like 'mushroom' configuration. On the other hand, if $D < R_f$, the lateral pressure between the overcrowded PEG extends the PEG chains to a semi-linear 'brush' configuration [214]. In general, the brush configuration of surface PEGs conveys greater protein repulsion and enhanced nanoparticle lifetime in the blood stream [215-217]. This surface configuration can also decrease the mobility of the PEG chains, thereby diminishing the stealth functionalities of the PEG layer [218], and hinder binding between the targeting ligands of the nanoparticles and the target cancer cells [213]. Therefore, the surface coverage of the nanoparticle must be optimized during the design of any theranostic system.

Despite the critical role of the targeting ligand density on the nanoparticle surfaces, few studies have reported maximization of a nanoparticle system targeting efficacy. Higher concentrations of the targeting ligands on the nanoparticles often increase cellular uptake [219,220]. Targeting ligands must be present on the nanoparticle surfaces at concentrations that exceed a minimum threshold for binding [221]. However, some studies also demonstrated that high ligand densities do not improve binding to the target cancer cells and can even promote nonspecific interactions with endothelial and other non-cancerous cells, which increases immunogenicity, thereby causing opsonization-mediated clearance of the nanoparticles [222]. Gao *et al.* prepared 0%, 5%, or 16% RGD ligand-immobilized Dox-loaded polymeric micelles to investigate their *in vitro* targeting and therapeutic properties [200]. The 16% RGD ligand-bearing nanoparticles displayed the highest cellular uptake and cytotoxicity in $\alpha\beta3$ integrin-overexpressing SLK cells. Berklund *et al.* modulated the reactive sites on the nanoparticle surfaces for peptide conjugation by controlling the mixture ratio of the two surfactants during nanoparticle fabrication [223]. They prepared PLGA nanoparticles with several ratios of the carboxyl and hydroxyl groups in the Pluronic® surfactant (100:0 75:25, 50:50, 25:75, and 0:100 (v/v)), and cLABEL peptides were conjugated to the surfaces to achieve intercellular cell adhesion molecule-1 (ICAM-1) targeting. Incubation of the cLABEL-PLGA nanoparticles with the target A549 cancer cells revealed a maximum uptake for surfactant ratios of 50:50 or 25:75. Interestingly, the minimum uptake occurred for the surfactant ratios of 100:0 and 75:25. The enhanced receptor binding at moderate ligand densities may have

been due to receptor behavior during the binding process. ICAM-1 mobility on the cell surface leads to clustering during ligand binding [224], and a high density of the targeting ligands can disturb the clustering. This result suggests that the ligand spacing should be considered during surface engineering of targeted nanoparticle systems. Recently, Ashley *et al.* developed targeted silica nanoporous particle-supported lipid bilayers that provided enhanced surface fluidity, which recruited multiple peptides to the target cancer cells to promote multivalent effects [6]. The unique long-range fluidity of the nanoparticle surface promoted a high affinity between the targeting peptides on the nanoparticles and the target cancer cells at low peptide densities (6 peptides per particle). This specific targeting is crucial for reducing nonspecific interactions and enhancing specific affinity, which maximize the selective delivery of a cargo.

It has become increasingly clear that the tumor-targeting properties of the nanoparticles optimized *in vitro* are not predictive of the *in vivo* performance. Farokhzad and Langer identified maximally targeted and maximally stealth surface engineering conditions for *in vitro* and *in vivo* performance using PSMA targeted aptamer-conjugated Dtxl-loaded self-assembled nanoparticles [225]. Nanoparticles were prepared with different compositions of the self-assembled diblock copolymers and aptamers, and the optimal aptamer density on the nanoparticle surface was initially determined *in vitro*. Increasing the ligand density to 5% significantly increased the nanoparticle uptake by the target cells (LNCaP), whereas further increase in aptamer density modestly increased the nanoparticle uptake. These results indicated that the optimum ligand density for PSMA-specific endocytosis *in vitro* was 10–80 nmol aptamer per μmol nanoparticle. LNCaP xenograft mouse models injected with the targeted nanoparticles showed that increasing the aptamer density from 0% to 5% significantly increased nanoparticle retention in tumors, but the retention decreased for aptamer densities beyond 10%. The authors suggested that higher aptamer densities may have reduced the nanoparticle stealth properties, resulting in rapid clearance by the liver. Gabizon *et al.* optimized the ligand density in the Her2-targeted PEGylated liposomal Dox system (HT-PLD) *in vivo* for ligand ratios of 7.5, 15, or 30 per liposome [226]. The best safety margin and *in vivo* performance resulted from a ligand density of 15 ligands per liposome in the HT-PLD formulation. A 30 ligand ratio accelerated plasma clearance in the tumor-bearing mice, and the 7.5 ligand ratio reduced cytotoxicity after *in vivo* passage.

The role of nanoparticle geometry in tumor tar-

getting has received relatively little attention, although it is important for determining the binding affinity for a target cell. Sailor *et al.* systemically optimized *in vivo* tumor targeting by varying the nanomaterial shape (elongated versus spherical), targeting ligand type (cell surface targeting versus extracellular matrix targeting), ligand surface coverage, and attachment chemistry (Figure 18) [227]. They prepared two types of tumor-targeting peptides (F3 or CREKA) and conjugated the peptides to magnetic nanoworms (NWs) or magnetic nanospheres (NSs) at varying numbers of targeting peptides and for varying PEG lengths. Intravenous injection of the magnetic nanostructures in the tumor xenograft mice models revealed that the *in vivo* tumor-targeting properties of the NWs were superior to those of the NSs due to multivalent interactions between the elongated NWs and the receptors on the tumor cell surfaces. The smaller neutral

CREKA targeting moiety was more effective than the larger positively charged F3 targeting moiety, presumably because multiple copies of the highly cationic F3 caused a large increase in the surface charge on the particles, which facilitated clearance by the MPS-related organs. The most effective number of CREKA peptides was 60 per NW. Above 60 peptides per NW, the blood circulation time decreased. For a given number of peptides bound to the NWs, the presence of a PEG linker facilitated peptide targeting by reducing conformational restriction as well as increasing the residence time of the nanostructures in the blood stream. The short SMCC linker restricted the targeting peptide conformation. These results suggest some design guidelines for the development of targeted multifunctional nanoparticle systems for cancer imaging and therapy.

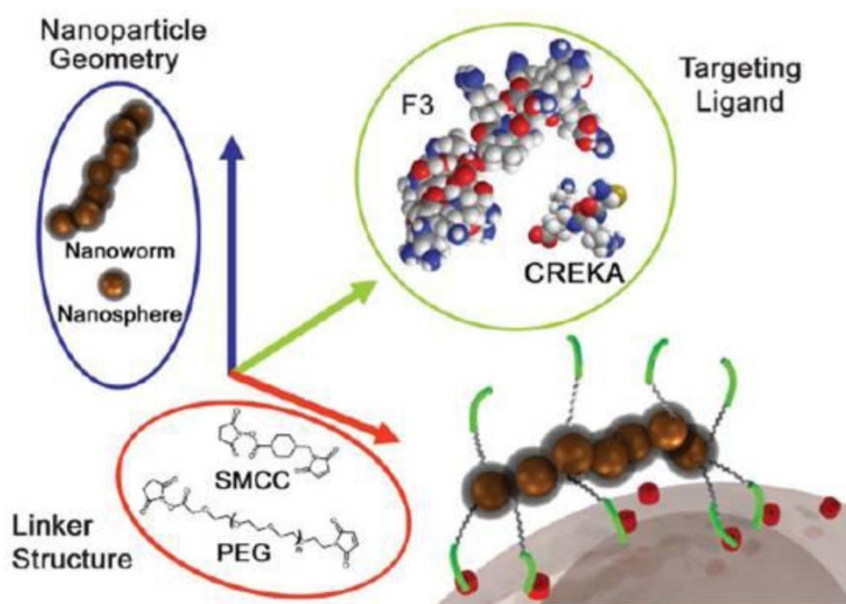


Figure 18. Three parameters were varied to optimize *in vivo* tumor targeting: the shape of the nanoparticle, the type of the targeting ligand, and the nature of the molecular linker. Two types of surface linkers were used to attach the targeting groups to the magnetic NWs or NSs. A short hydrocarbon places the targeting peptide (either F3 or CREKA, green lines) in close proximity to the dextran-coated nanostructure. A 5 kDa PEG linker places the targeting peptide further from the surface. The number of targeting groups per NW was varied to maximize the *in vivo* circulation time and optimize the *in vivo* tumor-targeting efficiency. These linker chemistries were tested on magnetic NSs. The NWs consisted of several NS cores linked together in a chain. Reproduced with permission from ref. [227].

5. Conclusions and perspectives

Considerable effort has been made toward the research and development of multifunctional nanoparticle systems for cancer targeted imaging and therapy. Among the nanoparticle platforms, magnetic

nanoparticle-based theranostic systems show particular promise. The intrinsic magnetic properties lend themselves to diagnostic MRI applications, and the surfaces may be easily modified using a variety of targeting moieties, such as antibodies, peptides, small molecules, aptamers, or therapeutic agents through a

number of conjugation strategies. Furthermore, magnetic nanoparticles unlike other inorganic nanoparticles such as gold- and carbon-based ones can be degraded to Fe ions in the body particularly in the acidic compartments of cells (e.g. lysosomes), alleviating the potential toxicity of long-term residence of nanoparticles. Therefore, magnetic nanoparticle formulations are considered valuable tool for disease diagnosis with anatomical details at an early stage, delivery of therapeutic agents to the target tumor sites, real-time monitoring of therapeutic responses, thereby currently attracting increasing interest for clinical utility. For the preparation of nanoparticles in potential clinical uses, it is critical to be aware of the design parameters discussed in this review. Better characterization methodologies are also needed, including pharmacokinetics and long-term toxicity studies. The costs required to integrate multiple components is an additional consideration for commercial viability. Although all such considerations are to be resolved in the near future, one should consider the regulatory hurdles encountered during clinical trials. The required regulatory processes become more complexed with the multifunctionalities of the nanoparticles because they are consisted of multiple additional components and also claim multiple indications with single nanoparticle. Nonetheless, there is high probability that cancer-specific nanoprobe arming with therapeutic capabilities are to be used in clinic in the near future because they are able to meet unmet medical needs for effective cancer treatments with minimal adverse effects.

Acknowledgements

This study was supported by a grant of the Korea Health technology R&D Project, Ministry of Health & Welfare, Republic of Korea (A101890).

Conflict of Interest

The authors have declared that no conflict of interest exists.

References

- Boyle P, Levin B. World Cancer Report. World Health Organization Press; 2008.
- Jemal A, Siegel R, Xu J, Ward E. Cancer statistics. *CA Cancer J Clin.* 2010; 60: 277-300.
- Maeda H. The enhanced permeability and retention (EPR) effect in tumor vasculature: the key role of tumor-selective macromolecular drug targeting. *Adv Enzyme Regul.* 2001; 41: 189-207.
- Allen TM. Ligand-targeted therapeutics in anticancer therapy. *Nat Rev Cancer.* 2002; 2: 705-63.
- Torchilin VP. Nanoparticulates as drug carriers. Imperial college press; 2006.

- Ashley CE, Carnes EC, Phillips GK, Padilla D, Durfee PN, Brown PA, et al. The targeted delivery of multicomponent cargos to cancer cells by nanoporous particle-supported lipid bilayers. *Nat Mater.* 2011; 10: 389-97.
- Cho EC, Glaus C, Chen J, Welch MJ, Xia Y. Inorganic nanoparticle-based contrast agents for molecular imaging. *Trends Mol Med.* 2010; 16: 561-73.
- Lee S, Kwon IC, Kim K. Multifunctional Nanoparticles for Cancer Theragnosis. In: Chen X, ed. *Nanoplatform-Based Molecular Imaging.* Hoboken, NJ, USA: John Wiley & Sons, Inc. 2011.
- Kievit FM, Zhang M. Surface engineering of iron oxide nanoparticles for targeted cancer therapy. *Acc Chem Res.* 2011; [Epub ahead of print].
- Varadan VK, Chen L, Xie J. Biomedical applications of magnetic nanoparticles, in *Nanomedicine: design and applications of magnetic nanomaterials, nanosensors and nanosystems.* Chichester, UK: John Wiley & Sons, Inc. 2008.
- Jones A, Harris AL. New developments in angiogenesis: a major mechanism for tumor growth and target for therapy. *Cancer J Sci Am.* 1998; 4: 209-17.
- Hobbs SK, Monsky WL, Yuan F, Roberts WG, Griffith L, Torchilin VP, et al. Regulation of transport pathways in tumor vessels: role of tumor type and microenvironment. *Proc Natl Acad Sci USA.* 1998; 95: 4607-12.
- Shubik P. Vascularization of tumors: a review. *J Cancer Res Clin Oncol.* 1982; 103: 211-26.
- Yaun F, Dellian M, Fukumura D, Leunig M, Berk DA, Torchilin VP, et al. Vascular permeability in a human tumor xenograft: molecular size dependence and cutoff size. *Cancer Res.* 1995; 55: 3752-56.
- Allen TM, Cullis PR. Drug delivery systems: entering the mainstream. *Science.* 2004; 303: 1818-22.
- Byrne JD, Betancourt T, Brannon-Peppas L. Active targeting schemes for nanoparticle systems in cancer therapeutics. *Adv Drug Deliv Rev.* 2008; 60:1615-26.
- Gabizon A, Martin F. Polyethylene glycol-coated (pegylated) liposomal doxorubicin. Rationale for use in solid tumours. *Drugs.* 1997; 54: 15-21.
- Gabizon A, Shmeeda H, Barenholz Y. Pharmacokinetics of pegylated liposomal Doxorubicin: review of animal and human studies. *Clin Pharmacokinet.* 2003; 42: 419-36.
- Allen TM, Martin FJ. Advantages of liposomal delivery systems for anthracyclines. *Semin Oncol.* 2004; 31: 5-15.
- Desai N, Trieu V, Yao Z, Louie L, Ci S, Yang A, et al. Increased antitumor activity, intratumor paclitaxel concentrations, and endothelial cell transport of cremophor-free, albumin-bound paclitaxel, ABI-007, compared with cremophor-based paclitaxel. *Clin Cancer Res.* 2006; 12: 1317-24.
- Miele E, Spinelli GP, Tomao F, Tomao S. Albumin-bound formulation of paclitaxel (Abraxane ABI-007) in the treatment of breast cancer. *Int J Nanomed.* 2009; 4: 99-105.
- Bae YH. Drug targeting and tumor heterogeneity. *J Control Release.* 2009; 133: 2-3.
- Mishra S, Webster P, Davis ME. PEGylation significantly affects cellular uptake and intracellular trafficking of non-viral gene delivery particles. *Eur J Cell Biol.* 2004; 83: 97-111.
- Romberg B, Hennink W, Storm G. Shedable Coatings for Long-Circulating Nanoparticles. *Pharm Res.* 2008; 25: 55-71.
- Hong RL, Huang CJ, Tseng YL, Pang VF, Chen ST, Liu JJ, et al. Direct comparison of liposomal doxorubicin with or without polyethylene glycol coating in C-26 tumor-bearing mice: Is surface coating with polyethylene glycol beneficial. *Clin Cancer Res.* 1999; 5: 3645-52.
- Gullotti E, Yeo Y. Extracellularly activated nanocarriers: a new paradigm of tumor targeted drug delivery. *Mol Pharm.* 2009; 6:1041-51.

27. Gottesman MM, Fojo T, Bates SE. Multidrug resistance in cancer: Role of ATP-dependent transporters. *Nature Rev Cancer*. 2002; 2: 48-58.
28. Peer D, Karp JM, Hong S, Farokhzad OC, Margalit R, Langer R. Nanocarriers as an emerging platform for cancer therapy. *Nat Nanotechnol*. 2007; 2: 751-60.
29. Pastan I, Hassan R, FitzGerald DJ, Kreitman RJ. Immunotoxin therapy of cancer. *Nat Rev Cancer*. 2006; 6: 559-65.
30. Shi J, Xiao Z, Kamaly N, Farokhzad OC. Self-Assembled Targeted Nanoparticles: Evolution of Technologies and Bench to Bedside Translation. *Acc Chem Res*. 2011; [Epub ahead of print]
31. Krown SE, Northfelt DW, Osoba D, Stewart JS. Use of liposomal anthracyclines in Kaposi's sarcoma. *Semin Oncol*. 2004; 31: 36-52.
32. Mrózek E, Rhoades CA, Allen J, Hade EM, Shapiro CL. Phase I trial of liposomal encapsulated doxorubicin (Myocet; D-99) and weekly docetaxel in advanced breast cancer patients. *Ann Oncol*. 2005; 16: 1087-93.
33. O'Brien ME, Wigler N, Inbar M, Rosso R, Grischke E, Santoro A, et al. Reduced cardiotoxicity and comparable efficacy in a phase III trial of pegylated liposomal doxorubicin HCl (CAELYX/Doxil) versus conventional doxorubicin for first-line treatment of metastatic breast cancer. *Ann Oncol*. 2004; 15: 440-9.
34. Sarris AH, Hagemester F, Romaguera J, Rodriguez MA, McLaughlin P, Tsimberidou AM, et al. Liposomal vincristine in relapsed non-Hodgkin's lymphomas: early results of an ongoing phase II trial. *Ann Oncol*. 2000; 11: 69-72.
35. Petrelli F, Borrono K, Barni S. Targeted delivery for breast cancer therapy: the history of nanoparticle-albumin-bound paclitaxel. *Expert Opin Pharmacother*. 2010; 11: 1413-32.
36. Lim WT, Tan EH, Toh CK, Hee SW, Leong SS, Ang PC, et al. Phase I pharmacokinetic study of a weekly liposomal paclitaxel formulation (Genexol-PM) in patients with solid tumors. *Ann Oncol*. 2010; 21: 382-8.
37. Davis ME. The first targeted delivery of siRNA in humans via a self-assembling, cyclodextrin polymer-based nanoparticle: from concept to clinic. *Mol Pharmaceutics*. 2009; 6: 659-68.
38. Sankhala KK, Mita AC, Adinin R, Wood L, Beeram M, Bullock S, et al. A phase I pharmacokinetic (PK) study of MBP-426, a novel liposome encapsulated oxaliplatin. *J Clin Oncol*. 2009; 27: S2535.
39. Matsumura Y, Gotoh M, Muro K, Yamada Y, Shirao K, Shimada Y, et al. Phase I and pharmacokinetic study of MCC-465, a doxorubicin (DXR) encapsulated in PEG immunoliposome, in patients with metastatic stomach cancer. *Ann Oncol*. 2004; 15: 517-25.
40. [Internet] BIND Biosciences initiates Phase 1 clinical study of BIND-014. [http://www.bindbio.com/content/pages/news/news_detail.jsp/q/news-id/55\(1/18/2011\)](http://www.bindbio.com/content/pages/news/news_detail.jsp/q/news-id/55(1/18/2011)).
41. Nemunaitis J, Senzer N, Bedell C, Nunan R, Sleer L, Chang E. A phase I study of escalating doses of SGT-53 for intravenous infusion of patients with advanced solid tumors. *Mol Ther*. 2009; 17: S226.
42. Kumar CS. *Nanomaterials for medical diagnosis and therapy*. Wiley-VCH. 2007.
43. Montet X, Funovics M, Montet-Abou K, Weissleder R, Josephson L. Multivalent effects of RGD peptides obtained by nanoparticle display. *J Med Chem*. 2006; 49: 6087-93.
44. Gao J, Gu H, Xu B. Multifunctional magnetic nanoparticles: design, synthesis, and biomedical applications. *Acc Chem Res*. 2009; 42: 1097-107.
45. Das M, Mishra D, Dhak P, Gupta S, Maiti TK, Basak A, et al. Biofunctionalized, Phosphonate-Grafted, Ultrasmall Iron Oxide Nanoparticles for Combined Targeted Cancer Therapy and Multimodal Imaging. *Small*. 2009; 5: 2883-93.
46. Pan D, Caruthers SD, Hu G, Senpan A, Scott MJ, Gaffney PJ, et al. Ligand-directed nanobialys as theranostic agent for drug delivery and manganese-based magnetic resonance imaging of vascular targets. *J Am Chem Soc*. 2008; 130: 9186-7.
47. Bae KH, Lee K, Kim C, Park TG. Surface functionalized hollow manganese oxide nanoparticles for cancer targeted siRNA delivery and magnetic resonance imaging. *Biomaterials*. 2011; 32: 176-84.
48. James JS, Dubs G. FDA approves new kind of lymphoma treatment. *AIDS Treat News* 1997; 284: 2-3.
49. Albanell J, Baselga J. Trastuzumab. A humanized anti-HER2 monoclonal antibody, for the treatment of breast cancer. *Drugs Today*. 1999; 35: 931-46.
50. Ferrara N. VEGF as a therapeutic target in cancer. *Oncology*. 2005; 69: 11-6.
51. Van Cutsem E, Köhne CH, Hitre E, Zaluski J, Chang Chien CR, Makhson A, et al. Cetuximab and chemotherapy as initial treatment for metastatic colorectal cancer. *N Engl J Med*. 2009; 360: 1408-17.
52. Hadjipanayis CG, Machaidze R, Kaluzova M, Wang L, Schuette AJ, Chen H, et al. EGFRvIII antibody-conjugated iron oxide nanoparticles for magnetic resonance imaging-guided convection-enhanced delivery and targeted therapy of glioblastoma. *Cancer Res*. 2010; 70: 6303-12.
53. Gao X, Cui Y, Levenson RM, Chung LW, Nie S. In vivo cancer targeting and imaging with semiconductor quantum dots. *Nat Biotechnol*. 2004; 22: 969-76.
54. Raghavan R, Brady ML, Rodríguez-Ponce MI, Hartlep A, Pedain C, Sampson JH. Convection-enhanced delivery of therapeutics for brain disease, and its optimization. *Neurosurg Focus*. 2006; 20: E12.
55. Bobo RH, Laske DW, Akbasak A, Morrison PF, Dedrick RL, Oldfield EH. Convection-enhanced delivery of macromolecules in the brain. *Proc Natl Acad Sci U S A* 1994; 91: 2076-80.
56. Hadjipanayis CG, Fellows-Mayle W, Deluca NA. Therapeutic efficacy of a herpes simplex virus in combination with radiation or temozolomide for intracranial glioblastoma after convection-enhanced delivery. *Mol Ther*. 2008; 16: 1783-8.
57. Morrison PF, Laske DW, Bobo H, Oldfield EH, Dedrick RL. High-flow microinfusion: tissue penetration and pharmacodynamics. *Am J Physiol*. 1994; 266: R292-305.
58. Ling Y, Wei K, Luo Y, Gao X, Zhong S. Dual docetaxel/superparamagnetic iron oxide loaded nanoparticles for both targeting magnetic resonance imaging and cancer therapy. *Biomaterials*. 2011; 32: 7139-50.
59. Wenthe MN, Jain A, Kono E, Berberat PO, Giese T, Reber HA, et al. Prostate stem cell antigen is a putative target for immunotherapy in pancreatic cancer. *Pancreas* 2005; 31: 119-25.
60. Chen G, Chen W, Wu Z, Yuan R, Li H, Gao J, et al. MRI-visible polymeric vector bearing CD3 single chain antibody for gene delivery to T cells for immunosuppression. *Biomaterials*. 2009; 30: 1962-70.
61. Tromsdorf UI, Bigall NC, Kaul MG, Bruns OT, Nikolic MS, Mollwitz B, et al. Size and surface effects on the MRI relaxivity of manganese ferrite nanoparticle contrast agents. *Nano Lett* 2007; 7: 2422-7.
62. Olenchock BA, Guo R, Carpenter JH, Jordan M, Topham MK, Koretzky GA, et al. Disruption of diacylglycerol metabolism impairs the induction of T cell anergy. *Nat Immunol* 2006; 7: 1174-81.
63. Zhong XP, Hainey EA, Olenchock BA, Zhao H, Topham MK, Koretzky GA. Regulation of T cell receptor-induced activation of the Ras-ERK pathway by diacylglycerol kinase zeta. *J Biol Chem*. 2002; 277: 31089-98.
64. Lu RM, Chang YL, Chen MS, Wu HC. Single chain anti-c-Met antibody conjugated nanoparticles for in vivo tumor-targeted imaging and drug delivery. *Biomaterials*. 2011; 32: 3265-74.

65. Birchmeier C, Birchmeier W, Gherardi E, Vande Woude GF. Met, metastasis, motility and more. *Nat Rev Mol Cell Biol.* 2003; 4: 915-25.
66. Cappuzzo F, Marchetti A, Skokan M, Rossi E, Gajapathy S, Felicioni L, et al. Increased MET gene copy number negatively affects survival of surgically resected non-small-cell lung cancer patients. *J Clin Oncol.* 2009; 27: 1667-74.
67. Ding S, Merkulova-Rainon T, Han ZC, Tobelem G. HGF receptor up-regulation contributes to the angiogenic phenotype of human endothelial cells and promotes angiogenesis in vitro. *Blood.* 2003; 101: 4816-22.
68. Wang AZ, Gu F, Zhang L, Chan JM, Radovic-Moreno A, Shaikh MR, et al. Biofunctionalized targeted nanoparticles for therapeutic applications. *Expert Opin Biol Ther.* 2008; 8: 1063-70.
69. McCarthy JR, Bhaumik J, Karver MR, Sibel Erdem S, Weissleder R. Targeted nanoagents for the detection of cancers. *Mol Oncol.* 2010; 4: 511-28.
70. Beekman KW, Colevas AD, Cooney K, Dipaola R, Dunn RL, Gross M, et al. Phase II evaluations of cilengitide in asymptomatic patients with androgen-independent prostate cancer: scientific rationale and study design. *Clin Genitourin Cancer.* 2006; 4: 299-302.
71. Kumar M, Yigit M, Dai G, Moore A, Medarova Z. Image-guided breast tumor therapy using a small interfering RNA nanodrug. *Cancer Res.* 2010; 70: 7553-61.
72. Perey L, Hayes DF, Maimonis P, Abe M, O'Hara C, Kufe DW. Tumor selective reactivity of a monoclonal antibody prepared against a recombinant peptide derived from the DF3 human breast carcinoma-associated antigen. *Cancer Res.* 1992; 52: 2563-8.
73. Veisheh O, Sun C, Fang C, Bhattarai N, Gunn J, Kievit F, et al. Specific targeting of brain tumors with an optical/magnetic resonance imaging nanoprobe across the blood-brain barrier. *Cancer Res.* 2009; 69: 6200-7.
74. Lyons SA, O'Neal J, Sontheimer H. Chlorotoxin, a scorpion-derived peptide, specifically binds to gliomas and tumors of neuroectodermal origin. *Glia.* 2002; 39: 162-73.
75. Packer RJ, Cogen P, Vezina G, Rorke LB. Medulloblastoma: clinical and biologic aspects. *Neuro Oncol.* 1999; 1: 232-50.
76. Hallahan AR, Pritchard JJ, Hansen S, Benson M, Stoek J, Hattton BA, et al. The SmoA1 mouse model reveals that notch signaling is critical for the growth and survival of sonic hedgehog-induced medulloblastomas. *Cancer Res.* 2004; 64: 7794-800.
77. Veisheh M, Gabikian P, Bahrami SB, Veisheh O, Zhang M, Hackman RC, et al. Tumor paint: a chlorotoxin: Cy5.5 bioconjugate for intraoperative visualization of cancer foci. *Cancer Res.* 2007; 67: 6882-8.
78. Mok H, Park JW, Park TG. Enhanced intracellular delivery of quantum dot and adenovirus nanoparticles triggered by acidic pH via surface charge reversal. *Bioconjugate Chem.* 2008; 19: 797-801.
79. Min KH, Kim JH, Bae SM, Shin H, Kim MS, Park S, et al. Tumoral acidic pH-responsive MPEG-poly(beta-aminoester) polymeric micelles for cancer targeting therapy. *J Control Release.* 2010; 144: 259-66.
80. Sethuraman VA, Na K, Bae YH. pH-responsive sulfonamide/PEI system for tumor specific gene delivery: an in vitro study. *Biomacromolecules.* 2006; 7: 64-70.
81. Mok H, Veisheh O, Fang C, Kievit FM, Wang FY, Park JO, et al. pH-Sensitive siRNA nanovector for targeted gene silencing and cytotoxic effect in cancer cells. *Mol Pharm.* 2010; 7: 1930-9.
82. Lee Y, Fukushima S, Bae Y, Hiki S, Ishii T, Kataoka K. A protein nanocarrier from charge-conversion polymer in response to endosomal pH. *J Am Chem Soc.* 2007; 129: 5362-3.
83. Gasparini G, Brooks PC, Biganzoli E, Vermeulen PB, Bonoldi E, Dirix LY, et al. Vascular integrin $\alpha v \beta 3$: A new prognostic indicator in breast cancer. *Clin Cancer Res.* 1998; 4: 2625-34.
84. Murphy EA, Majeti BK, Barnes LA, Makale M, Weis SM, Lutu-Fuga K, et al. Nanoparticle-mediated drug delivery to tumor vasculature suppresses metastasis. *Proc Natl Acad Sci U S A.* 2008; 105: 9343-8.
85. He X, Na MH, Kim JS, Lee GY, Park JY, Hoffman AS, et al. A novel peptide probe for imaging and targeted delivery of liposomal doxorubicin to lung tumor. *Mol Pharm.* 2011; 8: 430-8.
86. Ashley CE, Carnes EC, Phillips GK, Padilla D, Durfee PN, Brown PA, et al. The targeted delivery of multicomponent cargos to cancer cells by nanoporous particle-supported lipid bilayers. *Nat Mater.* 2011; 10: 389-97.
87. Simberg D, Duza T, Park JH, Essler M, Pilch J, Zhang L, et al. Biomimetic amplification of nanoparticle homing to tumors. *Proc Natl Acad Sci U S A.* 2007; 104: 932-6.
88. Dvorak HF, Senger DR, Dvorak AM, Harvey VS, McDonagh J. Regulation of extravascular coagulation by microvascular permeability. *Science.* 1985; 227: 1059-61.
89. Abe K, Shoji M, Chen J, Bierhaus A, Danave I, Micko C, et al. Regulation of vascular endothelial growth factor production and angiogenesis by the cytoplasmic tail of tissue factor. *Proc Natl Acad Sci USA.* 1999; 96: 8663-8.
90. Pilch J, Brown DM, Komatsu M, Jarvinen TA, Yang M, Peters D, et al. Peptides selected for binding to clotted plasma accumulate in tumor stroma and wounds. *Proc Natl Acad Sci USA.* 2006; 103: 2800-4.
91. von Maltzahn G, Park JH, Lin KY, Singh N, Schwöppe C, Mesters R, et al. Nanoparticles that communicate in vivo to amplify tumour targeting. *Nat Mater.* 2011; 10: 545-52.
92. Park JH, von Maltzahn G, Zhang L, Schwartz MP, Ruoslahti E, Bhatia SN, et al. Magnetic Iron Oxide Nanoworms for Tumor Targeting and Imaging. *Adv Mater.* 2008; 20: 1630-5.
93. Zhang H, Ma Y, Sun XL. Recent developments in carbohydrate-decorated targeted drug/gene delivery. *Med Res Rev.* 2010; 30: 270-89.
94. Shen Z, Wei W, Tanaka H, Kohama K, Ma G, Dobashi T, et al. A galactosamine-mediated drug delivery carrier for targeted liver cancer therapy. *Pharmacol Res.* 2011; 64: 410-9.
95. Kim EM, Jeong HJ, Moon MH. Asialoglycoprotein receptor targeted gene delivery using galactosylated Polyethylenimine-graft -Poly (ethylene glycol): In vitro and in vivo studies. *J Control Release.* 2005; 108: 557-67.
96. Yang Y, Zhang Z, Chen L, Gu W, Li Y. Galactosylated poly(2-(2-aminoethoxy)ethoxy)phosphazene/DNA complex nanoparticles: in vitro and in vivo evaluation for gene delivery. *Biomacromolecules.* 2010; 11: 927-33.
97. Cho CS, Park IK, Cho CS. Galactosylated Poly (ethylene glycol)-Chitosan - graft- Polyethylenimine as a gene carrier for hepatocyte-targeting. *J Control Release.* 2008; 131: 150-7.
98. Lu W, Zhang G, Zhang R, Flores LG 2nd, Huang Q, Gelovani JG, et al. Tumor site-specific silencing of NF-kappaB p65 by targeted hollow gold nanosphere-mediated photothermal transfection. *Cancer Res.* 2010; 70: 3177-88.
99. Karin M, Cao Y, Greten FR, Li ZW. NF-kB in cancer: from innocent bystander to major culprit. *Nat Rev Cancer.* 2002; 2: 301-10.
100. Hirsch LR, Stafford RJ, Bankson JA, Sershen SR, Rivera B, Price RE, et al. Nanoshell-mediated near-infrared thermal therapy of tumors under magnetic resonance guidance. *Proc Natl Acad Sci U S A.* 2003; 100: 13549-54.
101. Hu M, Chen J, Li ZY, Au L, Hartland GV, Li X, et al. Gold nanocages: engineering their structure for biomedical applications. *Adv Mater.* 2005; 17: 2255-61.
102. Melancon MP, Lu W, Yang Z, Zhang R, Cheng Z, Elliot AM, et al. In vitro and in vivo targeting of hollow gold nanoshells directed at epidermal growth factor receptor for photothermal ablation therapy. *Mol Cancer Ther.* 2008; 7: 1730-9.

103. Lu W, Xiong C, Zhang G, Huang Q, Zhang R, Zhang JZ, et al. Targeted photothermal ablation of murine melanomas with melanocyte-stimulating hormone analog-conjugated hollow gold nanospheres. *Clin Cancer Res*. 2009; 15: 876-86.
104. Foraker AB, Khantwal CM, Swaan PW. Current perspectives on the cellular uptake and trafficking of riboflavin. *Adv Drug Deliv Rev*. 2003; 55: 1467-83.
105. Karande AA, Sridhar L, Gopinath KS, Adiga PR. Riboflavin carrier protein: a serum and tissue marker for breast carcinoma. *Int J Cancer*. 2001; 95: 277-81.
106. Jayapaul J, Hostenius M, Arns S, Lederle W, Lammers T, Comba P, et al. FMN-coated fluorescent iron oxide nanoparticles for RCP-mediated targeting and labeling of metabolically active cancer and endothelial cells. *Biomaterials*. 2011; 32: 5863-71.
107. Lee CM, Jeong HJ, Kim EM, Kim DW, Lim ST, Kim HT, et al. Superparamagnetic iron oxide nanoparticles as a dual imaging probe for targeting hepatocytes in vivo. *Magn Reson Med*. 2009; 62: 1440-6.
108. Wilson DS, Szostak JW. In vitro selection of functional nucleic acids. *Ann Rev Biochem*. 1999; 68: 611-47.
109. Tuerk C, Gold L. Systematic evolution of ligands by exponential enrichment: RNA ligands to bacteriophage T4 DNA polymerase. *Science*. 1990; 249: 505-10.
110. Lee JF, Hesselberth JR, Meyers LA, Ellington AD. Aptamer database. *Nucleic Acids Res*. 2004; 32: D95-100.
111. Lee JF, Stovall GM, Ellington AD. Aptamer therapeutics advance. *Curr Opin Chem Biol*. 2006; 10: 282-9.
112. Bates PJ, Kahlon JB, Thomas SD, Trent JO, Miller DM. Antiproliferative activity of G-rich oligonucleotides correlates with protein binding. *J Biol Chem*. 1999; 274: 26369-77.
113. Bates PJ, Laber DA, Miller DM, Thomas SD, Trent JO. Discovery and development of the G-rich oligonucleotide AS1411 as a novel treatment for cancer. *Exp Mol Pathol*. 2009; 86: 151-64.
114. Mongelard F, Bouvet P. AS-1411, a guanosine-rich oligonucleotide aptamer targeting nucleolin for the potential treatment of cancer, including acute myeloid leukemia. *Curr Opin Mol Ther*. 2010; 12: 107-14.
115. Bouchard PR, Hutabarat RM, Thompson KM. Discovery and development of therapeutic aptamers. *Annu Rev Pharmacol Toxicol*. 2010; 50: 237-57.
116. Lupold SE, Hicke BJ, Lin Y, Coffey DS. Identification and characterization of nuclease-stabilized RNA molecules that bind human prostate cancer cells via the prostate-specific membrane antigen. *Cancer Res*. 2002; 62: 4029-33.
117. Bagalkot V, Farokhzad OC, Langer R, Jon S. An aptamer-doxorubicin physical conjugate as a novel targeted drug-delivery platform. *Angew Chem Int Ed*. 2006; 45: 8149-52.
118. Kolishetti N, Dhar S, Valencia PM, Lin LQ, Karnik R, Lippard SJ, et al. Engineering of self-assembled nanoparticle platform for precisely controlled combination drug therapy. *Proc Natl Acad Sci USA*. 2010; 107: 17939-44.
119. Farokhzad OC, Cheng J, Teply BA, Sherifi I, Jon S, Kantoff PW, et al. Targeted nanoparticle-aptamer bioconjugates for cancer chemotherapy in vivo. *Proc Natl Acad Sci USA*. 2006; 103: 6315-20.
120. Farokhzad OC, Jon S, Khademhosseini A, Tran TN, Lavan DA, Langer R. Nanoparticle-aptamer bioconjugates: a new approach for targeting prostate cancer cells. *Cancer Res*. 2004; 64: 7668-72.
121. Bagalkot V, Zhang L, Levy-Nissenbaum E, Jon S, Kantoff PW, Langer R, et al. Quantum dot-aptamer conjugates for synchronous cancer imaging, therapy, and sensing of drug delivery based on bi-fluorescence resonance energy transfer. *Nano Lett*. 2007; 7: 3065-70.
122. Dassie JP, Liu XY, Thomas GS, Whitaker RM, Thiel KW, Stockdale KR, et al. Systemic administration of optimized aptamer-siRNA chimeras promotes regression of PSMA-expressing tumors. *Nat Biotechnol*. 2009; 27: 839-49.
123. Yu MK, Kim D, Lee IH, So JS, Jeong YY, Jon S. Image-Guided Prostate Cancer Therapy Using Aptamer-Functionalized Thermally Cross-Linked Superparamagnetic Iron Oxide Nanoparticles. *Small*. 2011; 7: 2241-9.
124. Hwang do W, Ko HY, Lee JH, Kang H, Ryu SH, Song IC, et al. A nucleolin-targeted multimodal nanoparticle imaging probe for tracking cancer cells using an aptamer. *J Nucl Med*. 2010; 51: 98-105.
125. Derenzini M, Sirri V, Trere D, Ochs RL. The quantity of nucleolar proteins nucleolin and protein B23 is related to cell doubling time in human cancer cells. *Lab Invest*. 1995; 73: 497-502.
126. Antunes P, Ginj M, Zhang H, Waser B, Baum RP, Reubi JC, et al. Are radiogallium-labelled DOTA-conjugated somatostatin analogues superior to those labelled with other radiometals. *Eur J Nucl Med Mol Imaging*. 2007; 34: 982-93.
127. Li N, Larson T, Nguyen HH, Sokolov KV, Ellington AD. Directed evolution of gold nanoparticle delivery to cells. *Chem Commun*. 2010; 46: 392-4.
128. Davis ME, Zuckerman JE, Choi CH, Seligson D, Tolcher A, Alabi CA, et al. Evidence of RNAi in humans from systemically administered siRNA via targeted nanoparticles. *Nature*. 2010; 464: 1067-70.
129. Gatter KC, Brown G, Trowbridge IS, Wollston RE, Mason DY. Transferrin receptors in human tissues: their distribution and possible clinical relevance. *J Clin Pathol*. 1983; 36: 539-45.
130. Cerqueira NM, Pereira S, Fernandes PA, Ramos MJ. Overview of ribonucleotide reductase inhibitors: an appealing target in anti-tumor therapy. *Curr Med Chem*. 2005; 12: 1283-94.
131. Gunthert U, Hofmann M, Rudy W, Reber S, Zoller M, Haubmann I, et al. A new variant of glycoprotein CD44 confers metastatic potential to rat carcinoma cells. *Cell*. 1991; 65: 13-24.
132. Platt VM, Szoka Jr FC. Anticancer therapeutics: targeting macromolecules and nanocarriers to hyaluronan or CD44, a hyaluronan receptor. *Mol Pharmaceutics*. 2008; 5: 474-86.
133. Bhang SH, Won N, Lee T, Jin H, Nam J, Park J, et al. Hyaluronic acid-quantum dot conjugates for in vivo lymphatic vessel imaging. *ACS Nano*. 2009; 3: 1389-98.
134. Wu W, Shen J, Banerjee P, Zhou S. Core-shell hybrid nanogels for integration of optical temperature-sensing, targeted tumor cell imaging, and combined chemo-photothermal treatment. *Biomaterials*. 2010; 31: 7555-66.
135. Ge Y, Zhang Y, He S, Nie F, Teng G, Gu N. Fluorescence Modified Chitosan-Coated Magnetic Nanoparticles for High-Efficient Cellular Imaging. *Nanoscale Res Lett*. 2009; 4: 287-95.
136. Lee H, Yu MK, Park S, Moon S, Min JJ, Jeong YY, et al. Thermally cross-linked superparamagnetic iron oxide nanoparticles: synthesis and application as a dual imaging probe for cancer in vivo. *J Am Chem Soc*. 2007; 129: 12739-45.
137. Talanov VS, Regino CA, Kobayashi H, Bernardo M, Choyke PL, Brechbiel MW. Dendrimer-based nanoprobe for dual modality magnetic resonance and fluorescence imaging. *Nano Lett*. 2006; 6: 1459-63.
138. Veiseh O, Gunn JW, Zhang M. Design and fabrication of magnetic nanoparticles for targeted drug delivery and imaging. *Adv Drug Deliv Rev*. 2010; 62: 284-304.
139. Brunel FM, Lewis JD, Destito G, Steinmetz NF, Manchester M, Stuhlmann H, et al. Hydrazone ligation strategy to assemble multifunctional viral nanoparticles for cell imaging and tumor targeting. *Nano Lett*. 2010; 10: 1093-7.
140. Destito G, Yeh R, Rae CS, Finn MG, Manchester M. Folic acid-mediated targeting of cowpea mosaic virus particles to tumor cells. *Chem Biol*. 2007; 14: 1152-62.
141. Lewis JD, Destito G, Zijlstra A, Gonzalez MJ, Quigley JP, Manchester M, et al. Viral nanoparticles as tools for intravital vascular imaging. *Nat Med*. 2006; 12: 354-60.

142. McLain L, Durrani Z, Wisniewski LA, Porta C, Lomonosoff GP, Dimmock NJ. Stimulation of neutralizing antibodies to human immunodeficiency virus type 1 in three strains of mice immunized with a 22 amino acid peptide of gp41 expressed on the surface of a plant virus. *Vaccine*. 1996; 14: 799-810.
143. Zhang J, Misra RD. Magnetic drug-targeting carrier encapsulated with thermosensitive smart polymer: core-shell nanoparticle carrier and drug release response. *Acta Biomater*. 2007; 3: 838-50.
144. Xie J, Chen K, Lee HY, Xu C, Hsu AR, Peng S, et al. Ultrasmall c(RGDyK)-coated Fe₃O₄ nanoparticles and their specific targeting to integrin alpha(v)beta3-rich tumor cells. *J Am Chem Soc*. 2008; 130: 7542-3.
145. Koole R, van Schooneveld MM, Hilhorst J, Castermans K, Cormode DP, Strijkers GJ, et al. Paramagnetic lipid-coated silica nanoparticles with a fluorescent quantum dot core: a new contrast agent platform for multimodality imaging. *Bioconjug Chem*. 2008; 19: 2471-9.
146. Reddy GR, Bhojani MS, McConville P, Moody J, Moffat BA, Hall DE, et al. Vascular targeted nanoparticles for imaging and treatment of brain tumors. *Clin Cancer Res*. 2006; 12: 6677-86.
147. Yu MK, Park J, Jeong YY, Moon WK, Jon S. Integrin-targeting thermally cross-linked superparamagnetic iron oxide nanoparticles for combined cancer imaging and drug delivery. *Nanotechnology*. 2010; 21: 415102.
148. Derfus AM, Chen AA, Min DH, Ruoslahti E, Bhatia SN. Targeted quantum dot conjugates for siRNA delivery. *Bioconjug Chem*. 2007; 18: 1391-6.
149. Green NM. Avidin and streptavidin. *Methods Enzymol*. 1990; 184: 51-67.
150. Mok H, Lee SH, Park JW, Park TG. Multimeric small interfering ribonucleic acid for highly efficient sequence-specific gene silencing. *Nat Mater*. 2010; 9: 272-8.
151. Jain TK, Morales MA, Sahoo SK, Leslie-Pelecky DL, Labhasetwar V. Iron oxide nanoparticles for sustained delivery of anticancer agents. *Mol Pharm*. 2005; 2: 194-205.
152. Gonzalez H, Hwang SJ, Davis ME. New class of polymers for the delivery of macromolecular therapeutics. *Bioconjug Chem*. 1999; 10: 1068-74.
153. Slamon DJ, Godolphin W, Jones LA, Holt JA, Wong SG, Keith DE, et al. Studies of the HER-2/neu proto-oncogene in human breast and ovarian cancer. *Science*. 1989; 244: 707-12.
154. Artemov D, Mori N, Okollie B, Bhujwalla ZM. MR molecular imaging of the Her-2/neu receptor in breast cancer cells using targeted iron oxide nanoparticles. *Magn Reson Med*. 2003; 49: 403-8.
155. Frederick CA, Williams LD, Ughetto G, van der Marel GA, van Boom JH, Rich A, et al. Structural comparison of anticancer drug-DNA complexes: adriamycin and daunomycin. *Biochemistry*. 1990; 29: 2538-49.
156. Kim D, Jeong YY, Jon S. A drug-loaded aptamer-gold nanoparticle bioconjugate for combined CT imaging and therapy of prostate cancer. *ACS Nano*. 2010; 4: 3689-96.
157. Kolb HC, Finn MG, Sharpless KB. Click Chemistry: Diverse Chemical Function from a Few Good Reactions. *Angew Chem Int Ed Engl*. 2001; 40: 2004-21.
158. Hein CD, Liu XM, Wang D. Click chemistry, a powerful tool for pharmaceutical sciences. *Pharm Res*. 2008; 25: 2216-30.
159. Devaraj NK, Upadhyay R, Haun JB, Hilderbrand SA, Weissleder R. Fast and sensitive pretargeted labeling of cancer cells through a tetrazine/trans-cyclooctene cycloaddition. *Angew Chem Int Ed Engl*. 2009; 48: 7013-6.
160. von Maltzahn G, Ren Y, Park JH, Min DH, Kotamraju VR, Jayakumar J, et al. In vivo tumor cell targeting with "click" nanoparticles. *Bioconjug Chem*. 2008; 19: 1570-8.
161. Rubinstein DB, Stortchevoi A, Boosalis M, Ashfaq R, Ghebrehiwet B, Peerschke EI, et al. Receptor for the globular heads of Clq (gClq-R, p33, hyaluronan-binding protein) is preferentially expressed by adenocarcinoma cells. *Int J Cancer*. 2004; 110: 741-50.
162. Santra S, Kaittanis C, Grimm J, Perez JM. Drug/dye-loaded, multifunctional iron oxide nanoparticles for combined targeted cancer therapy and dual optical/magnetic resonance imaging. *Small*. 2009; 5: 1862-8.
163. Haun JB, Devaraj NK, Hilderbrand SA, Lee H, Weissleder R. Bioorthogonal chemistry amplifies nanoparticle binding and enhances the sensitivity of cell detection. *Nat Nanotechnol*. 2010; 5: 660-5.
164. Haun JB, Devaraj NK, Marinelli BS, Lee H, Weissleder R. Probing intracellular biomarkers and mediators of cell activation using nanosensors and bioorthogonal chemistry. *ACS Nano*. 2011; 5: 3204-13.
165. Lee H, Yoon TJ, Figueiredo JL, Swirski FK, Weissleder R. Rapid detection and profiling of cancer cells in fine-needle aspirates. *Proc Natl Acad Sci U S A*. 2009; 106: 12459-64.
166. Javier DJ, Nitin N, Levy M, Ellington A, Richards-Kortum R. Aptamer-targeted gold nanoparticles as molecular-specific contrast agents for reflectance imaging. *Bioconjug Chem*. 2008; 19: 1309-12.
167. Gref R, Minamitake Y, Peracchia MT, Trubetskoy V, Torchilin V, Langer R. Biodegradable long-circulating polymeric nanospheres. *Science*. 1994; 263: 1600-3.
168. Berry CC, Curtis ASG. Functionalisation of magnetic nanoparticles for applications in biomedicine. *Journal of Physics D: Applied Physics*. 2003; 36: R198-206.
169. Moghimi SM, Hunter AC, Murray JC. Long-circulating and target-specific nanoparticles: Theory to practice. *Pharmacol Rev*. 2001; 53: 283-318.
170. Xie J, Xu C, Kohler N, Hou Y, Sun S. Controlled PEGylation of monodisperse Fe₃O₄ nanoparticles for reduced non-specific uptake by macrophage cells. *Adv Mater*. 2007; 19: 3163-6.
171. Lutz JF, Stiller S, Hoth A, Kaufner L, Pison U, Cartier R. One-pot synthesis of PEGylated ultrasmall iron-oxide nanoparticles and their in vivo evaluation as magnetic resonance imaging contrast agents. *Biomacromolecules*. 2006; 7: 3132-8.
172. Larsen EK, Nielsen T, Wittenborn T, Birkedal H, Vorup-Jensen T, Jakobsen MH, et al. Size-Dependent Accumulation of PEGylated Silane-Coated Magnetic Iron Oxide Nanoparticles in Murine Tumors. *ACS Nano*. 2009; 3: 1947-51.
173. Chung HJ, Lee H, Bae KH, Lee Y, Park J, Cho SW, et al. Facile synthetic route for surface-functionalized magnetic nanoparticles: cell labeling and magnetic resonance imaging studies. *ACS Nano*. 2011; 5: 4329-36.
174. Flesch C, Unterfinger Y, Bourgeat-Lami E, Duguet E, Delaite C, Dumas P. Poly(ethylene glycol) surface coated magnetic particles. *Macromol Rapid Comm*. 2005; 26: 1494-8.
175. Lu Y, Yin YD, Mayers BT, Xia YN. Modifying the surface properties of Superparamagnetic iron oxide nanoparticles through a sol-gel approach. *Nano Lett*. 2002; 2: 183-6.
176. Veiseh O, Sun C, Gunn J, Kohler N, Gabikian P, Lee D, et al. Optical and MRI multifunctional nanoprobe for targeting gliomas. *Nano Lett*. 2005; 5: 1003-8.
177. Gunn J, Wallen H, Veiseh O, Sun C, Fang C, Cao JH, et al. A multimodal targeting nanoparticle for selectively labeling T cells. *Small*. 2008; 4: 712-5.
178. Sun C, Veiseh O, Gunn J, Fang C, Hansen S, Lee D, et al. In vivo MRI detection of gliomas by chlorotoxin-conjugated superparamagnetic nanoprobe. *Small*. 2008; 4: 372-9.
179. Kumar M, Muzzarelli RAA, Muzzarelli C, Sashiwa H, Domb AJ. Chitosan chemistry and pharmaceutical perspectives. *Chem Rev*. 2004; 104: 6017-84.
180. Park J, Yu MK, Jeong YY, Kim JW, Lee K, Phan VN, et al. Antibiofouling amphiphilic polymer-coated superparamagnetic

- iron oxide nanoparticles: synthesis, characterization, and use in cancer imaging in vivo. *J Mater Chem*. 2009; 19: 6412-7.
181. Weissleder R, Stark DD, Engelstad BL, Bacon BR, Compton CC, White DL, et al. Superparamagnetic iron oxide - pharmacokinetic and toxicity. *AJR Am J Roentgenol*. 1989; 152: 167-73.
182. Weissleder R, Elizondo G, Wittenberg J, Lee AS, Josephson L, Brady TJ. Ultrasmall superparamagnetic iron oxide - an intravenous contrast agent for assessing lymph-nodes with MR imaging. *Radiology*. 1990; 175: 494-8.
183. Stark DD, Weissleder R, Elizondo G, Hahn PF, Saini S, Todd LE, et al. Superparamagnetic iron oxide - clinical application as a contrast agent for MR imaging of the liver. *Radiology*. 1988; 168: 297-301.
184. Josephson L, Tung CH, Moore A, Weissleder R. High-efficiency intracellular magnetic labeling with novel superparamagnetic-Tat peptide conjugates. *Bioconjug Chem*. 1999; 10: 186-91.
185. [185] Wunderbaldinger P, Josephson L, Weissleder R. Cross-linked iron oxides (CLIO): A new platform for the development of targeted MR contrast agents. *Acad Radiol*. 2002; 9: S304-6.
186. McCarthy JR, Weissleder R. Multifunctional magnetic nanoparticles for targeted imaging and therapy. *Adv Drug Deliv Rev*. 2008; 60: 1241-51.
187. Wang Y, Teng XW, Wang JS, Yang H. Solvent-free atom transfer radical polymerization in the synthesis of Fe₂O₃@ polystyrene core-shell nanoparticles. *Nano Lett*. 2003; 3: 789-93.
188. Li GF, Fan JD, Jiang R, Gao Y. Cross-linking the linear polymeric chains in the ATRP synthesis of iron oxide/polystyrene core/shell nanoparticles. *Chem Mater*. 2004; 16: 1835-7.
189. Chastellain M, Petri A, Hofmann H. Superparamagnetic iron oxide nanoparticles for biomedical applications: a focus on PVA as a coating. *Quantum Dots, Nanoparticles and Nanowires* 2004; 789: 269-72.
190. Liu HL, Ko SP, Wu JH, Jung MH, Min JH, Lee JH, et al. One-pot polyol synthesis of monosize PVP-coated sub-5 nm Fe₃O₄ nanoparticles for biomedical applications. *J Magn Magn Mater*. 2007; 310: E815-7.
191. Ma YH, Wu SY, Wu T, Chang YJ, Hua MY, Chen JP. Magnetically targeted thrombolysis with recombinant tissue plasminogen activator bound to polyacrylic acid-coated nanoparticles. *Biomaterials*. 2009; 30: 3343-51.
192. Portet D, Denizot B, Rump E, Lejeune JJ, Jallet P. Nonpolymeric coatings of iron oxide colloids for biological use as magnetic resonance imaging contrast agents. *J Colloid Interface Sci*. 2001; 238: 37-42.
193. Fauconnier N, Pons JN, Roger J, Bee A. Thiolation of maghemite nanoparticles by dimercaptosuccinic acid. *J Colloid Interface Sci*. 1997; 194: 427-33.
194. Zhang C, Wangler B, Morgenstern B, Zentgraf H, Eisenhut M, Untenecker H, et al. Silica- and alkoxysilane-coated ultrasmall superparamagnetic iron oxide particles: a promising tool to label cells for magnetic resonance imaging. *Langmuir*. 2007; 23: 1427-34.
195. Jun YW, Huh YM, Choi JS, Lee JH, Song HT, Kim S, et al. Nanoscale size effect of magnetic nanocrystals and their utilization for cancer diagnosis via magnetic resonance imaging. *J Am Chem Soc*. 2005; 127: 5732-3.
196. Choi JS, Park JC, Nah H, Woo S, Oh J, Kim KM, et al. A hybrid nanoparticle probe for dual-modality positron emission tomography and magnetic resonance imaging. *Angew Chem Int Ed Engl*. 2008; 47: 6259-62.
197. Lee JH, Lee K, Moon SH, Lee Y, Park TG, Cheon J. All-in-one target-cell-specific magnetic nanoparticles for simultaneous molecular imaging and siRNA delivery. *Angew Chem Int Ed Engl*. 2009; 48: 4174-9.
198. Martina MS, Fortin JP, Ménager C, Clément O, Barratt G, Grabelle-Madelmont C, et al. Generation of superparamagnetic liposomes revealed as highly efficient MRI contrast agents for in vivo imaging. *J Am Chem Soc*. 2005; 127: 10676-85.
199. Yang J, Lee CH, Ko HJ, Suh JS, Yoon HG, Lee K, et al. Multifunctional magneto-polymeric nanohybrids for targeted detection and synergistic therapeutic effects on breast cancer. *Angew Chem Int Ed Engl*. 2007; 46: 8836-9.
200. Nasongkla N, Bey E, Ren J, Ai H, Khemtong C, Guthi JS, et al. Multifunctional polymeric micelles as cancer-targeted, MRI-ultrasensitive drug delivery systems. *Nano Lett*. 2006; 6: 2427-30.
201. Kim J, Kim HS, Lee N, Kim T, Kim H, Yu T, et al. Multifunctional uniform nanoparticles composed of a magnetite nanocrystal core and a mesoporous silica shell for magnetic resonance and fluorescence imaging and for drug delivery. *Angew Chem Int Ed Engl*. 2008; 47: 8438-41.
202. Kim J, Park S, Lee JE, Jin SM, Lee JH, Lee IS, et al. Designed fabrication of multifunctional magnetic gold nanoshells and their application to magnetic resonance imaging and photothermal therapy. *Angew Chem Int Ed Engl*. 2006; 45: 7754-8.
203. Zhang Z, Chao T, Chen SF, Jiang SY. Superlow fouling sulfobetaine and carboxybetaine polymers on glass slides. *Langmuir* 2006; 22: 10072-7.
204. Ostuni E, Chapman RG, Liang MN, Meluleni G, Pier G, Ingber DE, et al. Self-assembled monolayers that resist the adsorption of proteins and the adhesion of bacterial and mammalian cells. *Langmuir*. 2001; 17: 6336-43.
205. Ladd J, Zhang Z, Chen S, Hower JC, Jiang S. Zwitterionic polymers exhibiting high resistance to nonspecific protein adsorption from human serum and plasma. *Biomacromolecules*. 2008; 9: 1357-61.
206. Holmlin RE, Chen XX, Chapman RG, Takayama S, Whitesides GM. Zwitterionic SAMs that resist nonspecific adsorption of protein from aqueous buffer. *Langmuir*. 2001; 17: 2841-50.
207. Choi HS, Liu W, Misra P, Tanaka E, Zimmer JP, Itty Ipe B, et al. Renal clearance of quantum dots. *Nat Biotechnol*. 2007; 25: 1165-70.
208. Liu W, Choi HS, Zimmer JP, Tanaka E, Frangioni JV, Bawendi M. Compact cysteine-coated CdSe(ZnCdS) quantum dots for in vivo applications. *J Am Chem Soc*. 2007; 129: 14530-1.
209. Yang W, Zhang L, Wang S, White AD, Jiang S. Functionalizable and ultra stable nanoparticles coated with zwitterionic poly(carboxybetaine) in undiluted blood serum. *Biomaterials*. 2009; 30: 5617-21.
210. Zhang L, Xue H, Gao C, Carr L, Wang J, Chu B, et al. Imaging and cell targeting characteristics of magnetic nanoparticles modified by a functionalizable zwitterionic polymer with adhesive 3,4-dihydroxyphenyl-L-alanine linkages. *Biomaterials*. 2010; 31: 6582-8.
211. Sun C, Lee JS, Zhang M. Magnetic nanoparticles in MR imaging and drug delivery. *Adv Drug Deliv Rev*. 2008; 60: 1252-65.
212. Knop K, Hooogenboom R, Fischer D, Schubert US. Poly(ethylene glycol) in drug delivery: pros and cons as well as potential alternatives. *Angew Chem Int Ed Engl*. 2010; 49: 6288-308.
213. Wang M, Thanou M. Targeting nanoparticles to cancer. *Pharmacol Res*. 2010; 62: 90-9.
214. Degennes PG. Polymers at an interface-a simplified view. *Adv Colloid Interface*. 1987; 27: 189-209.
215. Szleifer I. Polymers proteins: interactions at interfaces. *Curr Opin Solid St M*. 1997; 2: 337-44.
216. Owens DE 3rd, Peppas NA. Opsonization, biodistribution, and pharmacokinetics of polymeric nanoparticles. *Int J Pharm*. 2006; 307: 93-102.
217. Gbadamosi JK, Hunter AC, Moghimi SM. PEGylation of microspheres generates a heterogeneous population of particles with differential surface characteristics and biological performance. *Febs Lett*. 2002; 532: 338-44.

218. Storm G, Belliot SO, Daemen T, Lasic DD. Surface modification of nanoparticles to oppose uptake by the mononuclear phagocyte system. *Adv Drug Deliv Rev.* 1995; 17: 31-48.
219. Garg A, Tisdale AW, Haidari E, Kokkoli E. Targeting colon cancer cells using PEGylated liposomes modified with a fibronectin-mimetic peptide. *Int J Pharm.* 2009; 366: 201-10.
220. Gindy ME, Ji S, Hoye TR, Panagiotopoulos AZ, Prud'homme RK. Preparation of poly(ethylene glycol) protected nanoparticles with variable bioconjugate ligand density. *Biomacromolecules.* 2008; 9: 2705-11.
221. Olivier V, Meisen I, Meckelein B, Hirst TR, Peter-Katalinic J, Schmidt MA, et al. Influence of targeting ligand flexibility on receptor binding of particulate drug delivery systems. *Bioconjug Chem.* 2003; 14: 1203-8.
222. Ferrari M. Nanogeometry: beyond drug delivery. *Nat Nanotechnol.* 2008; 3: 131-2.
223. Fakhari A, Baoum A, Siahaan TJ, Le KB, Berkland C. Controlling ligand surface density optimizes nanoparticle binding to ICAM-1. *J Pharm Sci.* 2011; 100: 1045-56.
224. Wülfing C, Sjaastad MD, Davis MM. Visualizing the dynamics of T cell activation: intracellular adhesion molecule 1 migrates rapidly to the T cell/B cell interface and acts to sustain calcium levels. *Proc Natl Acad Sci U S A.* 1998; 95: 6302-7.
225. Gu F, Zhang L, Teply BA, Mann N, Wang A, Radovic-Moreno AF, et al. Precise engineering of targeted nanoparticles by using self-assembled biointegrated block copolymers. *Proc Natl Acad Sci U S A.* 2008; 105: 2586-91.
226. Shmeeda H, Tzemach D, Mak L, Gabizon A. Her2-targeted pegylated liposomal doxorubicin: retention of target-specific binding and cytotoxicity after in vivo passage. *J Control Release.* 2009; 136: 155-60.
227. Park JH, von Maltzahn G, Zhang L, Derfus AM, Simberg D, Harris TJ, et al. Systematic surface engineering of magnetic nanoworms for in vivo tumor targeting. *Small.* 2009; 5: 694-700.